2014

Topics in Quantum Metrology, Control, and Communications

Bhaskar Roy Bardhan
Louisiana State University and Agricultural and Mechanical College, bhasiitg@gmail.com

TOPICS IN QUANTUM METROLOGY, CONTROL, AND COMMUNICATIONS

A Dissertation

Submitted to the Graduate Faculty of the
Louisiana State University and
Agricultural and Mechanical College
in partial fulfillment of the
requirements for the degree of
Doctor of Philosophy

in

The Department of Physics and Astronomy

by
Bhaskar Roy Bardhan
B.Sc., University of Calcutta, 2006
M.Sc., Indian Institute of Technology Guwahati, 2008
December 2014

Acknowledgements

First of all, I would like to thank my PhD advisor Professor Jonathan Dowling whose guidance, inspiration, and support have steered me through my doctoral studies. I consider it to be one of my greatest privileges to have him as my advisor. I will be ever grateful to him for teaching me how to learn physics, for identifying my strengths and weaknesses, for inspiring me to think innovatively, and for countless other reasons. Working with a legendary and visionary physicist like Professor Dowling will always remain as one of the most cherishable experiences in my scientific career.

I am immensely grateful to my co-advisor Professor Mark Wilde with whom I worked for a few recent projects after he joined LSU. He has opened a new horizon to my knowledge by introducing me to the field of the quantum information theory. I had little to no understanding of this newly emerging field when he started to teach the course on it at LSU, but within a short period of time his dedication and motivating teaching style have ignited great interest in me to explore some problems in quantum information theory. I am especially thankful to him for patiently answering all of my questions during our discussions, which helped me to clarify many subtle points of our projects.

I am greatly indebted to Professor Hwang Lee for his guidance, encouragement, and support all along. I am very much thankful to my committee members Professor Ravi Rau and Professor Jeffrey Blackmon for being a part of my committee. I would also like to thank Professor Helmut Schneider from the Department of Information Systems and Decision Sciences for being on my committee as the dean's representative.

I have greatly benefitted from many collaborative research works during the course of my doctoral studies, and all of my collaborators have influenced me in different ways. In particular, I would like to thank Dr. Saikat Guha at Raytheon BBN and Professor Girish Agarwal at Oklahoma State University. The collaboration with Saikat was very remarkable to me in the sense that he introduced me to many practical aspects of optical communication and quantum information theory, and I had the opportunity to participate in many stimulating and interesting discussions. Professor Agarwal kindly agreed to host me at his university to complete a collaborative project, and from him I learnt many basic but invaluable lessons in quantum optics.

I would like to extend my thanks to the current and former postdocs in our research group. In particular, I am greatly thankful to Dr. Petr Anisimov and Dr. Katherine Brown for mentoring me in the initial years of my PhD, and helping me out with many numerical and analytical issues for the projects that I completed with them. I thank my colleagues Kaushik Seshadreesan, Kebei Jiang, Ashkan Balouchi, Robinjeet Singh, and Jonathan Olson for helpful discussions and company. It is a pleasure of mine to thank my best friend and roommate Brajesh Gupt whose company was a very significant and inseparable part of my life at LSU.

Finally, and most importantly, no words are enough to thank my parents and family members whose continued love and support have played a key role to pursue my dreams. Without their sacrifices and unconditional support it would not have been possible for me to overcome many rough phases of my life.

Table of Contents

List of Figures

Abstract

Noise present in an environment has significant impacts on a quantum system affecting properties like coherence, entanglement and other metrological features of a quantum state. In this dissertation, we address the effects of different types of noise that are present in a communication channel (or medium) and an interferometric setup, and analyze their effects in the contexts of preserving coherence and entanglement, phase sensitivity, and limits on rate of communication through noisy channels.

We first consider quantum optical phase estimation in quantum metrology when phase fluctuations are introduced in the system by its interaction with a noisy environment. By considering path-entangled dual-mode photon Fock states in a Mach-Zehnder optical interferometric configuration, we show that such phase fluctuations affect phase sensitivity and visibility by adding noise to the phase to be estimated. We also demonstrate that the optimal detection strategy for estimating a phase in the presence of such phase noise is provided by the parity detection scheme.

We then investigate the random birefringent noise present in an optical fiber affecting the coherence properties of a single photon polarization qubit propagating through it. We show that a simple but effective control technique, called dynamical decoupling, can be used to suppress the effects of the dephasing noise, thereby preserving its ability to carry the encoded quantum information in a long-distance optical fiber communication system.

Optical amplifiers and attenuators can also add noise to an entangled quantum system, deteriorating the non-classical properties of the state. We show this by considering a two-mode squeezed vacuum state, which is a Gaussian entangled state, propagating through a noisy medium, and characterizing the loss of entanglement in the covariance matrix and the symplectic formalism for this state.

Finally, we discuss limits on the rate of communication in the context of sending messages through noisy optical quantum communication channels. In particular, we prove that a strong converse theorem holds under a maximum photon number constraint for these channels, guaranteeing that the success probability in decoding the message vanishes in the asymptotic limit for the rate exceeding the capacity of the channels.

Chapter 1
Introduction

Quantum theory allows us to understand the behavior of systems at the atomic length scale or smaller levels. It contains elements that are radically different from the classical description of nature and has revolutionized the way we see nature. The cornerstone of this fascinating theory was laid down by the pioneering work of Max Planck in 1900 when he came up with the remarkable postulate that the energy spectrum of a harmonic oscillator is discrete and quantized. This quantized nature of the energy spectrum not only helped to construe the spectral distribution of thermal light but also led to several immediate implications that in turn contributed to the formulation of the quantum description of nature. In particular, in 1905 Albert Einstein applied Planck's idea of discrete energy to explain the phenomenon called the photo-electric effect, where light incident on a piece of metal results in the emission of electrons from the metal.

Einstein also contributed to the quantum theory of electromagnetic radiation by establishing a theory in 1917 for understanding the absorption and emission of light from atoms. In 1927, Paul Adrien Maurice Dirac put forward a complete quantum mechanical treatment of the emission and absorption of light, leading to the quantum description of optics. Unlike classical optics, this new theory is based on quantized electromagnetic fields, and explains the concept of *photon* as the elementary quanta of light radiation. Roy Glauber, in his seminal work in 1963, provided the quantum formulation of optical coherence that fully established the field of quantum optics.

Along with the quantization of electromagnetic fields and atomic energy levels, the quantum mechanical description of nature also makes use of principles such as superposition, entanglement, teleportation and uncertainty principle. Based on these quantum principles, extensive efforts have been taken over the last few decades, contributing towards the development of technologies for computation, communication, cryptography, metrology, lithography and microscopy, etc. The reason for this growing interest in exploiting quantum phenomena is that they promise major 'quantum' leaps over the existing technologies (that are based on classical concepts) in the above mentioned areas.

One serious impediment for using the aforementioned quantum principles is that a quantum state is extremely fragile. The quantum state of a system gets affected by an environment, leading to the loss of information from the system to the environment. In general, the behavior of a quantum system is significantly influenced by noise present in the environment that surrounds the system. The noisy environment can in general have significant effects on properties like phase coherence, entanglement and metrological characteristics of quantum states.

In this dissertation, we address the effects of different types of noise that are present in a communication channel (or medium) or an interferometric setup, and analyze their effects in the contexts of preserving coherence and entanglement, phase sensitivity, and limits on the rate of communication through noisy channels. In Chapter 1, we begin with a brief overview of the essential topics of quantum mechanics, quantum optics, and quantum information theory, providing a foundation for discussions in later chapters. We first consider quantum optical

phase estimation in quantum metrology when phase fluctuations are introduced in the system by its interaction with a noisy environment. In Chapter 2, by considering path-entangled dual-mode photon Fock states in a Mach-Zehnder optical interferometric configuration, we show that such phase fluctuations affect phase sensitivity and visibility by adding noise to the phase to be estimated. We also demonstrate that a specific detection scheme, known as parity detection, provides the optimal detection strategy for estimating the phase in presence of such phase noise for these states.

In Chapter 3, we investigate the random birefringent noise present in an optical fiber and its effects on the coherence of a single photon polarization qubit propagating through the fiber. We show that a simple but effective control technique, called dynamical decoupling, can be used to suppress the effects of the dephasing noise thereby preserving its ability to carry the encoded quantum information for a long-distance optical fiber communication system.

Optical amplifiers and attenuators can also add noise to an entangled quantum system deteriorating the non-classical properties of the state. We show this by considering a two-mode squeezed vacuum state, which is a Gaussian entangled state, propagating through a noisy medium, and by characterizing the loss of entanglement in the covariance matrix and the symplectic formalism for this state. In Chapter 4, we present a case study as an application of this to provide an estimate of the tolerable noise for a given entanglement to be preserved and also to detect the presence or absence of an object embedded in such noisy medium.

We also study the ultimate limits on reliable communication through noisy optical quantum communication channels that are allowed by the laws of quantum mechanics. In Chapter 5, we consider phase-insensitive bosonic Gaussian channels that represent the most practically relevant models to describe free space or optical fiber transmission, or transmission of classical messages through dielectric media. In particular, we prove that a strong converse theorem for these channels holds under a maximum photon number constraint, guaranteeing that the success probability in decoding the message vanishes for many independent uses of the channel when the rate exceeds the capacity of the respective channels.

In the following, we give a brief overview of the essential concepts of quantum mechanics and its principles, providing a foundation for the works that will be covered in this thesis.

1.1 Brief review of quantum mechanics

1.1.1 Pure and mixed states

A pure state of a quantum system is conventionally denoted by a vector $|\psi\rangle$ having unit length and which resides in a complex Hilbert space $\mathcal{H}$. A pure state $|\psi\rangle$ can be expressed in terms of a set of complete orthonormal basis vectors $\{|\phi_n\rangle\}$ spanning the Hilbert space $\mathcal{H}$ as

$$|\psi\rangle = \sum_n c_n |\phi_n\rangle. \tag{1.1}$$

Here c_n are a set of complex numbers such that $\sum_n |c_n|^2 = 1$. As a simple example of a pure state, we can consider a 'qubit'—a two-level system, which is regarded as the fundamental unit of quantum information. A general qubit can be written in terms of the orthonormal basis vectors $|0\rangle$ and $|1\rangle$ as $|\psi\rangle = \alpha|0\rangle + \beta|1\rangle$, where α and β are two complex numbers with $|\alpha|^2 + |\beta|^2 = 1$.

A mixed state, on the contrary, is a statistical ensemble of pure states. Mixed states represent the most frequently encountered states in real experiments because of the fact that in reality the quantum systems cannot be completely isolated from their surroundings. Both pure and mixed states, however, can be represented by their density operator or density matrix (denoted by $\hat{\rho}$). The density matrix $\hat{\rho}$ in general is positive definite, and Hermitian ($\hat{\rho}^\dagger = \hat{\rho}$). The trace of $\hat{\rho}$ is unity, i.e. $\mathrm{Tr}\,\hat{\rho} = \sum_n \langle\phi_n|\hat{\rho}|\phi_n\rangle = 1$. For a pure state $|\psi\rangle$, the density operator can be written as $\hat{\rho} = |\psi\rangle\langle\psi|$, and it also satisfies $\hat{\rho}^2 = |\psi\rangle\langle\psi|\psi\rangle\langle\psi| = \hat{\rho}$. In fact, the quantity $\mathrm{Tr}[\hat{\rho}^2]$ is also referred to as the *purity* of the state.

As an example, take the pure state $|\psi\rangle = \frac{|0\rangle+|1\rangle}{\sqrt{2}}$. The density operator for this state in the basis $\{|0\rangle, |1\rangle\}$ can be written as $\hat{\rho} = \frac{1}{2}\begin{pmatrix} 1 & 1 \\ 1 & 1. \end{pmatrix}$

The density operator for a mixed state, which is a probabilistic mixture of the pure states $\{|\psi_k\rangle\langle\psi_k|\}$, is defined as

$$\hat{\rho} = \sum_k p_k |\psi_k\rangle\langle\psi_k|, \tag{1.2}$$

where the sum of the probabilities $\sum_k p_k = 1$.

As a special case, consider the maximally mixed state for which the probabilities of the basis states are equal. In that case, the density operator $\hat{\rho}$ is given by $\hat{\rho} = \frac{1}{N}\hat{I}$, where N is the dimension of the Hilbert space $\mathcal{H}$ and $\hat{I}$ is the identity operator.

The decomposition of the mixed state in Equation (1.2) is not unique. Since the density operator is Hermitian in nature, it has a spectral decomposition $\hat{\rho} = \sum_i a_i |i\rangle\langle i|$ for some orthonormal basis $|i\rangle$. The eigenvalues a_i here form a probability distribution.

1.1.2 Product states and entangled states

The pure and mixed states of a composite quantum system AB can be classified into two classes—separable states and entangled states. Let us consider two quantum systems A and B with respective Hilbert spaces $\mathcal{H}_A$ and $\mathcal{H}_B$. The pure states and the mixed states of the composite system AB can be identified following the same way as for the individual systems but in the joint Hilbert space $\mathcal{H}_{AB} = \mathcal{H}_A \otimes \mathcal{H}_B$.

A quantum state $\hat{\rho}^{AB} \in \mathcal{H}_{AB}$ in general is said to be separable if $\hat{\rho}^{AB}$ can be expressed as a convex combination of the product states:

$$\hat{\rho}^{AB} = \sum_k p_k \hat{\rho}_k^A \otimes \hat{\rho}_k^B, \tag{1.3}$$

where $\sum_k p_k = 1$. Such a separable state can be prepared in the laboratory by local operations and classical communication.

On the other hand, if a state is not separable, it is called an *entangled* state. As an example, we can consider the pure state

$$|\psi\rangle = \frac{|0\rangle|_A 1\rangle_B + |1\rangle_A|0\rangle_B}{\sqrt{2}},$$

which can not be written as a separable state of the above form, and represents an entangled state.

One can always consider a mixed state $\hat{\rho}^A$ of a system A as entangled with some auxiliary reference system R. First, consider its spectral decomposition

$$\hat{\rho}^A = \sum_k a_k |\phi_k\rangle\langle\phi_k|, \tag{1.4}$$

in some orthonormal basis $|\phi_k\rangle$. Then, the following state is called a *purification* of $\hat{\rho}^A$

$$|\psi\rangle^{RA} = \sum_k \sqrt{a_k} |\phi_k\rangle^A |k\rangle^R \tag{1.5}$$

for some set of orthonormal states $\{|k\rangle\}$ of the system R. The above idea of purification has the implication that the noise in the state can be thought to be arising from the interaction of the system with an external environment to which we do not have access. This remarkable notion of the purification extends, by considering an isometric extension of a channel, to the case of the noisy quantum channels as well.

1.1.3 Dynamical evolution of quantum states

How a *closed* quantum system evolves with time is, in general, governed by a unitary transformation U of the state. This means that the state $|\psi(t_0)\rangle$ of the system at time t_0 is *reversibly* related to the state at time t by a unitary transformation $\hat{U}(t, t_0)|\psi(t_0)\rangle$:

$$|\psi(t)\rangle = \hat{U}(t, t_0)|\psi(t_0)\rangle = \exp\left(\frac{-iH(t - t_0)}{\hbar}\right)|\psi(t_0)\rangle, \tag{1.6}$$

where $\hbar$ is a constant known as Planck's constant. For a mixed state with the density operator $\hat{\rho}$, the evolution looks like

$$\hat{\rho}(t) = \hat{U}(t, t_0)\hat{\rho}(t_0)\hat{U}^\dagger(t, t_0). \tag{1.7}$$

The unitary evolution of a closed quantum system implies the *reversibility* which means that one can recover the initial state before the evolution from the knowledge of the evolution. Furthermore, the unitarity of the evolution also ensures that the unit-norm constraint is preserved.

In almost all real-life scenarios, the system interacts with a surrounding environment where the evolution of such an *open* quantum system is not governed by unitary evolution in general. However, the state of the system *together* with the environment is still a closed system, and its time evolution is again given by a unitary evolution. But for the system alone, the evolution is non-unitary, and can be conveniently represented by a noisy map $\mathcal{N}$ acting on the density operator $\hat{\rho}$.

This map $\mathcal{N}$ is a trace-preserving map, meaning that $\mathrm{Tr}\{\mathcal{N}(\hat{\rho})\} = 1$. It is also completely positive. It means that the output of the tensor product map $(I^k \otimes \mathcal{N})(\hat{\rho})$ for any finite k is a positive operator where the input $\hat{\rho}$ to the channel is a positive operator. We note that such a completely positive trace-preserving (CPTP) map is the mathematical model that we will use for a quantum channel (see Chapter 5) since it represents the most general noisy evolution of a quantum state. Such a model of the noisy channel can be expressed in an operator sum representation with Kraus operators $\hat{A}_k$ so that $\mathcal{N}(\hat{\rho}) = \sum_k \hat{A}_k \hat{\rho} \hat{A}_k^\dagger$ with $\sum \hat{A}_k^\dagger \hat{A}_k = \hat{I}$.

1.1.4 Quantum measurements

As with all measurements, we try to extract some classical information when we make a measurement on a system. However, there exist some fundamental subtleties regarding the notion of quantum measurements. In quantum mechanics, measurements are described by a set of Hermitian (self-adjoint) operators, and the act of measurement on a quantum system inevitably disturbs the quantum state.

In the following, we discuss two types of quantum measurements that we generally encounter—the one is called projective measurement (or von Neumann measurement), and the other is known as Positive Operator-Valued Measure (POVM).

A *projective measurement* in quantum mechanics refers to the kind of measurement in which the measurement projects a quantum state onto an eigenstate of the measurement operator. Let $\hat{M}$ denote the measurement operator which is Hermitian in nature and has a complete set of orthonormal eigenstates $\{|\phi\rangle\}$. The measurement of this operator $\hat{M}$ on a quantum state $\hat{\rho}$ yields an outcome which is an eigenvalue ϕ of $\hat{M}$, i.e.

$$\hat{M}|\phi\rangle = \phi|\phi\rangle, \tag{1.8}$$

with the probability $p(\phi) = \langle\phi|\hat{\rho}|\phi\rangle$. Note that the eigenvalue ϕ is real since $\hat{M}$ is a Hermitian operator. The post-measurement state of the system is then the eigenstate $|\phi\rangle$ with the corresponding eigenvalue ϕ. Thus, the measurement projects the state onto its eigenspace, and hence the name projective measurement. However, if the system is already in one of the eigenstates of the operator $\hat{M}$, then the measurement does not change the state of the system.

A generalization of the above projective measurement is called the *Positive Operator-Valued Measurement (POVM).* A set of positive operators $\{\Pi_m\}$ that satisfy $\sum_m \hat{\Pi}_m = \hat{I}$ is called a POVM. For a pure quantum state $|\psi\rangle$, the probability of getting m as the outcome of a POVM is $\langle\psi|\hat{\Pi}_m|\psi\rangle$, while for a mixed state $\hat{\rho}$ the probability of getting m as the outcome is $\mathrm{Tr}\{\hat{\Pi}_m\rho\}$. Unlike projective measurements, the POVM operators do not uniquely determine the post-measurement state.

For instance, we consider classical data transmission over a noisy quantum channel, where it is appropriate for the receiver at the end of the channel to perform a POVM since he is merely concerned about knowing the probabilities of the outcomes of the measurement and not the post-measurement state.

1.2 Brief review of quantum optics

In this section we review some concepts in quantum optics that will be relevant for our works in later chapters. We start with the quantization of electromagnetic fields and discuss some key features associated with it, by following the notations used in Reference [133]). Then we present a brief study on the quantum mechanical states and their phase space representations. We then discuss the notion of phase in quantum optics and delineate the methods of its estimation in an optical interferometric setup. Finally, we present a brief overview of the approaches to determine the lower bounds in estimation of such an optical phase, e.g., by evaluating the quantum Cramér-Rao bound. The quantum Cramér-Rao bound also helps us to decide if a given detection strategy is optimal for estimating the optical phase.

1.2.1 Quantization of the electromagnetic field

In order to understand the quantization of the electromagnetic field, we start with the classical electromagnetic field in free space in the absence of any source of radiation, which is described by Maxwell's equations:

$$\nabla.\mathbf{E} = 0 \tag{1.9}$$

$$\nabla \times \mathbf{E} = -\frac{\partial \mathbf{B}}{\partial t} \tag{1.10}$$

$$\nabla.\mathbf{B} = 0 \tag{1.11}$$

$$\nabla \times \mathbf{B} = \frac{1}{c^2}\frac{\partial \mathbf{E}}{\partial t}, \tag{1.12}$$

where $\mathbf{E} = \mathbf{E}(\mathbf{r}, t)$ and $\mathbf{B} = \mathbf{B}(\mathbf{r}, t)$ represent the electric field and magnetic field vectors in free space in terms of the spatial vector $\mathbf{r} = \mathbf{r}(x, y, z)$ and time t, and c is the speed of light. In order to obtain a general solution of the above equations, we introduce the vector potential $\mathbf{A}(\mathbf{r}, t)$ which is defined in terms of the electric and the magnetic fields as

$$\mathbf{E} = -\frac{\partial \mathbf{A}}{\partial t} \tag{1.13}$$

$$\mathbf{B} = \nabla \times \mathbf{A}. \tag{1.14}$$

Since there is no source present, we can choose to work in the Coulomb gauge, i.e.

$$\nabla.\mathbf{A} = 0. \tag{1.15}$$

Using the above Gauge condition, we obtain a vector wave equation for the vector potential $\mathbf{A}(\mathbf{r}, t)$ which is of the form

$$\nabla^2 \mathbf{A}(\mathbf{r}, t) = \frac{1}{c^2}\frac{\partial^2 \mathbf{A}}{\partial t^2}. \tag{1.16}$$

We can now separate out the vector potential $\mathbf{A}(\mathbf{r}, t)$ into two terms, and confine the field to a finite volume (say $V = L^3$ for a cubical cavity of side L) so that $\mathbf{A}(\mathbf{r}, t)$ can now be written in terms of a discrete set of orthogonal mode functions $\mathbf{u}_k(\mathbf{r})$ corresponding to the frequency ω_k

$$\mathbf{A}(\mathbf{r}, t) = \sum_k \alpha_k \mathbf{u}_k(\mathbf{r}) e^{i\omega_k t} + \sum_k \alpha_k^\dagger \mathbf{u}_k^*(\mathbf{r}) e^{-i\omega_k t} \tag{1.17}$$

Substituting this into Equation (1.16), we then get

$$\left(\nabla^2 + \frac{\omega_k^2}{c^2}\right) \mathbf{u}_k(\mathbf{r}) = 0. \tag{1.18}$$

For a cubical cavity of side L confining the field, the solution of the above equation takes the form

$$\mathbf{u}_k(\mathbf{r}) = \frac{1}{L^{3/2}} \hat{\varepsilon}_\lambda e^{i\mathbf{k}.\mathbf{r}}, \tag{1.19}$$

where $\hat{\varepsilon}_\lambda$ is the unit polarization vector ($\lambda = 1, 2$ corresponding to two orthogonal polarizations) perpendicular to the wave vector $\mathbf{k}$, and components of k are given by

$$k_x = \frac{2\pi n_x}{L}, k_y = \frac{2\pi n_y}{L}, k_z = \frac{2\pi n_z}{L}. \tag{1.20}$$

With the solution of $\mathbf{u}_k(\mathbf{r})$ in Equation (1.19), the vector potential $\mathbf{A}(\mathbf{r},t)$ can be written as

$$\mathbf{A}(\mathbf{r},t) = \sum_k \left(\frac{\hbar}{2\varepsilon_0\omega_k}\right)^{1/2} \left[a_k\mathbf{u}_k(\mathbf{r})e^{i\omega_k t} + a_k^\dagger\mathbf{u}_k^*(\mathbf{r})e^{-i\omega_k t}\right], \tag{1.21}$$

where ε_0 is the permittivity of free space. The associated electric field can then be written as

$$\mathbf{E}(\mathbf{r},t) = \sum_k \left(\frac{\hbar}{2\varepsilon_0\omega_k}\right)^{1/2} \left[a_k\mathbf{u}_k(\mathbf{r})e^{i\omega_k t} + a_k^\dagger\mathbf{u}_k^*(\mathbf{r})e^{-i\omega_k t}\right]. \tag{1.22}$$

We now proceed to the quantization of the electromagnetic field which we can do by generalizing the amplitudes a_k and $a_k^\dagger$ in the above equations to be mutually adjoint operators $\hat{a}_k$ and $\hat{a}_k^\dagger$ satisfying the following bosonic commutation relations:

$$[\hat{a}_k, \hat{a}_{k'}] = [\hat{a}_k^\dagger, \hat{a}_{k'}^\dagger] = 0, \tag{1.23}$$

$$[\hat{a}_k, \hat{a}_{k'}^\dagger] = \delta_{kk'}. \tag{1.24}$$

The operators $\hat{a}_k$ and $\hat{a}_k^\dagger$ are known as the annihilation and creation operators for a quantum mechanical harmonic oscillator (the reasons for such names will be clearer in the next subsection).

The quantum theory of the radiation field associates each mode of the field to a quantum harmonic oscillator. The energy stored in the electromagnetic field in the cavity is given by the Hamiltonian

$$H = \frac{1}{2}\int_{V=L^3} \left(\varepsilon_0\mathbf{E}^2 + \frac{1}{\mu_0}\mathbf{B}^2\right) d^3\mathbf{r}, \tag{1.25}$$

where μ_0 is the permeability of free space. The above Hamiltonian may be rewritten in the following form:

$$H = \sum_k \hbar\omega_k \left(\hat{a}_k^\dagger\hat{a}_k + \frac{1}{2}\right), \tag{1.26}$$

which represents the sum of two terms—the first is the number of photons in each mode of the radiation field multiplied by the energy of a photon $\hbar\omega_k$ in each mode, while the second term $\frac{1}{2}\hbar\omega_k$ is the energy corresponding to the vacuum fluctuations in each mode of the field.

1.2.2 Quadratures of the field

The last subsection described how the bosonic field operators $\hat{a}$ and $\hat{a}^\dagger$ represent the bosonic system such as the modes of the electromagnetic field that can be associated with independent quantum harmonic oscillators. There is another kind of field operator known as the quadrature operator that can be used to describe bosonic systems. We define the following two Hermitian quadrature operators $\hat{X}$ and $\hat{Y}$ in terms of $\hat{a}$ and $\hat{a}^\dagger$

$$\hat{X} = \frac{\hat{a} + \hat{a}^\dagger}{\sqrt{2}},\ \hat{Y} = \frac{\hat{a} - \hat{a}^\dagger}{\sqrt{2}i}, \tag{1.27}$$

which satisfy the commutation relation $[\hat{X}, \hat{Y}] = i$, and Heisenberg's uncertainty relation:

$$\Delta X\Delta Y \geq \frac{1}{2},\ \text{where } (\Delta X)^2 = \langle X^2\rangle - \langle X\rangle^2,\ (\Delta Y)^2 = \langle Y^2\rangle - \langle Y\rangle^2, \tag{1.28}$$

where ΔX and ΔY denote the uncertainties in the quadratures X and Y, respectively.

1.2.3 Quantum states of the electromagnetic field

The Hamiltonian operator from Equation (1.26) has the eigenvalues $\hbar\omega(n+\frac{1}{2})$ where $n = 0, 1, 2, \ldots$ (For the sake of brevity, we henceforth drop the mode index k). The eigenstates $|n\rangle$ are known as *photon number states* or Fock states. The operator $\hat{n} = \hat{a}^\dagger\hat{a}$ is called the photon number operator:

$$\hat{n}|n\rangle = n|n\rangle. \tag{1.29}$$

The vacuum state of the field mode is given by $\hat{a}|0\rangle = 0$, and has energy $\frac{1}{2}\hbar\omega$. The photon number states form a complete orthonormal basis for representing any arbitrary state of a single-mode bosonic field, since $\langle n|k\rangle = \delta_{nk}$ (orthonormal), and $\sum_{n=0}^{\infty}|n\rangle\langle n| = \hat{I}$(complete), where $\hat{I}$ is the identity operator.

The action of the creation and annihilation operators on the number state $|n\rangle$ is

$$\hat{a}|n\rangle = \sqrt{n}|n-1\rangle, \tag{1.30}$$

$$\hat{a}^\dagger|n\rangle = \sqrt{n+1}|n+1\rangle. \tag{1.31}$$

Also, the number state $|n\rangle$ can be obtained from the ground state $|0\rangle$ in the following way

$$|n\rangle = \frac{(\hat{a}^\dagger)^n}{\sqrt{n!}}|0\rangle. \tag{1.32}$$

For Fock states, the mean values of the field operator $\hat{a}$ and the quadrature operators vanish, i.e.

$$\langle n|\hat{a}|n\rangle = \langle n|\hat{X}|n\rangle = \langle n|\hat{Y}|n\rangle = 0 \tag{1.33}$$

These states contain equal uncertainties in the two quadratures, i.e. $(\Delta X)^2 = (\Delta Y)^2 = n+\frac{1}{2}$, leading to $\Delta X\Delta Y = n + \frac{1}{2}$. It can also be noted here that the photon number states or the Fock states are highly non-classical in nature, and have well-defined number of photons but phase distribution is completely random (see Figure 1.1).

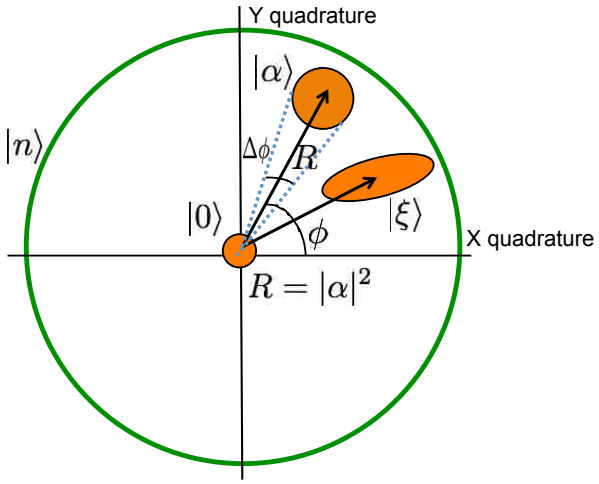

Figure 1.1: Phase space diagram of the quantum states. A number state $|n\rangle$ is shown as a circle with a fixed number of photons but completely random phase distribution. A coherent state $|\alpha\rangle$, with amplitude $|\alpha|^2$ and phase ϕ, has equal uncertainties in the two quadratures, and it can be generated by displacing the vacuum state $|0\rangle$ in the phase space. A squeezed state $|\xi\rangle$ in which fluctuations in one quadrature are reduced is also shown in the figure.

The *coherent states* of light, contrary to the Fock states $|n\rangle$ discussed above, are the "most classical-like" states in the sense that they are the closest analogue of the classical electromagnetic wave, having fixed amplitude and phase (for example a coherent laser light).

The coherent states $|\alpha\rangle$ are defined as the eigenstates of the annihilation operator $\hat{a}$, i.e. $\hat{a}|\alpha\rangle = \alpha|\alpha\rangle$, where $|\alpha|^2$ is the amplitude of the coherent state $|\alpha\rangle$. In the number state basis, the coherent states $|\alpha\rangle$ can be written as superposition of the Fock states $|n\rangle$

$$|\alpha\rangle = \sum_{n=0}^{\infty} \frac{e^{-|\alpha|^2/2}\alpha^n}{\sqrt{n!}}|n\rangle, \tag{1.34}$$

which can be generated by "displacing" the vacuum state $|0\rangle$ (see Figure 1.1) with a displacement operator $\hat{D}(\alpha)$:

$$|\alpha\rangle = \hat{D}(\alpha)|0\rangle. \tag{1.35}$$

The displacement operator $\hat{D}(\alpha)$ is defined as : $\hat{D}(\alpha) = \exp(\alpha\hat{a}^\dagger - \alpha^*\hat{a})$.

The probability of finding n photons in a coherent state $|\alpha\rangle$ is represented by the following Poisson distribution with mean $|\alpha|^2 = \langle n\rangle$ (where $\hat{n} = \hat{a}^\dagger\hat{a}$ is the photon number operator)

$$p_n = \frac{e^{-|\alpha|^2}\alpha^{2n}}{n!}. \tag{1.36}$$

The coherent states of light have uncertainties in the quadratures $(\Delta X)^2 = (\Delta Y)^2 = \frac{1}{2}$, leading to the minimum uncertainty product $\Delta X \Delta Y = \frac{1}{2}$. Also, the mean values of the field operator $\hat{a}$ and the quadrature operators are non-zero,

$$\langle\alpha|\hat{a}|\alpha\rangle = \alpha,\ \langle\alpha|\hat{X}|\alpha\rangle = \frac{\mathrm{Re}(\alpha)}{\sqrt{2}},\ \langle\alpha|\hat{Y}|\alpha\rangle = \frac{\mathrm{Im}(\alpha)}{\sqrt{2}}. \tag{1.37}$$

Unlike the Fock states, the coherent states are non-orthogonal

$$\langle\alpha|\beta\rangle = \exp\left(\alpha^*\beta - \frac{1}{2}|\alpha|^2 - \frac{1}{2}|\beta|^2\right), \tag{1.38}$$

but they form a complete basis of states

$$\hat{I} = \int |\alpha\rangle\langle\alpha|\frac{d^2\alpha}{\pi} = \sum_{n=0}^{\infty} |n\rangle\langle n|. \tag{1.39}$$

We can see that the thermal state ρ_{th} of a mode (which is a mixed state of the radiation field) is written as an isotropic Gaussian mixture of the coherent states $|\alpha\rangle$

$$\rho_{\mathrm{th}} = \int \frac{e^{-|\alpha|^2/N_{\mathrm{th}}}}{\pi N_{\mathrm{th}}}|\alpha\rangle\langle\alpha|d^2\alpha, \tag{1.40}$$

where N_{th} is the mean number of photons in the thermal state ρ_{th}.

The next class of states that we consider are *squeezed states* $|\xi\rangle$ that can be generated by applying the unitary single-mode squeezing operator

$$\hat{S}(\xi) = \exp\left(\frac{1}{2}\xi\hat{a}^{\dagger 2} - \frac{1}{2}\xi^*\hat{a}^2\right),\ \xi = re^{i\phi}, \tag{1.41}$$

on the vacuum state, i.e $\hat{S}(\xi)|0\rangle = |\xi\rangle$. Here r is called the squeezing parameter. The mean number of photons in the squeezed state is $\langle \hat{a}^\dagger \hat{a}\rangle = \sinh^2 r$. In terms of the Fock states $|n\rangle$, the squeezed state can be written as

$$|\xi\rangle = \frac{1}{\sqrt{\cosh(r)}} \sum_{n=0}^{\infty} e^{in\phi} (\tanh r)^n \frac{\sqrt{(2n)!}}{(n!)^2 2^{2n}} |2n\rangle. \tag{1.42}$$

It shows that $|\xi\rangle$ has only even photon number states in the superposition. This is the case when a nonlinear crystal is pumped with a bright laser light—some of the pump photons having frequency 2ω are divided into pairs of photons each with frequency ω. The outgoing mode for a degenerate parametric amplifier consists of a superposition of even photon-number states.

In order to see the quadrature squeezing in such states, let us first define a more general quadrature operator (which is a linear combination of the quadrature operators $\hat{X}$ and $\hat{Y}$)

$$\hat{X}_\theta \equiv \frac{\hat{a}e^{-i\theta} + \hat{a}^\dagger e^{i\theta}}{\sqrt{2}}, \tag{1.43}$$

with the commutation relation $[\hat{X}_\theta, \hat{X}_{\theta+\pi/2}] = i$. For the single-mode squeezed state $|\xi\rangle$, one can show that

$$\left(\Delta X_{\phi/2}\right)^2 = \frac{1}{2}e^{2r}, \left(\Delta X_{\phi/2+\pi/2}\right)^2 = \frac{1}{2}e^{-2r}, \tag{1.44}$$

$$\Delta X_{\phi/2} \Delta X_{\phi/2+\pi/2} = \frac{1}{2}. \tag{1.45}$$

From the above, we see that the quadrature denoted by $\Delta X_{\phi/2}$ is stretched, while the other quadrature $\Delta X_{\phi/2+\pi/2}$ is squeezed at the same time.

The *squeezed coherent states* $|\xi, \alpha\rangle$ can be generated by applying the squeezing operator $\hat{S}(\xi)$ on the coherent state $|\alpha\rangle$:

$$|\xi, \alpha\rangle = \hat{S}(\xi)|\alpha\rangle = \hat{S}(\xi)\hat{D}(\alpha)|0\rangle. \tag{1.46}$$

Since the displacement $\hat{D}(\alpha)$ in phase space does not produce further squeezing, the squeezing properties of this state $|\xi, \alpha\rangle$ are the same as those for the single-mode squeezed vacuum state $|\xi\rangle$.

Finally, we consider the *two-mode squeezed vacuum state* $|\xi\rangle_{\text{TMSV}}$ that can be generated by applying the unitary two-mode squeezing operator

$$\hat{S}_2(\xi) = \exp\left(\xi \hat{a}^\dagger \hat{b}^\dagger - \xi^* \hat{a}\hat{b}\right), \tag{1.47}$$

on the two-mode vacuum state, i.e $\hat{S}_2(\xi)|0,0\rangle = |\xi\rangle_{\text{TMSV}}$, where $\hat{a}$ and $\hat{b}$ denote the annihilation operators corresponding to the two modes. The correlation between these two modes $\langle ab\rangle$ gives rise to the non-classical properties of the state $|\xi\rangle_{\text{TMSV}}$, such as squeezing.

The two-mode squeezed vacuum state $|\xi\rangle_{\text{TMSV}}$ can be written in terms of the Fock states $|n\rangle$ as

$$|\xi\rangle_{\text{TMSV}} = \frac{1}{\cosh r} \sum_{n=0}^{\infty} e^{in\phi} (\tanh r)^n |n_a, n_b\rangle, \tag{1.48}$$

showing that the photon pairs are created by the two-mode squeezing operation on the vacuum state.

1.2.4 Phase in quantum optics and its estimation

In quantum metrology, we seek to exploit the quantum mechanical properties of a state to improve the sensitivity and resolution in estimating a physical parameter. In particular, the physical parameter that is of the most significance in the context of quantum optical metrology is the optical phase. However, there exists no Hermitian operator in quantum mechanics that can represent such an optical phase, and consequently it calls for an estimation scheme in which the optical phase is the parameter to be estimated.

Let us consider a single mode of the radiation field **E** having an unknown phase. One can use the standard technique, known as the *balanced homodyne detection* to measure the phase difference, as shown in Figure 1.2. A local oscillator excited in a strong coherent state (such as a laser), say $\alpha e^{i\theta}$, is applied on the other input port of a 50-50 beam splitter. A phase difference is established between the two input modes since the phase of the local oscillator is known. The detectors placed in the output beams measure the difference in the intensities $I_1 - I_2$, from which the phase of the unknown signal can be measured.

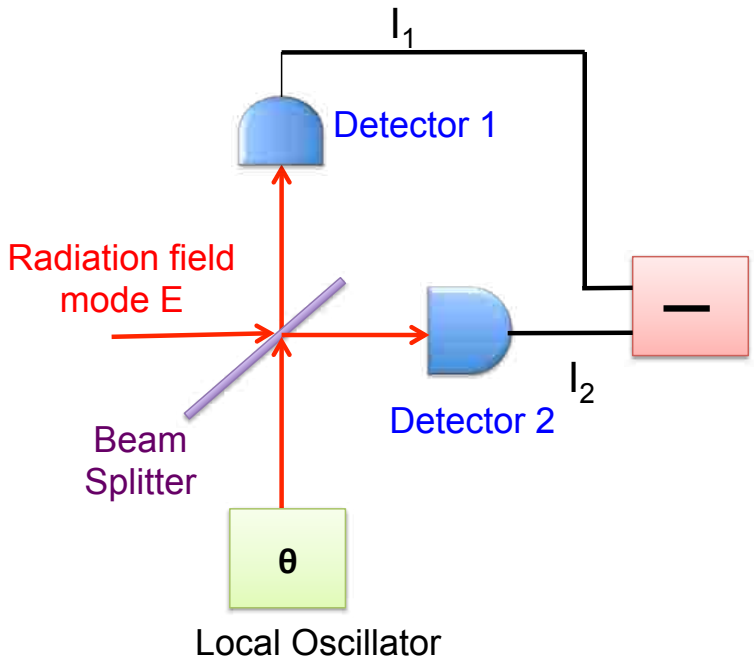

Figure 1.2: Balanced homodyne detection to measure unknown phase difference. **E** represents the electric field of the radiation field incident on the 50-50 beam-splitter, where it is mixed with a local oscillator in a strong coherent state with phase θ. The outputs are incident on two photodetectors, and the corresponding photocurrents give the difference of the intensities $I_1 - I_2$, revealing the phase of the unknown signal.

In the following, we discuss the optical interferometric setup, commonly known as the Mach-Zehnder interferometer, to detect the phase shift between *two modes* that can be treated as a quantum mechanical extension of homodyne detection.

A typical setup of a Mach-Zehnder interferometer (MZI) is shown schematically in Figure 1.3. In a MZI configuration, laser light in the port A is split by the first beam-splitter, then it is reflected from the two mirrors followed by accumulation of the phase difference ϕ, and finally is recombined at the second beam-splitter. If we denote the annihilation operators for the input and output pair of modes by $\hat{a}, \hat{b}$, and $\hat{a}', \hat{b}'$, respectively, the effective mode

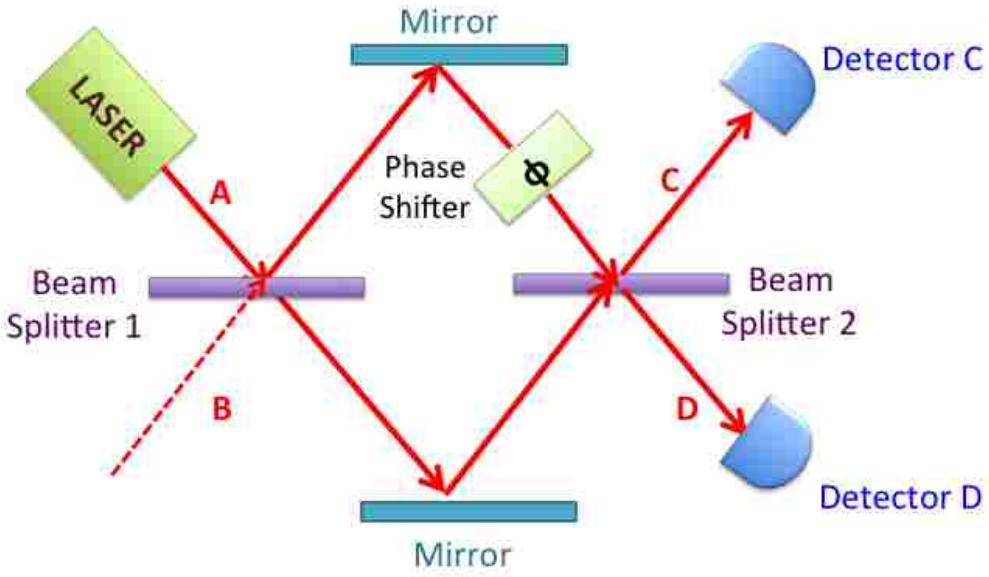

Figure 1.3: Schematic diagram of a Mach-Zehnder interferometer. Laser light in the port A is split by the first beam-splitter, then it is reflected from the two mirrors followed by accumulation of the phase difference ϕ due to the phase-shifter, and finally is recombined at the second beam-splitter, emerging in the ports C and D.

transformation relation between them can be written as

$$\begin{pmatrix} \hat{a}' \\ \hat{b}' \end{pmatrix} = \frac{1}{2}\begin{pmatrix} 1 & i \\ i & 1 \end{pmatrix}\begin{pmatrix} 1 & 0 \\ 0 & e^{-i\phi} \end{pmatrix}\begin{pmatrix} 1 & -i \\ i & 1 \end{pmatrix}\begin{pmatrix} \hat{a} \\ \hat{b} \end{pmatrix} = ie^{-i\phi/2}\begin{pmatrix} \sin(\phi/2) & \cos(\phi/2) \\ \cos(\phi/2) & -\sin(\phi/2) \end{pmatrix}\begin{pmatrix} \hat{a} \\ \hat{b} \end{pmatrix}. \quad (1.49)$$

In the above, ϕ is the relative phase shift between the two paths, which is also proportional to the optical path difference between the these two paths. In order to estimate this phase shift ϕ, we write the phase uncertainty $\Delta\phi$ as

$$(\Delta\phi)^2 = \langle\phi^2\rangle - \langle\phi\rangle^2. \quad (1.50)$$

This quantifies the precision with which ϕ can be estimated for a given interferometric detection scheme. Using the simple error-propagation formula, we can write

$$\Delta\phi = \frac{\Delta\hat{A}}{|\frac{\partial\langle\hat{A}\rangle}{\partial\phi}|}, \quad (1.51)$$

where $\hat{A}$ represents an observable (Hermitian operator) for the detection scheme used at the output of the interferometer.

When a coherent state is used in one port in conjunction with the vacuum at the other, the above relation in Equation (1.51) gives the phase estimate $\Delta\phi$ that scales as $1/\sqrt{\bar{n}}$, where $\bar{n}$ is the average number of photons in the coherent state. Furthermore, regardless of the state used in the first port, the phase uncertainty $\Delta\phi$ is lower bounded by $1/\sqrt{\bar{n}}$ as long as the vacuum state is fed into the second port of the interferometer. This bound given by $1/\sqrt{\bar{n}}$ is known as the *shot-noise limit* (SNL), and is a manifestation of vacuum fluctuations. Note that this agrees with the number-phase uncertainty relation $\Delta n\Delta\phi \geq 1$ since $\Delta n = \sqrt{\bar{n}}$ for the coherent state.

Any state for which it is possible to attain a phase-sensitivity lower than the SNL is said to achieve super-sensitivity. Numerous proposals exist in the literature for reducing the phase uncertainty below the SNL by using quantum states of light, and approaching $1/\bar{n}$ is known as the Heisenberg limit (HL) of phase-sensitivity. The first among those is due to Caves [1], where he showed that using coherent light and squeezed vacuum states at the two input ports of the MZI can give rise to Heisenberg-limited phase sensitivity.

1.2.5 Phase estimation and the Cramér-Rao bound

Here we briefly review the essential ingredients of estimation theory. We first present the Fisher information approach from classical estimation theory and then show how it generalizes in the quantum estimation of the optical phase, providing a lower bound on the phase sensitivity $\Delta\phi$, known as the Cramér-Rao bound.

In classical estimation theory, one aims to construct an estimate for a set of unknown parameters $\{\phi_1, \phi_2, \ldots, \phi_n\}$ that gives the most accurate estimate of the set of parameters based on a given data set of the measurement outcomes. Here we consider the the ultimate limit in estimating a *single* parameter ϕ by using the classical Fisher information for a given measurement X. Each measurement provides an outcome x which depends on the value of ϕ.

The performance of a given estimator of ϕ can be quantified by the error estimate $\Delta\phi \equiv \sqrt{\langle(\phi_{\text{est}} - \phi_{\text{real}})^2\rangle}$. Here $\langle \ldots \rangle$ denotes the average over all possible experimental results, while ϕ_{est} and ϕ_{real} are the estimated and the real value of the unknown parameter ϕ, respectively. For ν repetitions of the given measurement, this error estimate $\Delta\phi$ is bounded by the classical Cramér-Rao bound [2]

$$\Delta\phi \geq \frac{1}{\sqrt{\nu F(\phi)}}, \tag{1.52}$$

where $F(\phi)$ is the classical Fisher information, given by

$$F(\phi) = \sum_x p(x|\phi) \left\{ \frac{dp(x|\phi)}{d\phi} \right\}. \tag{1.53}$$

Here the probability distribution $p(x|\phi)$ corresponds to the probability of getting the experimental result x for estimating the parameter ϕ. This relation applies to both classical and quantum physics whenever the estimator is unbiased, i.e. $\langle\phi_{\text{est}}\rangle = \phi_{\text{real}}$ and the probability distribution $p(x|\phi)$ is fixed.

In quantum mechanics, we can model the experiment using the POVM operators Π_x, where Π_x is associated to a measurement outcome x. For a quantum state denoted by the density matrix $\rho(\phi)$ that carries the encoded information about the unknown parameter ϕ, we can write

$$p(x|\phi) = \text{Tr}\left[\rho(\phi)\Pi_x\right]. \tag{1.54}$$

Maximizing over all possible measurement strategies, we can arrive at the quantum Fisher information $F_Q\left(\rho(\phi)\right)$ (which depends only on the probe state $\rho(\phi)$), leading to the following lower bound on the estimation of ϕ, known as the quantum Cramér-Rao bound

$$\Delta\phi \geq \frac{1}{\sqrt{\nu F_Q\left(\rho(\phi)\right)}}. \tag{1.55}$$

For a closed system, prepared in a pure state $\rho = |\psi\rangle\langle\psi|$, which evolves under a unitary transformation $\hat{U}_\phi$, the quantum Fisher information is given by [3]

$$F_Q\left(\rho'(\phi)\right) = 4\langle\Delta\hat{H}^2\rangle, \tag{1.56}$$

where $\rho'(\phi) = \hat{U}_\phi\rho\hat{U}_\phi^\dagger$, $\hat{H}(\phi) = i\left(\frac{d\hat{U}_\phi^\dagger}{d\phi}\right)\hat{U}_\phi$, and $\langle\Delta\hat{H}\rangle^2 = \Big[\langle\psi|\hat{H}^2(\phi)|\psi\rangle - \langle\psi|\hat{H}(\phi)|\psi\rangle^2\Big]$. For instance, when we use the coherent state as the probe state, the quantum Fisher information can be evaluated to be $F_Q = 4\langle(\Delta\hat{n})^2\rangle$ associated with the unitary evolution operator $U_\phi = e^{i\hat{n}\phi}$ ($\hat{n}$ is the photon number operator). Since for the coherent state $\Delta n = \sqrt{\bar{n}}$, this leads us to the SNL where the phase sensitivity $\Delta\phi$ scales as $1/\sqrt{\bar{n}}$. By using quantum states of light, it is possible to increase the precision of the phase estimation—for example, maximizing this variance corresponds to the case of the N00N state [4] where the variance is increased to $\langle(\Delta\hat{n})^2\rangle = \frac{N^2}{4}$, leading to the HL of the phase sensitivity, i.e. the phase sensitivity $\Delta\phi$ scaling as $1/N$ where N is the mean input photon number of the N00N state.

1.3 Brief review of quantum information theory

In quantum information theory, we study the ultimate limits on reliable communication that are allowed by the laws of quantum mechanics, and also seek to determine the ways by which these limits can be achieved in realistic systems. The mathematical foundations of quantum information theory were laid out in the ground-breaking 1948 paper of Claude Shannon that introduced the idea of channel capacity, the maximum mutual information between a channel's input and output, as the highest rate at which error-free reliable communication is possible for a given channel. This idea is captured in his famous noisy channel coding theorem [5]. Holevo, Schumacher, and Westmoreland provided a generalization of the Shannon's classical channel coding theorem to the quantum setting [6, 7], establishing an *achievable* rate at which a sender can transmit classical data to a receiver over a noisy quantum channel using the channel a large number of times.

It is worthwhile to note that quantum information science is an overwhelmingly rich and broad subject by its own virtue, encompassing fields as diverse as quantum computation, quantum complexity, quantum algorithms, entanglement theory, quantum key distribution, and so on. However, in the following we present a very brief review of the topics in quantum information theory that will be extensively used in our study in Chapter 5. For a detailed review on the subject, the interested readers are referred to Reference [8].

1.3.1 Quantum entropy and information

For quantifying the amount of information and correlations in quantum systems, we define the von Neumann entropy $H(\rho)$ of a quantum state ρ

$$H(\rho) = -\mathrm{Tr}(\rho\log\rho). \tag{1.57}$$

This entropy is also known as the quantum entropy, and gives a measure of how mixed the quantum state is. The base of the logarithm is taken to be 2. We can also express the von Neumann entropy in terms of the eigenvalues λ_i of the density operator ρ as

$$H(\rho) = -\sum_i \lambda_i\log\lambda_i. \tag{1.58}$$

Note that for a pure state, the von Neumann entropy is zero, while for a maximally mixed state it is given by $\log D$ where D is the dimension of the system.

For a bipartite system AB in a joint state ρ^{AB}, the joint quantum entropy is defined as

$$H(AB) = -\mathrm{Tr}(\rho^{AB} \log \rho^{AB}). \tag{1.59}$$

The joint entropy of the bipartite system is subadditive, i.e.

$$H(AB) \leq H(A) + H(B),$$

where the equality holds when ρ^{AB} is a tensor-product state ($\rho^{AB} = \rho^A \otimes \rho^B$).

The conditional quantum entropy $H(A|B)$ of the bipartite state ρ^{AB} is defined as

$$H(A|B) = H(AB) - H(B), \tag{1.60}$$

i.e., the difference between the joint entropy and the marginal entropy.

1.3.2 Quantum mutual information

Quantum mutual information is a measure of correlations between two systems A and B. The quantum mutual information $I(A;B)$ of a bipartite state ρ^{AB} is defined as

$$I(A;B) = H(A) + H(B) - H(AB). \tag{1.61}$$

The quantum mutual information can also be written alternatively in terms of the conditional quantum entropies

$$I(A;B) = H(A) - H(A|B) = H(B) - H(B|A). \tag{1.62}$$

1.3.3 Holevo bound

In quantum information theory, the Holevo bound serves as an upper bound on the accessible information. Suppose that a sender (Alice) prepares an ensemble $\xi = \{p_X(x), \rho_x\}$ before handing it over to a receiver (Bob). In order to determine which value of X Alice chose, Bob performs a measurement on his system B which are described by the POVM elements $\{\Lambda_y\}$. The accessible information in this case is the information that Bob can access about the random variable X, and is defined as

$$I_{\mathrm{acc}}(\xi) = \max_{\Lambda_y} I(X;Y), \tag{1.63}$$

where Y is a random variable representing the outcome of the measurements that Bob performs.

The Holevo bound can then be written as

$$I(X;Y) \leq H\left(\sum_x p_X \rho_x\right) - \sum_x p_X H\left(\rho_x\right), \tag{1.64}$$

where the quantity on the right hand side $\chi(\xi) = H\left(\sum_x p_X \rho_x\right) - \sum_x p_X H\left(\rho_x\right)$ is also known as the Holevo χ quantity or the Holevo information of the ensemble of the states $\xi = \{p_X(x), \rho_x\}$. The implication of the Holevo bound is that this upper bound can be achieved asymptotically by employing a joint (collective) quantum measurement on Bob's side. This gives the maximum information that Bob can gain about ξ by such joint quantum measurements.

1.3.4 Capacity of classical communication: HSW theorem

The notion of the Holevo bound introduced above leads us to determining the achievable rates of communication for a noisy quantum channel. Holevo, Schumacher, and Westmoreland (HSW) characterized the classical capacity of a quantum channel $\mathcal{N}$ in terms of the Holevo information [6, 7]

$$\chi(\mathcal{N}) \equiv \max_{\{p_X(x),\rho_x\}} I(X;B)_\rho, \tag{1.65}$$

and showed that this Holevo information serves as an achievable rate for communicating classical data over the quantum channel $\mathcal{N}$. Here, $\{p_X(x), \rho_x\}$ represents an ensemble of quantum states, and the quantum mutual information $I(X;B)_\rho \equiv H(X)_\rho + H(B)_\rho - H(XB)_\rho$, is defined with respect to a classical-quantum state $\rho_{XB} \equiv \sum_x p_X(x) |x\rangle\langle x|_X \otimes \mathcal{N}(\rho_x)_B$. The above formula given by HSW for certain quantum channels is additive whenever

$$\chi(\mathcal{N}^{\otimes n}) = n\chi(\mathcal{N}). \tag{1.66}$$

For such quantum channels, the HSW formula is indeed equal to the classical capacity of those channels. However, a regularization is necessary for the quantum channels for which the HSW formula cannot be shown to be additive. The classical capacity in general is then characterized by the following regularized formula:

$$\chi_{\text{reg}}(\mathcal{N}) \equiv \lim_{n\to\infty} \frac{1}{n}\chi(\mathcal{N}^{\otimes n}). \tag{1.67}$$

1.4 Distance measures in quantum information

Noisy quantum channels affect the input states, resulting in an output state which is different from the input. It is, therefore, necessary to characterize how close two quantum states are by using some distance measures. In this section, we review two such distance measures—the *trace distance* and the *fidelity*. These distance measures are important in quantum information theory because they help us to compare the performance of different quantum protocols. We conclude this chapter with a brief discussion on the gentle measurement lemma, that concerns the disturbance of the quantum states upon measurement. This helps us to characterize the distance between the original state and the post-measurement state.

1.4.1 Trace distance

The trace norm $\|A\|_1$ of an Hermitian operator A is defined as

$$\|A\|_1 = \text{Tr}\left\{\sqrt{A^\dagger A}\right\}. \tag{1.68}$$

The trace distance between two operators A and B is given by

$$\|A - B\|_1 = \text{Tr}\left\{\sqrt{(A-B)^\dagger (A-B)}\right\}. \tag{1.69}$$

In particular, when we consider any two operators ρ and σ, the trace distance between them is bounded by

$$0 \leq \|\rho - \sigma\|_1 \leq 2. \tag{1.70}$$

The above trace distance is invariant under unitary operations, i.e.

$$\|\rho - \sigma\|_1 = \|U\rho U^\dagger - U\sigma U^\dagger\|_1. \tag{1.71}$$

The trace distance between two quantum states ρ and σ is equal to twice the largest probability difference that these two states could yield the same measurement outcome Π [8], i.e.,

$$\|\rho - \sigma\|_1 = 2 \max_{0 \leq \Pi \leq I} \mathrm{Tr}\left\{\Pi(\rho - \sigma)\right\}, \tag{1.72}$$

where the maximization is done over all positive operators Π with eigenvalues between 0 and 1.

As an example, we can use the trace distance between two quantum states to obtain the minimum probability of error to distinguish between two quantum states (say ρ_0 and ρ_1) in the setting of the quantum binary hypothesis testing.

Suppose that Alice prepares, with equal probability 1/2, either ρ_0 or ρ_1, and Bob wants to distinguish between them. In order to do so, he performs a binary POVM with elements $\{\Pi_0, \Pi_1\}$. Let us say the decision rule is: Bob declares the state to be ρ_0 if he receives "0" as a measurement outcome or otherwise (for the "1" outcome) declares it to be ρ_1. The probability of error in distinguishing these two states can then be written as (using the relation in Equation (1.72))

$$p_e = \frac{1}{2}\left(\mathrm{Tr}\{\Pi_0\rho_1\} + (\mathrm{Tr}\{\Pi_1\rho_0\}\right) = \frac{1}{2}\left(1 - \mathrm{Tr}\{\Pi_0(\rho_0 - \rho_1)\}\right). \tag{1.73}$$

Another important relation that we will use quite often is the one that concerns the measurement on two approximately close states [8]: For two quantum states ρ and σ and a positive operator Π ($0 \leq \Pi \leq I$), we can write

$$\mathrm{Tr}\{\Pi\rho\} \geq \mathrm{Tr}\{\Pi\sigma\} - \frac{1}{2}\|\rho - \sigma\|_1. \tag{1.74}$$

Consider two quantum states, for example, ρ and σ that are ε-close in trace distance to each other (ε is a very small positive number), i.e. $\|\rho - \sigma\|_1 \leq \varepsilon$. Suppose that the probability of successful decoding of the state ρ with the measurement operator Π is very high so that

$$\mathrm{Tr}\left\{\Pi\rho\right\} \geq 1 - \varepsilon, \tag{1.75}$$

then for the state σ, we have [using Equation (1.74)]

$$\mathrm{Tr}\left\{\Pi\sigma\right\} \geq 1 - 2\varepsilon \tag{1.76}$$

which states that the same measurement also succeeds with high probability for the state σ.

1.4.2 Fidelity

Here we introduce the fidelity as an alternative measure of how close two quantum states are to each other. The fidelity between an input state $|\psi\rangle$ and an output state $|\phi\rangle$ when both of them are pure states is given by

$$F\left(|\psi\rangle, |\phi\rangle\right) = |\langle\psi|\phi\rangle|^2. \tag{1.77}$$

This fidelity is equal to one if the states overlap with each other, while it is equal to zero when the states are orthogonal to each other.

However, a noisy quantum communication protocol could map a pure input state $|\psi\rangle$ to a mixed state ρ. In such case, we define the expected fidelity between these two states in the following way. The expected fidelity between a pure input state ψ and mixed output state ρ is given by

$$F\left(|\psi\rangle, \rho\right) = \langle\psi|\rho|\psi\rangle. \tag{1.78}$$

In the most general case, both the above states could be mixed. We can incorporate the idea of purification (with respect to a reference system R) to define the fidelity between the two mixed states ρ_A and σ_A for a common quantum system A. This fidelity is known as the Uhlmann fidelity [8].

Suppose we want to determine the fidelity between the two mixed states ρ_A and σ_A of the quantum system a. Consider the purifications of these two states as $|\phi_\rho\rangle^{RA}$ and $|\phi_\sigma\rangle^{RA}$ with respect to the reference system R. The Uhlmann fidelity between the two mixed states is then defined as

$$F(\rho, \sigma) = \max_{|\phi_\rho\rangle^{RA}, |\phi_\sigma\rangle^{RA}} |\langle\phi_\rho|\phi_\sigma\rangle|^2, \tag{1.79}$$

where the maximization is over all purifications $|\phi_\rho\rangle^{RA}$ and $|\phi_\sigma\rangle^{RA}$.

For two quantum states ρ and σ, the relation between the trace distance and fidelity for two quantum states can be expressed as

$$1 - \sqrt{F(\rho, \sigma)} \leq \frac{1}{2}\|\rho - \sigma\|_1 \leq \sqrt{1 - F(\rho, \sigma)}. \tag{1.80}$$

As an example of the relation in Equation (1.80), we can establish a useful relation between the trace distance and the fidelity for two very close states ρ and σ. Suppose for a very small positive constant ε we have

$$F(\rho, \sigma) \geq 1 - \varepsilon, \tag{1.81}$$

then it follows that

$$\|\rho - \sigma\|_1 \leq 2\sqrt{\varepsilon}, \tag{1.82}$$

i.e., these two states are $2\sqrt{\varepsilon}$-close in trace distance to each other.

1.4.3 Gentle measurement

The notion of gentle measurement that we describe below is associated with the disturbance of the quantum states when some quantum measurement is performed on them. This follows by applying the relation Equation 1.80 considering a measurement operator Λ (or an element of a POVM) on a quantum state ρ. In the following lemma describing the "gentle" effect of the quantum measurement on the quantum state we follow the notations and definitions used in Reference [8].

Lemma 1 *If the measurement operator Λ detects the quantum state ρ with a very high probability, i.e. for a very small positive constant ε*

$$\mathrm{Tr}\left\{\Lambda\rho\right\} \geq 1 - \varepsilon, \tag{1.83}$$

then the "gently" perturbed post-measurement state is given by

$$\rho' = \frac{\sqrt{\Lambda}\rho\sqrt{\Lambda}}{\mathrm{Tr}\{\Lambda\rho\}}, \tag{1.84}$$

which is $2\sqrt{\varepsilon}$-close in trace distance to ρ, i.e.,

$$\|\rho - \rho'\|_1 \leq 2\sqrt{\varepsilon}. \tag{1.85}$$

Finally, we specify a variation of the above lemma that we will explicitly use in our work.

Lemma 2 *If the measurement operator Λ detects the quantum state ρ with a very high probability, i.e.,*

$$\mathrm{Tr}\left\{\Lambda\rho\right\} \geq 1 - \varepsilon, \tag{1.86}$$

then $\sqrt{\Lambda}\rho\sqrt{\Lambda}$ is $2\sqrt{\varepsilon}$-close in trace distance to ρ, i.e.,

$$\|\rho - \sqrt{\Lambda}\rho\sqrt{\Lambda}\|_1 \leq 2\sqrt{\varepsilon}. \tag{1.87}$$

Chapter 2
Effects of phase fluctuation noise in quantum metrology [1]

In this chapter, we discuss the effects of phase fluctuations on the quantum metrological properties of the two-mode path-entangled photon-number states and compare their performances in an optical interferometric setup in the presence of such noise. In particular, we consider the maximally path-entangled state, known as the N00N state, along with a more generalized version of it, called the mm' state in the context of quantum phase estimation. NOON states of light have been shown to achieve Heisenberg limited supersensitivity as well as super resolution in quantum metrology [9, 10] but they are extremely susceptible to photon loss [11, 12, 13, 14, 15]. In order to combat this disadvantage of the N00N states under photon loss, Huver *et al.* proposed mm' states, and showed that such states provide more robust metrological performance than N00N states in the presence of photon loss [14].

In real life applications such as a quantum sensor or radar, phase fluctuations due to different noise sources can further aggravate the phase sensitivity by adding significant noise to the phase ϕ to be estimated. For instance, when one considers the propagation of entangled states over distances of kilometers, through, say, the atmosphere, then atmospheric turbulence becomes an issue as it can cause uncontrollable noise or fluctuation in the phase. In this sense, phase fluctuation can render the quantum metrological advantage for achieving super-sensitivity and super-resolution totally useless. This has motivated us to investigate the impacts of such random phase fluctuations on the metrological properties (such as the phase sensitivity and the visibility) of quantum mechanically entangled states.

Considering the path-entangled photon Fock states, viz. N00N and mm' states in the presence of such phase noise, we study the parity detection [16] for the interferometry to calculate the phase-fluctuated sensitivity. This detection scheme has been shown to reach Heisenberg limited sensitivity when combined with the N00N state in the absence of photon loss [16, 17, 18, 19]. Here we calculate the minimum detectable phase shift in the presence of phase fluctuation, and show that the lower bound of the phase-fluctuated sensitivity for both the states saturates the quantum Cramér-Rao bound [20, 21], which gives the ultimate limit to the precision of phase measurement. This shows that the parity detection serves as an optimal detection strategy when the above states are subject to phase fluctuations.

Here, we first introduce in Section 2.1 the N00N and mm' states, i.e., the class of path-entangled two-mode photon Fock states that we will study for investigating the effects of the phase noise on the metrological properties of these states. In Section 2.2, we describe how the density matrices corresponding to these states evolve under phase fluctuations in a typical optical interferometric configuration. Section 2.2 contains the discussion of the parity detection scheme that is used in our work to evaluate the phase sensitivity and visibility.

[1] This chapter previously appeared as B. Roy Bardhan, K. Jiang, and J. P. Dowling, Physical Review A **88**, 023857 (2013) (Copyright(2013) American Physical Society) [22]. It is reprinted by permission of the American Physical Society. See Appendix C for details.

In order to provide the tightest bound on the uncertainty of the phase, we provide explicit calculation of the quantum Fisher information that in turn gives the quantum Cramér-Rao bound, the lowest bound on phase sensitivity that can be attained with these states. Finally, we conclude this chapter with a brief summary of the main results obtained from the work presented here. For the sake of completeness, we provide in Appendix A calculations of phase sensitivity and visibility in the presence of both photon loss and phase fluctuation for the states considered above.

2.1 Path entangled photon Fock states—N00N and mm' states

Quantum states of light have long been known to attain greater precision, resolution and sensitivity in metrology, image production, and object ranging [4, 23, 24] than their classical counterparts. The maximally path-entangled N00N state is one of the most prominent examples of such non-classical states [9, 25, 26], which is a superposition of all N photons in one path of a Mach-Zehnder interferometer (MZI) with none in the other, and vice versa. This state is entangled between the two paths, and has been shown to violate the Bell inequality for non-classical correlations [27]. The N00N state can be written as

$$|N :: 0\rangle_{a,b} = \frac{1}{\sqrt{2}}(|N, 0\rangle_{a,b} + |0, N\rangle_{a,b}), \tag{2.1}$$

where a and b represent the two paths of the interferometer. This state is in the class of Schrödinger-cat states [26], and a measurement of the photon number in either of the paths results in random collapse of all the N photons into one or the other path.

N00N states are known to achieve Heisenberg limited super-sensitivity as well as super-resolution in quantum metrology [9, 10]. In recent years, several schemes for reliable production of such states have been proposed, making them useful in super-precision measurements in optical interferometry, atomic spectroscopy, gravitational wave detection, and magnetometry along with potential applications in rapidly evolving fields such as quantum imaging and sensing [28, 29, 30, 31, 32, 33, 34].

The superiority of the N00N state in phase sensitivity and resolution, compared to a coherent state $|\alpha\rangle$, can be attributed to the fact that the number state evolves N-times faster in phase than the coherent state. This in turn results in the sub-Rayleigh-diffraction-limited resolution (super-resolution) as well as the sub-shot-noise-limited phase sensitivity (super-sensitivity) achieved with the N00N state [4].

However, the N00N states are vulnerable to photon loss which is present in almost all realistic interferometric configurations. For instance, the N00N state is transformed, when a single photon is lost from the system, to the state $|N-1, 0\rangle\langle N-1, 0| + |0, N-1\rangle\langle 0, N-1|$ which is unusable for estimation of the phase ϕ. In order to overcome such disadvantage of the N00N state in the presence of photon loss, the authors in Reference [14] proposed a class of the generalized path-entangled Fock states, by introducing decoy photons to both paths of the interferometer. These states are known as the mm' states and have been shown to be more robust against photon loss than N00N states. The mm' states can be written as

$$|m :: m'\rangle_{a,b} = \frac{1}{\sqrt{2}}(|m, m'\rangle_{a,b} + |m', m\rangle_{a,b}), \tag{2.2}$$

where m and m' are the number of input photons injected into the two modes of the interferometer.

For this class of path-entangled Fock states, Jiang *et al.* provided strategies for choosing the optimal m and m' for a given photon loss [15]. The mm' states can be produced, for example, by post-selecting on the output of a pair of optical parametric oscillators [35]. Note that the mm' state reduces to a N00N state when $m = N$ and $m' = 0$.

In the following sections, we study the behavior of the phase sensitivity and the visibility of the mm' and the N00N states under phase fluctuations.

2.2 Dynamical evolution of the mm' and N00N states under phase fluctuations

We start with the propagation of mm' and N00N states through a MZI (schematically shown in Figure 2.1) in the presence of the phase fluctuations $\Delta\phi$, where the photon number difference ($\Delta m = m - m'$) between the two arms in the initial state is fixed.

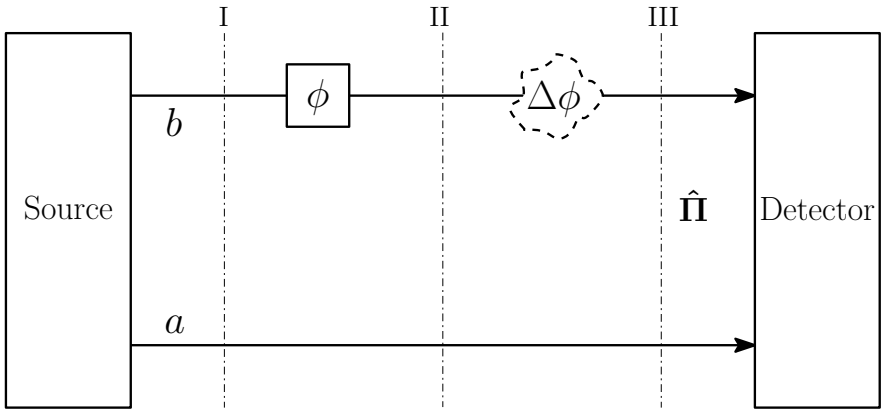

Figure 2.1: Schematic diagram of a two-mode optical interferometer. Here a and b denote the two modes for the mm' and N00N states as the input. The source and the detector are represented by the respective boxes. Effects of the phase fluctuations due to the phase noise is represented by $\Delta\phi$ in the upper path b of the interferometer. The upper beam passes through a phase-shifter ϕ, and the phase acquired depends on the total number of photons $\Delta m = m - m'$ (or N) passing throughout the upper path. Parity detection is used as the detection scheme at either of the two output ports of the interferometer.

The presence of the phase shifter in the upper path b introduces a phase shift ϕ to the photons traveling through it, so that the state at stage II becomes

$$\begin{aligned} |\psi\rangle_{\rm II} =& \frac{1}{\sqrt{2}}(e^{im'\phi}|m, m'\rangle + e^{im\phi}|m', m\rangle) \\ =& \alpha|m, m'\rangle + \beta|m', m\rangle, \end{aligned} \tag{2.3}$$

where $\alpha = e^{im'\phi}/\sqrt{2}$ and $\beta = e^{im\phi}/\sqrt{2}$. Because of the different number of photons being phase-shifted on the upper path b, phase shifts accumulated are different along the two paths, thus providing the possibility of interference upon detection.

The combined effects of random phase fluctuations are represented by $\Delta\phi$ in the upper path in Figure 2.1, and the mm' state at stage III is then given by,

$$|\psi(\Delta\phi)\rangle_{\rm III} = \alpha e^{im'\Delta\phi}|m, m'\rangle + \beta e^{im\Delta\phi}|m', m\rangle. \tag{2.4}$$

Notice that because of the random nature of the phase fluctuations, the state of the system becomes a mixed state and the associated density matrix is then

$$\rho_{mm'} = \langle |\psi(\Delta\phi)\rangle_{\text{III}}\ {}_{\text{III}}\langle\psi(\Delta\phi)|\rangle. \tag{2.5}$$

Random fluctuations $\Delta\phi$ in the phase effectively cause the system to undergo pure dephasing. As a result, the off-diagonal terms in the density matrix will acquire decay terms, while the diagonal terms representing the population will remain intact, *i.e.* the photon number will be preserved along the path [36].

We can expand the exponential in Equation (2.3) in a series expansion, and consider the terms up to the second order in $\Delta\phi$. We assume the random phase fluctuation $\Delta\phi$ to have Gaussian statistics described by Wiener process, *i.e.* with zero mean and non-zero variance $\langle\Delta\phi^2\rangle = 2\Gamma L$ (L is the length of the dephasing region, and Γ is the dephasing rate). Ensemble averaging over all realizations of the random process then gives,

$$\begin{aligned}\langle e^{i\Delta m\Delta\phi}\rangle &= 1 + i\Delta m\langle\Delta\phi\rangle - (\Delta m)^2\langle\Delta\phi^2\rangle/2 \\ &= 1 - (\Delta m)^2\Gamma L \approx e^{-(\Delta m)^2\Gamma L}.\end{aligned}$$

The density matrix for the mm' state is approximated by

$$\begin{aligned}\rho_{mm'} = \ & |\alpha|^2|m,m'\rangle\langle m,m'| + |\beta|^2|m',m\rangle\langle m',m| \\ & + \alpha^*\beta e^{-(\Delta m)^2\Gamma L}|m,m'\rangle\langle m',m| \\ & + \alpha\beta^* e^{-(\Delta m)^2\Gamma L}|m',m\rangle\langle m,m'|.\end{aligned} \tag{2.6}$$

A similar equation for the N00N state can be obtained from Equation (2.1) as

$$\begin{aligned}\rho_{\text{N00N}} = & |\alpha|^2|N,0\rangle\langle N,0| + |\beta|^2|0,N\rangle\langle 0,N| \\ & + \alpha^*\beta e^{-N^2\Gamma L}|N,0\rangle\langle 0,N| + \ \alpha\beta^* e^{-N^2\Gamma L}|0,N\rangle\langle N,0|.\end{aligned} \tag{2.7}$$

2.3 Parity operator

Achieving super-resolution and super-sensitivity depends not only on the state preparation, but also on the optimal detection schemes with specific properties. Here, we study parity detection, which was originally proposed by Bollinger *et al.* in the context of trapped ions [37] and it was later adopted for optical interferometry by Gerry [16]. The original parity operator can be expressed as $\hat{\pi} = \exp(i\pi\hat{n})$, which distinguishes states with even and odd number of photons without having to know the full photon number counting statistics. Usually the parity detection is only applied to one of two output modes of the Mach-Zehnder interferometer. In our case, the parity operator inside the interferometer, following the Reference [38], can be written as

$$\hat{\Pi} = i^{(m+m')}\sum_{k=0}^{m}(-1)^k|k,n-k\rangle\langle n-k,k|, \tag{2.8}$$

where $\hat{\Pi}^2 = 1$ and $n = m + m'$, is the total number of photons. It should be noticed that the parity operator inside the interferometer detects both modes a and b of the field.

The expectation value of the parity for the mm' state is then calculated as

$$\begin{aligned}\langle\hat{\Pi}\rangle_{mm'} &= \mathrm{Tr}\left[\hat{\Pi}\rho_{mm'}\right] \\ &= (-1)^{(m+m')}e^{-(\Delta m)^2\Gamma L}\cos[\Delta m(\phi-\pi/2)],\end{aligned} \tag{2.9}$$

where the density matrix $\rho_{mm'}$ is given by Equation (2.6). If we put a half-wave plate in front of the phase shifter, which amounts to replace ϕ by $\phi+\pi/2$, the expectation value becomes,

$$\langle\hat{\Pi}\rangle_{mm'} =(-1)^{(m+m')}e^{-(\Delta m)^2\Gamma L}\cos[\Delta m\phi]. \tag{2.10}$$

Using the density matrix ρ_{N00N} in Equation (2.7) for the N00N state, we can also obtain the expectation value of the parity operator for the N00N state as

$$\begin{aligned}\langle\hat{\Pi}\rangle_{\mathrm{N00N}} &= \mathrm{Tr}\left[\hat{\Pi}\rho_{\mathrm{N00N}}\right] \\ &= (-1)^N e^{-N^2\Gamma L}\cos[N\phi].\end{aligned} \tag{2.11}$$

2.3.1 Phase sensitivity

In quantum optical metrology, the precision of the phase measurement is given by its phase sensitivity. We now calculate the phase sensitivity for both the mm' and N00N states using the expectation values of the parity operator obtained above.

Phase sensitivity using the parity detection is defined by the linear error propagation method [39]

$$\delta\phi = \frac{\Delta\hat{\Pi}}{|\partial\langle\hat{\Pi}\rangle/\partial\phi|}, \tag{2.12}$$

where $\Delta\hat{\Pi} = \sqrt{\langle\hat{\Pi}^2\rangle - \langle\hat{\Pi}\rangle^2}$. Given $\langle\hat{\Pi}^2_{mm'}\rangle = 1$, the phase sensitivity with the parity detection for the mm' state is

$$\delta\phi_{mm'} = \sqrt{\frac{1-e^{-2(\Delta m)^2\Gamma L}\cos^2(\Delta m\phi)}{(\Delta m)^2 e^{-2(\Delta m)^2\Gamma L}\sin^2(\Delta m\phi)}}. \tag{2.13}$$

For the N00N state, the phase sensitivity with the parity detection is similarly obtained as

$$\delta\phi_{\mathrm{N00N}} = \sqrt{\frac{1-e^{-2N^2\Gamma L}\cos^2 N\phi}{N^2 e^{-2N^2\Gamma L}\sin^2 N\phi}}. \tag{2.14}$$

We note that in the limit of no dephasing ($\Gamma\to 0$), $\delta\phi_{mm'}\to 1/(\Delta m)$. For the N00N state, $\Gamma\to 0$ case leads to $\delta\phi_{\mathrm{N00N}}\to 1/N$ (Heisenberg limit of the phase sensitivity for the NOON state).

In Figure 2.2, we plot the phase sensitivities $\delta\phi_{mm'}$ and $\delta\phi_{\mathrm{N00N}}$ for the various dephasing rates Γ choosing $\Delta m = N$, so that the amount of phase information is the same for either state. For $\Delta m = N$, Equations (2.13) and (2.14) show that the mm' and N00N states give rise to the same phase sensitivity. In particular, we show the phase sensitivity for the states $|4::0\rangle$ and $|5::1\rangle$, and find that both the states perform equally well in presence of phase

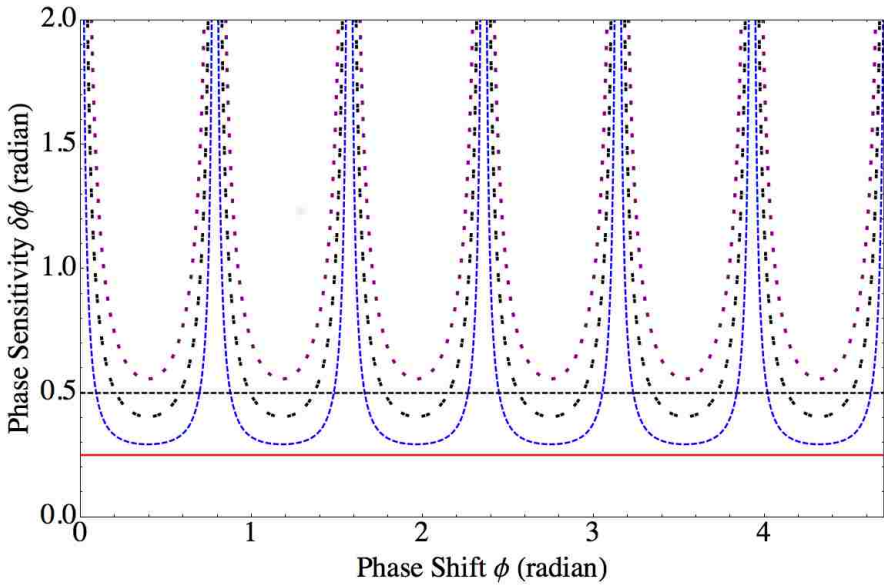

Figure 2.2: Phase sensitivity $\delta\phi$ of the mm' and the N00N states with phase fluctuation. We show the phase sensitivity $\delta\phi$ of the mm' state $|5::1\rangle$), or the N00N state $|4::0\rangle$, having the same phase information, as a function of phase shift ϕ for different values of Γ: $\Gamma = 0.1$ (curved blue dashed line), $\Gamma = 0.3$ (curved black double-dotted line), $\Gamma = 0.5$ (curved purple dotted line). The Heisenberg limit $(1/N)$ and the shot noise limit $(1/\sqrt{N})$ of the phase sensitivity for the N00N state are shown by the red solid line and the black dashed line, respectively, for comparison.

fluctuations when parity detection is used, although the former has been shown to outperform N00N states in presence of photon loss [14, 15].

The minimum phase sensitivities $\delta\phi_{\rm min}$ can be obtained from Equations (2.13) and (2.14) for $\phi = \pi/(2\Delta m)$, or $\phi = \pi/(2N)$ for the mm' or N00N states, respectively. Also, note that the HL for a general mm' state is $1/(m + m')$ in terms of the total number of photons available, and is equal to $1/N$ for the N00N state. The SNL for these two states is given by $1/(\sqrt{m + m'})$ and $1/\sqrt{N}$, respectively. For the $|4::0\rangle$ and $|5::1\rangle$ states, we plot the minimum phase sensitivity $\delta\phi_{\rm min}$ in Figure 2.3 as a function of Γ, and compare with the SNL and HL for both the states. We see that the minimum phase sensitivity $\delta\phi_{\rm min}$ hits the HL for the NOON state for $\Gamma = 0$ only, while it never reaches the HL for the mm' state.

2.3.2 Visibility

We define a relative visibility in the following to quantify the degree of measured phase information

$$V_{mm'} = \frac{\langle\hat{\Pi}_{mm'}\rangle_{\rm max} - \langle\hat{\Pi}_{mm'}\rangle_{\rm min}}{\langle\hat{\Pi}_{mm'}(\Gamma = 0)\rangle_{\rm max} - \langle\hat{\Pi}_{mm'}(\Gamma = 0)\rangle_{\rm min}}, \tag{2.15}$$

where the numerator corresponds to the difference in the maximum and minimum parity signal in presence of phase fluctuations, while the denominator corresponds to the one with no dephasing, i.e. $\Gamma = 0$. Visibility for the N00N state is similarly defined as

$$V_{\rm N00N} = \frac{\langle\hat{\Pi}_{\rm N00N}\rangle_{\rm max} - \langle\hat{\Pi}_{\rm N00N}\rangle_{\rm min}}{\langle\hat{\Pi}_{\rm N00N}(\Gamma = 0)\rangle_{\rm max} - \langle\hat{\Pi}_{\rm N00N}(\Gamma = 0)\rangle_{\rm min}}. \tag{2.16}$$

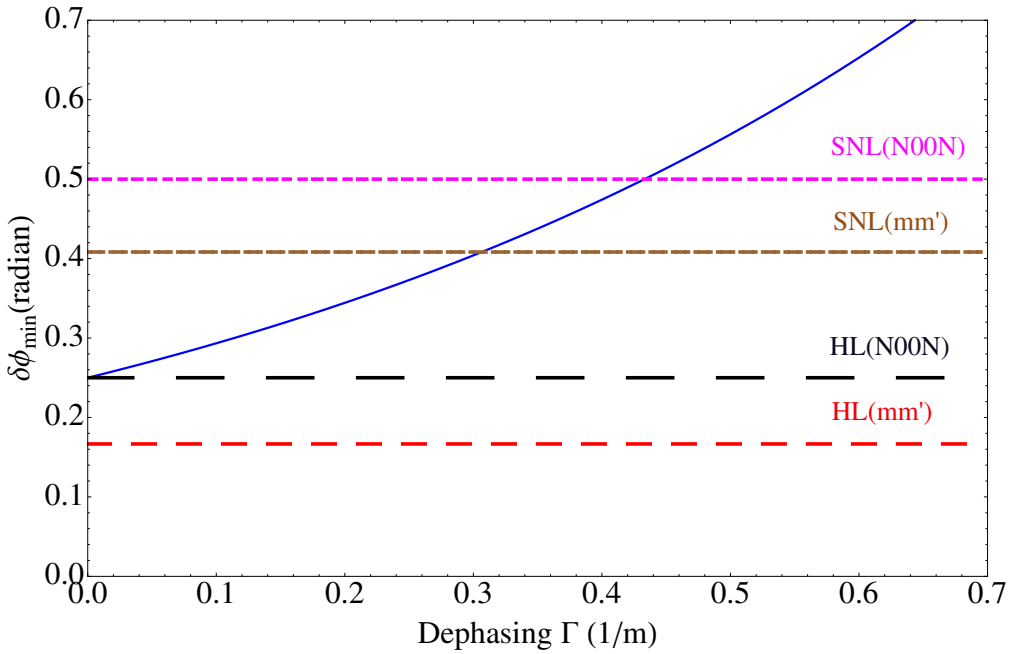

Figure 2.3: Minimum phase sensitivity $\delta\phi_{\min}$ with phase fluctuation. We show the minimum phase sensitivity $\delta\phi_{\min}$ of the mm' state $|5::1\rangle$), or the N00N state $|4::0\rangle$ as a function of Γ. The shot noise limits (SNL) and the Heisenberg limits (HL) of the phase sensitivity for both the states are also shown for comparison.

Using Equations (2.10) and (2.11), we then obtain the visibilities for the mm' state

$$V_{mm'} = e^{-(\Delta m)^2 \Gamma L}, \tag{2.17}$$

and for the N00N state

$$V_{\text{N00N}} = e^{-N^2 \Gamma L}. \tag{2.18}$$

We note that the visibility of the N00N state with the parity detection in Equation (2.18) agrees with the visibility in Reference [36].

The visibility in Equations (2.17) and (2.18) depends on the value of the dephasing rate Γ and N (or $\Delta m = m - m'$), and for a given value of Γ, the visibility falls down faster as N increases. Hence, high-N00N states (or mm' states) with large number of photons are very much susceptible to the phase fluctuations compared to the low-NOON states, and hence are not suitable to achieve metrological advantage with robustness in presence of phase noise. This is shown in Figure 2.4, where we plotted the visibility for different N (or Δm) with respect to the dephasing rate Γ.

2.4 Quantum Fisher information: bounds for phase sensitivity

In order to minimize the uncertainty $\delta\phi$ of the measured phase, we now seek to provide the lowest bound on the uncertainty of the phase. This bound is given by the quantum Cramér-Rao bound $\delta\phi_{\text{QCRB}}$, and is related to the quantum Fisher information $F(\phi)$ [40, 41, 20, 21] as $\delta\phi_{\text{QCRB}} \geq \frac{1}{\sqrt{F(\phi)}}$.

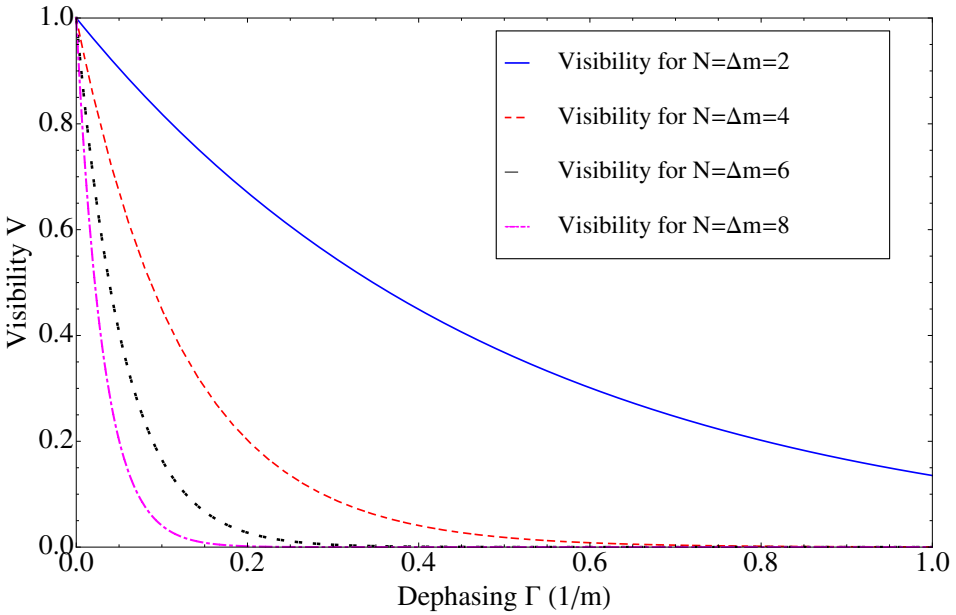

Figure 2.4: Visibility V of the mm' and the N00N state with phase fluctuation. We show the visibility V of the mm' state for different Δm (for different N in case of N00N states with the same phase information) as a function of Γ. The visibility V is plotted for N(or Δm)=2 [solid blue line], N(or Δm)=4 [dashed red line], N(or Δm)=6 [double dotted black line], and N(or Δm)=8 [dot-dashed purple line]. We see that the visibility drops faster for larger values of Δm (or N).

A general framework for estimating the ultimate precision limit in noisy quantum-enhanced metrology has been studied by Escher *et al* [42]. In the following, we first obtain the quantum Fisher information, leading to the quantum Cramér-Rao bound for both the mm' and N00N states in the presence of phase fluctuations, and show that parity detection attains the quantum Cramér-Rao bound for both of these states subject to dephasing.

The quantum Cramér-Rao bound has been shown to be always reached asymptotically by maximum likelihood estimations and a projective measurement in the eigenbasis of the symmetric logarithmic derivative L_ϕ [43, 20, 21], which is a self-adjoint operator satisfying the equation

$$\frac{L_\phi \rho_\phi + \rho_\phi L_\phi}{2} = \frac{\partial \rho_\phi}{\partial \phi}, \tag{2.19}$$

where ρ_ϕ is given by Equation (2.6) for mm' state and by Equation (2.7) for a N00N state. The quantum Fisher information $F(\rho_\phi)$ is then expressed as [44]

$$F(\rho_\phi) = \mathrm{Tr}(\rho_\phi L_\phi L_\phi^\dagger) = \mathrm{Tr}(\rho_\phi L_\phi^2). \tag{2.20}$$

The symmetric logarithmic operator L_ϕ is given by

$$\frac{\lambda_i + \lambda_j}{2} \langle i|L_\phi|j\rangle = \langle i|\frac{\partial \rho_\phi}{\partial \phi}|j\rangle, \tag{2.21}$$

for all i and j, where λ_i and $|i\rangle$ are the eigenvalue and the corresponding eigenvector of ρ_ϕ. Evaluating ρ_ϕ and $\partial\rho_\phi/\partial\phi$ from Equation (2.6) and then using Equations (2.20) and (2.21),

we obtain the quantum Fisher information for the mm' state

$$F_{mm'} = (\Delta m)^2 e^{-2(\Delta m)^2 \Gamma L}, \tag{2.22}$$

leading to the quantum Cramér-Rao bound

$$\delta\phi_{\mathrm{QCRB},mm'} \geq \frac{1}{\sqrt{F_{mm'}}} = \frac{1}{\Delta m e^{-(\Delta m)^2 \Gamma L}}. \tag{2.23}$$

For the N00N states, similar calculation with Equation (2.7) yields

$$F_{\mathrm{N00N}} = N^2 e^{-2N^2 \Gamma L}, \tag{2.24}$$

and

$$\delta\phi_{\mathrm{QCRB,\ N00N}} \geq \frac{1}{\sqrt{F_{\mathrm{N00N}}}} = \frac{1}{N e^{-N^2 \Gamma L}}. \tag{2.25}$$

Equations (2.23) and (2.24) represent the lowest bound on the uncertainty of the phase measurement for the mm' and N00N states, respectively.

For a detection scheme to be optimal, it has to saturate the quantum Cramér-Rao bound. Equations (2.13) and (2.14) represent phase sensitivity for the mm' and N00N states respectively, and these expressions can be shown to be identical to the quantum Cramér-Rao bounds in Equations (2.23) and (2.24) for $\phi = \pi/(2\Delta m)$, or $\phi = \pi/(2N)$ for the mm' or N00N states respectively. Thus, parity detection saturates the quantum Cramér-Rao bounds and is optimal for both states in the presence of phase fluctuations.

Note that in the most general scenario, the photon loss and phase fluctuation can both affect the phase sensitivity and visibility of such states, and we can model photon loss from the system into the environment by adding two fictitious beam splitters are added before stage I as shown in Fig 2.5.

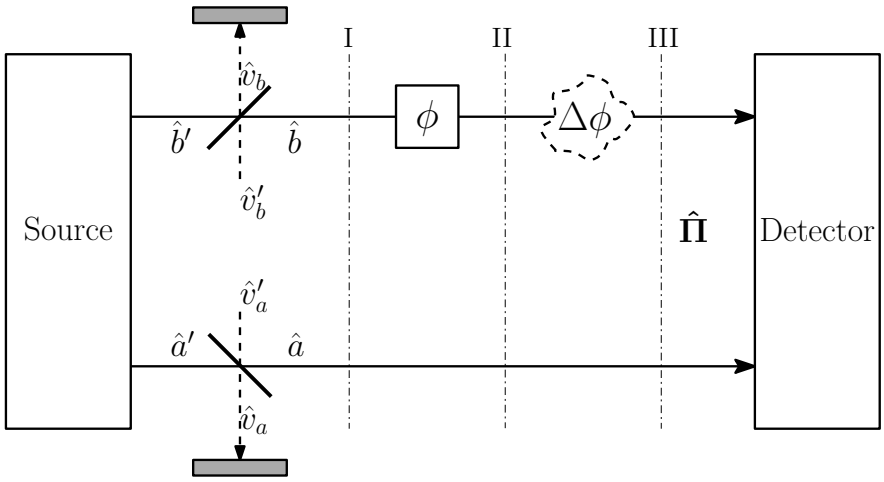

Figure 2.5: Effects of both phase fluctuation and photon loss on the N00N and mm' states. Two fictitious beam splitters are introduced to the Figure 2.1 of Chapter 2 to mimic the loss of photon from the system into the environment. After tracing out the environment mode v_b and v_a, the system results in a mixed state at stage I.

2.5 Conclusion

In this chapter, we studied the effects of phase fluctuations on the phase sensitivity and visibility of path-entangled photon Fock states such as mm' and N00N states in an optical interferometric setup. Although $mm^{'}$ states are more robust than N00N states against photon loss, we showed that they do not provide any better performance in presence of such phase fluctuations than their equivalent N00N counterpart. We have used the parity detection technique for phase estimation, that can be readily implemented using photon-number-resolving detectors [45] in the low power regime and using optical nonlinearities and homodyning in the high power regime [16, 46, 47, 48]. We have also presented a brief study on the quantum Fisher information for such states and showed that for both the states parity detection serves as the optimal detection strategy as it saturates the quantum Cramér-Rao bound of the interferometric scheme.

Chapter 3
Effects of dephasing noise on photon polarization qubits [1]

Quantum computers manipulate quantum states, rather than classical bits and have the potential to solve certain problems much faster than their classical counterparts. These problems include factorization of a large number (essential for the security of quantum cryptographic system) by using Shor's algorithm [49]. It can also provide a quadratic speedup for searching a large unsorted database using Grover's algorithm [50] and efficiently simulate quantum systems [51, 52]. In a quantum computer, calculations are performed by controlled time evolution of a set of coupled two-level quantum systems known as qubits. These qubits are the building blocks for quantum information processing. They are used to store, process and transmit information in a quantum computer.

However, there is a major obstacle to the practical realization of quantum computers. Inevitable interaction of the qubits with a noisy environment causes a loss of coherence, leading to errors in the processing of quantum information. Various strategies have been extensively developed over the last few decades to effectively counteract such decoherence processes, including decoherence free subspaces [53, 54], quantum error correction techniques [55, 56, 57] and dynamical decoupling (DD) [58, 59, 60].

Dynamical decoupling is based on the idea of suppressing undesirable influences on quantum dynamics by appropriately applied external pulses. In general, a DD scheme can be regarded as an open-loop control technique acting on *open* quantum system to *coherently average* out these undesirable interactions. This technique is comparatively simple to implement experimentally, and unlike other conventional quantum error correction protocols, it does not require any measurement protocol or ancilla qubits or encoding overhead.

The development of DD has been motivated from nuclear magnetic resonance (NMR) refocusing techniques developed since the discovery of the spin echo effect [63]. DD was first introduced to quantum information processing for preserving single qubit coherence within the spin-boson model [58]. It was then generalized to preserving states of open quantum systems interacting with arbitrary environments. Since then a wide variety of DD schemes have been proposed and analyzed. Prominent examples of DD schemes are the periodic DD (PDD) [64], Carr-Purcell DD (CP) [65], Carr-Purcell-Meiboom-Gill (CPMG) [66], concatenated DD (CDD) [59, 61] and Uhrig DD (UDD) [60].

However, the majority of theoretical works on DD have considered only the case of ideal pulses, i.e., the case when the decoupling pulses are assumed to be instantaneous and infinitely strong. In that case, we can ignore the effect of a noise-inducing environment *during* the application of the pulses. In any realistic physical implementation, the non-ideal properties of these pulses reduce the efficiency of the decoupling techniques. For instance, pulses generally

[1] Parts of this chapter previously appeared as B. Roy Bardhan, K. L. Brown, and J. P. Dowling, Physical Review A **88**, 052311 (2013) (Copyright(2013) American Physical Society) [79] and B. Roy Bardhan *et al.*, Physical Review A **85**, 022340 (2012) (Copyright(2012) American Physical Society) [80]. They are reprinted by permission of the American Physical Society. See Appendix C for details.

have a finite duration ($\tau_{\rm p}$), and they also may not implement the desired rotations that are required for *averaging out* the interaction of the system with the environment. These imperfections can lead to the accumulation of a considerable amount of overall error, for a large number of pulses, destroying the qubit coherence.

Photons are a prominent candidate for being mediators in quantum communication processes since they move fast and interact weakly with the environment. Quantum information is typically encoded in the polarization or phase of a photon. Recent developments in the above schemes of DD have motivated us to study whether we can find a suitable DD strategy to preserve polarization photonic qubits against decoherence effects. Previous works have looked at the suppression of these effects by using methods including bang-bang decoupling. Wu and Lidar [67] analytically showed that dynamical decoupling [58] could be used for reducing quantum noise in optical fibers and Lucamarini *et al.* [68] showed the application of DD for polarization qubits confined in a ring-cavity. Massar and Popescu presented a method to reduce polarization-mode dispersion in an optical fiber using controlled polarization rotations [69]. Entanglement between a single photon and a single trapped atom was reported by [70], which provided a step towards long-distance quantum networking with individual neutral atoms. Damodarakurup *et al.* experimentally reported on the suppression of polarization decoherence in a ring cavity using bang-bang control of polarization qubits [71].

We propose the application of the CPMG sequence of dynamical decoupling for minimizing the random dephasing in birefringent optical fibers. This sequence [66] has been shown to be robust against a variety of dephasing and control pulse errors [72, 73]. We apply this sequence to flying polarization qubits in order to extend the useful range of a quantum communication channel. We simulate the CPMG pulses with spatially separated half-wave plates to suppress the dephasing of the input polarization qubits. This will be useful for the BB84 protocol [74] of quantum key distribution, along with applications in optical quantum computing [25]. Our method might also be useful in quantum teleportation [75], where the entanglement is distributed with photonic qubits (as in quantum repeaters).

We also investigate the issue of polarization dephasing by using *finite width* wave plates which are likely to cause some additional errors, apart from the random birefringent dephasing noise. Finite widths of the birefringent waveplates directly affect the phase of the photon transmitted through the waveplates leading to a further loss of coherence. Introducing tailored refractive index profiles within the waveplates, we show that it is possible to address such detrimental effects with DD techniques when implemented with waveplates at the prescribed locations along the fiber. Estimates of the required inter-waveplate distance are provided for each of the refractive index profiles, and this information will be enough for an experimenter to know for successfully implementing a faithful long-distance quantum communication channel in practice.

In this chapter, we first present a brief overview of the dynamical decoupling technique along with its paradigmatic example: the spin-boson model. It will help us to understand how this technique is useful in suppressing decoherence of a single qubit coupled to a purely dephasing environment. In Section 3.2 we discuss the nature of random birefringent fluctuations in an optical fiber which are likely to cause dephasing of a photon polarization qubit. We will then show in Section 3.3 how the DD technique can help in mitigating this random phase error to preserve the coherence for a long-distance optical communication fiber. In Section 3.4, we provide a detailed description of the proposed application of the CPMG sequence of dynamical decoupling to combat such dephasing and preserve the input state through the fiber. We address the issue of the additional phase error introduced by the finite

widths of the waveplates implementing the DD in the optical fiber in Section 3.5, and present our numerical results and comparative analysis for various tailored refractive index profiles in the fiber. We conclude with a brief summary and implications of our work, along with suggestions for experimentally implementing the DD sequence in optical fibers.

3.1 Overview of dynamical decoupling

The most general Hamiltonian describing the evolution of a system coupled to a bath can be written as

$$H = H_{\mathrm{S}} \otimes I_{\mathrm{B}} + I_{\mathrm{S}} \otimes H_{\mathrm{B}} + H_{\mathrm{SB}}, \tag{3.1}$$

where H_S and H_B are the system and bath Hamiltonians, respectively. The interaction Hamiltonian H_{SB} can be written as

$$H_{\mathrm{SB}} = \sum_{\alpha} S_{\alpha} \otimes B_{\alpha}, \tag{3.2}$$

with S_α acting only on the system and B_α acting only on the bath.

The aim is to reduce or eliminate the errors by modifying the time evolution of the system and the bath using external control Hamiltonians. This is done by repeatedly applying external control pulses that act on the system such that the coupling of the system to the bath can be time reversed and thus canceled. These control pulses are often called "dynamical decoupling pulses" due to their original objective of decoupling the system from the bath. Typically, DD is used to reduce or eliminate phase errors on a qubit. But, this method can also be used, by nesting two decoupling sequences in orthogonal directions, to mitigate both bit-flip and phase errors [81, 62]. In Figure 3.1, we show a typical dynamical decoupling pulse cycle which can be used to suppress phase error accumulated during the free propagation of the system under the system-bath interaction Hamiltonian H_{SB}.

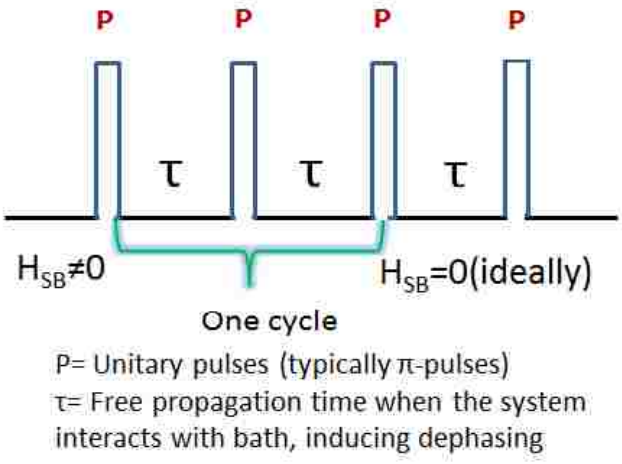

Figure 3.1: A typical DD pulse sequence for removing pure dephasing noise. We show one cycle of a typical dynamical decoupling with ideal (zero-width) pulses. The phase error accumulates during the free propagation time τ.

3.1.1 Example: DD for spin-boson model

Let us consider a qubit realized by a spin-1/2 system coupled to a quantized environment that can be regarded as a continuum of harmonic modes [58]. The overall dynamics of the qubit + environment system is governed by the Hamiltonian

$$H = \hbar\omega_0 \frac{\sigma_z}{2} + \sum_k \hbar\omega_k b_k^\dagger b_k + \sum_k \hbar\sigma_z (g_k b_k^\dagger + g_k^* b_k), \tag{3.3}$$

where ω_0 denotes the energy difference between computational basis states $|0\rangle, |1\rangle$ of the qubit, the second term corresponds to the bath $H_B = \sum_k \hbar\omega_k b_k^\dagger b_k$ with $b_k^\dagger, b_k$ being the bosonic operators of the k-th field mode, and the last term represents the system-bath interaction characterized by the coupling parameter g_k, i.e.

$$H_{\text{SB}} = \sum_k \hbar\sigma_z (g_k b_k^\dagger + g_k^* b_k). \tag{3.4}$$

The associated decoherence mechanism is dephasing in which the qubits lose coherence (represented by the off-diagonal terms in the density matrix) without any energy exchange between the qubit and the bath.

In the Schrödinger picture, let us write the state of the system combined with the bath at time t as $\rho(t)$. However, if we want to work in the interaction picture that corresponds to the free dynamics of $H_S + H_B$, then the transformed state is given by

$$\tilde{\rho}(t) = e^{i(H_S+H_B)t/\hbar} \rho(t) e^{-i(H_S+H_B)t/\hbar}, \tag{3.5}$$

and the transformed time-dependent interaction Hamiltonian by

$$\tilde{H}_{SB}(t) = \tilde{H}(t) = \hbar\sigma_z \sum_k (g_k b_k^\dagger e^{i\omega_k t} + g_k^* b_k e^{-i\omega_k t}). \tag{3.6}$$

The corresponding unitary operator can be written as

$$\tilde{U}(0,t) = \mathcal{T} \exp\left\{ -\frac{i}{\hbar} \int_0^t du \tilde{H}(u) \right\}, \tag{3.7}$$

where $\mathcal{T}$ is the time-ordering operator. For the sake of simplicity, we will henceforth set $\hbar = 1$.

We can now consider the following two standard assumptions: (1) the qubit and the bath are initially decoupled from each other, i.e., $\rho(0) = \rho_S(0) \otimes \rho_B(0)$, and (2) the bath is initially in thermal equilibrium at temperature T. The unitary evolution operator in Equation (3.7) can then be exactly evaluated for this model which in turn gives the qubit coherence $\rho_{01}(t) = \langle 0|\rho(t)|1\rangle$ as [58]

$$\rho_{01}(t) = \rho_{01}(0) e^{i\omega_0 t - \Gamma_0(t)}, \; \Gamma_0(t) = \int_0^\infty d\omega J(\omega) \frac{1 - \cos\omega t}{\omega^2}, \tag{3.8}$$

where $J(\omega) = I(\omega)(2\bar{n}(\omega, T)+1)$ is the power spectrum of the bath specifying the effect of the bath in terms of the oscillator spectral density $I(\omega)$. Here $\bar{n}(\omega, T)$ denotes the average number of field excitations at the temperature T. The above equation determines the evolution of the qubit coherence when there is *no control* (decoupling pulses) present.

In the presence of the decoupling pulses, the decoherence properties of the qubit are modified, resulting in a renormalized spectral density function $J_c(\omega)$ [58]. For a train of instantaneous and infinitely strong π pulses about the x-axis (also known as the Bang-bang pulses), it is given by:

$$J_c(\omega) = J_(\omega) \tan^2\left(\frac{\omega T_c}{4}\right), \tag{3.9}$$

where N is the number of pulses and T_c is the cycle time. The corresponding *controlled* dynamics of the qubit coherence is

$$\rho_{01}(t) = \rho_{01}(0)e^{i\omega_0 t - \Gamma_c(t)},\ \Gamma_c(t) = \int_0^\infty d\omega J_c(\omega)\frac{1-\cos\omega t}{\omega^2}. \tag{3.10}$$

For arbitrarily fast control, i.e. for $T_c \to 0, N \to \infty$, this reduces to

$$\lim_{T_c\to 0, N\to\infty} \rho_{01}(t = NT_c) = \rho_{01}(0). \tag{3.11}$$

This implies the possibility of preserving the qubit coherence of arbitrary single qubit states using such instantaneous and infinitely strong pulses, and essentially signifies the ideal limit of the suppression of the decoherence using the DD technique.

3.1.2 DD in the semiclassical picture of decoherence

Instead of the quantized environment affecting the coherence of the qubit, we can now consider the semiclassical picture in which a local classical external field $B(t)$ causes the pure dephasing of the qubit. In the limit of weak system-bath coupling, we can invoke the Born-Markov approximation and write the semiclassical interaction Hamiltonian as $H_{SB} = B(t)\sigma_z$, where $B(t)$ is a scalar function of time. Suppose the qubit is initially in the coherent superposition state (in the computational basis states $|0\rangle, |1\rangle$)

$$|\psi(0)\rangle = a|0\rangle + b|1\rangle. \tag{3.12}$$

At the end of the evolution for a time τ in the presence of the field $B(t)$ aligned in the z direction, the qubit accumulates a random relative phase $\phi(\tau) = 2\int_0^\tau B(t)dt$. As a result, the qubit state is transformed into

$$|\psi(0)\rangle = a|0\rangle e^{-i\phi(\tau)/2} + b|1\rangle e^{i\phi(\tau)/2}. \tag{3.13}$$

If we control the qubit with rotations around the x-axis on the Bloch sphere, then the complete system Hamiltonian with dephasing is

$$H(t) = B(t)\sigma_z + f(t)\sigma_x, \tag{3.14}$$

where $f(t)$ is the time-dependent control field for the dynamical decoupling pulses [82].

The underlying principle of dynamical decoupling is to select a "pulse sequence" $f(t)$ which causes the integrated time evolution of the interaction Hamiltonian to coherently average to zero [83]. We suppose that the control field is given by $f(t) = \frac{\pi}{2}\sum_{k=1}^{M}\delta(t - t_k)$, consisting of instantaneous "π pulses" at prescribed time instants $\{t_1, \ldots, t_M\}$. In the reference frame co-rotating with this control field $f(t)$, we can rewrite the system Hamiltonian from Equation (3.14) as

$$\tilde{H}(t) = y(t)B(t)\sigma_z. \tag{3.15}$$

In the above, $y(t)$ is a "switching function" which takes on values ± 1, switching polarity at each time t_k corresponding to a π pulse in the control sequence. To see the effect of a dynamical decoupling sequence, we calculate the system propagator in the interaction picture as

$$\tilde{U}(0,T) = \exp\left(-i\left[\int_0^T y(t)B(t)dt\right]\sigma_z\right). \tag{3.16}$$

We can drop time-ordering in the propagator because the simplified Hamiltonian in Equation (3.15) commutes with itself at all times $t \in [0,T]$.

The ideal decoupling sequence would eliminate any dephasing from the system propagator, but since $B(t)$ is in general unknown, decoupling sequences must attempt to make $\int_0^T y(t)B(t)dt \approx 0$ by appropriate choice of pulse locations $\{t_1,\ldots,t_M\}$. In the simplest example, consider a time-independent $B(t) = B_0$ and a single π pulse at $t = T/2$. In this case, a simplified form of the Hahn spin-echo sequence [63], the system is fully decoupled at time T.

A group theoretic understanding of the unitary symmetrization procedure to eliminate errors up to the first order in the Magnus expansion is provided in Reference [84]. Typically, the coupling terms contributing to the decoherence errors undergo an effective renormalization. This renormalization transformation can be considered as the cancelation of the terms in the Magnus expansion of the effective Hamiltonian [85]. This analysis assumes ideal pulses having zero width, in which case it has been shown that DD sequences can be designed to make higher-order system-bath coupling terms vanish [86, 82, 59].

3.1.3 Recent improvements

In the field of magnetic resonance, pulse sequence techniques have been studied as a method of reducing spin ensemble dephasing for many decades [83, 87]. With the advent of quantum computing, these techniques have been re-explored for overcoming decoherence effects, resulting in the development of a wide variety of DD strategies. In quantum computing, DD has been typically used as an open-loop control scheme to reduce the errors which occur during the evolution of the quantum state.

The simplest case DD is the spin-echo sequence [63], where it is possible to reduce the pure dephasing due to low-frequency ($\omega < 1/\tau$) noise by applying a π pulse at time $\tau/2$ during the free evolution. However, this is not very effective in the presence of high-frequency noise. Moreover, errors are introduced by imperfections in realistic pulses. These issues can be addressed by repeating the π pulses used in the spin-echo technique N times. Typically, DD strategies assume ideal pulses having zero width, in which case it has been shown that DD sequences can be designed to make higher-order system-bath coupling terms vanish [86, 82, 59]. Such ideal, instantaneous pulses, however, are not achievable in actual physical systems, and some researchers have considered finite-width pulses, which decouple to higher order than simple rectangular pulses [88, 89].

Another choice of pulse sequence is known as CPMG dynamical decoupling [66], which is a multi-pulse generalization of the spin echo. The CPMG sequence acts as a high-pass filter, which effectively filters out the components of H_{SB} varying slowly compared to τ. The CPMG sequence has been shown to be robust against a variety of dephasing and control pulse errors [72, 94, 95].

In the context of optical quantum processing, DD can be used to preserve the coherence of photonic qubits. Wu and Lidar [67] showed that dynamical decoupling could be used for reducing quantum noise in optical fibers. Massar and Popescu presented a method to reduce polarization mode dispersion in an optical fiber using controlled polarization rotations [69]. The suppression of polarization decoherence in a ring cavity using bang-bang control of polarization qubits has been reported in Reference [71].

3.2 Birefringent dephasing of polarization qubits in optical fibers

3.2.1 Propagation of polarization qubits in optical fiber

In optical quantum information processing, photons are used to store, process and transmit information. They are a prominent candidate for being mediators in quantum communication processes since they move fast and interact weakly with the environment. Quantum information is encoded in the state of a photon, such as in photon number or polarization, and the photons are typically routed through optical fibers or waveguides. Transmission of the photons through such optical fibers can be helpful in using them as optical quantum memory [96, 97], distributed quantum computation [98] and quantum cryptography [99]. Consequently, quantum communication using propagation of the photons through optical fibers has emerged as a very active area of research for the last few decades.

However, as a photonic qubit propagates through the fiber, it interacts with the optical fiber. This interaction causes the qubit to lose its ability to exhibit coherent behavior. As a result, the phase of the qubit becomes randomized and the information stored in it is eventually lost. Hence, it is crucial to protect the polarization qubits against such detrimental dephasing effects induced by the fiber.

In the BB84 protocol of quantum key distribution [74], it is necessary to preserve the input polarized signals against decoherence effects during propagation through the noisy communication channel. Polarization-maintaining (PM) fibers can be used to preserve two orthogonal states of single photon polarization qubit, e.g. photon states with vertical and horizontal polarizations [100, 101]. However, the sender needs to choose the input polarized light signals from either the horizontal-vertical basis or the diagonal basis randomly. Therefore, it is important to preserve all of these states against unpredictable changes in the polarization state due to dephasing in the fiber [102].

3.2.2 Dephasing in optical fiber and noise model

Due to the random fluctuations in uncontrollable factors like mechanical stress (internal or external) [78], temperature, etc., in the optical fiber, the polarization state of single photons changes very rapidly as it propagates through the fiber. These effects cause the birefringence $\triangle n = |n_e - n_o|$ (the subscripts e and o stand for the extraordinary and the ordinary rays) to change randomly along the fiber. For practical fiber lengths of the order of several hundreds of kilometers, the birefringence in such optical fibers can totally destroy the information stored in the polarization qubits.

To combat such large-scale dephasing errors in the fiber, we propose the application of dynamical decoupling implemented with waveplates along the communication channel. We approximate the communication channel as continuously connected fiber elements, as shown in Figure 3.2, which have sections of constant birefringence on the order of the length scale of 10 m (which is fairly realistic for the long-distance communication purposes) along the

fiber. We consider the communication channel provided by a polarization maintaining fiber. As the optical losses are small for the wavelength in the telecommunication band, we restrict our calculations for this wavelength region (around 1550 nm) [103, 104].

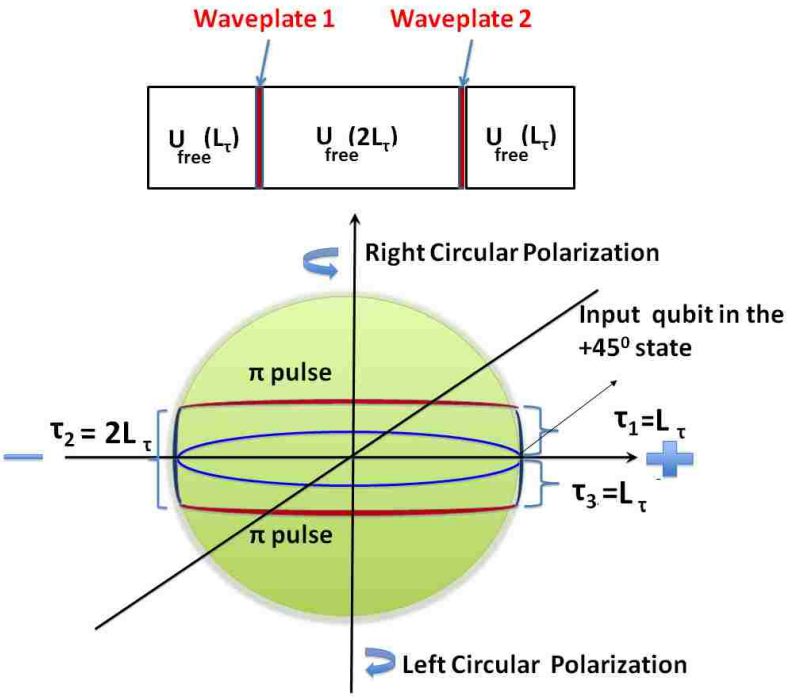

Figure 3.2: CPMG pulse sequence implemented in optical fiber with half-wave plates. Top : CPMG sequence implemented with half-wave plates in the diagonal basis along the fiber; U_{free}'s are the propagators corresponding to the free propagations through the dephasing segments. Bottom : Free propagations and π rotations caused by the waveplates for the input qubit in the $+45^\circ$ state are shown on the Poincare sphere.

Assuming that single-photon sources are available, we initialize the qubit in the $+45^\circ$ or -45° states which can be written as

$$|\psi(0)\rangle = \frac{1}{\sqrt{2}}(|H\rangle \pm |V\rangle). \tag{3.17}$$

It should be pointed out here that the following analysis is valid for a general polarization state of single photons, not only the $+45^\circ$ or -45° states [80]. If we now allow the input photons to propagate freely for a length L, then the qubit state becomes

$$|\psi(L)\rangle = \frac{1}{\sqrt{2}}(e^{i\phi_H}|H\rangle \pm e^{i\phi_V}|V\rangle). \tag{3.18}$$

The phase accumulated by the qubit is given by

$$\triangle\phi = \phi_H - \phi_V = (2\pi/\lambda)\int_0^L \triangle n(x)dx, \tag{3.19}$$

where the refractive index difference $\Delta n(x)$ between the two orthogonal polarizations is referred to as the birefringent noise, resulting in the dephasing error $\triangle\phi = \phi_H - \phi_V$.

If we describe the fluctuations in the fiber to be random, stochastic fluctuations of the refractive index difference $\Delta n(x)$ can be simulated as a Gaussian-distributed zero-mean random process. In this case, the noise is completely defined by the first-order correlation function at two points x_1 and x_2 inside the fiber given by

$$\langle \triangle n(x_1) \triangle n(x_2) \rangle = \exp\left[-\triangle n(x)^2 / 2\sigma^2_{\triangle n} \right]. \tag{3.20}$$

The above form of the two-point correlation function $\langle \triangle n(x_1) \triangle n(x_2) \rangle$ follows from the fact that the fluctuating random birefringence noise $\Delta n(x)$ is assumed to have Gaussian statistics with $\langle \Delta n \rangle = 0$ and standard deviation $\sigma_{\Delta n}$, leading to the random dephasing $\Delta\phi$ in Equation (3.19). The separation $|x_1 - x_2|$ between the two points x_1 and x_2 in Equation (3.20) is considered to be less than the correlation length. (Estimates of the correlation lengths for a typical optical fiber are given in Reference [105].) The Fourier transform $S(k)$ of the correlation function is $S(k) = \exp(-\frac{k^2\sigma_n^2}{2})$.

In the presence of such random birefringent dephasing, the off-diagonal density matrix element propagates according to

$$\rho_{12}(x = L) = \rho_{12}(0) \langle \exp\left(-i \triangle \phi\right) \rangle \approx \rho_{12}(0) \exp\left(-\frac{\langle \Delta \phi^2 \rangle}{2} \right), \tag{3.21}$$

where $\langle \ldots \rangle$ represents the stochastic average, i.e. with respect to the realizations of the birefringent noise. The second line in the above equation follows by expanding the exponential in the first line in series expansion up to the second order of the dephasing $\Delta\phi$. Considering $\Delta\phi$ to be a zero-mean Gaussian process, i.e. $\langle \Delta\phi \rangle = 0$, we obtain the last line in Equation (3.21) showing that the off-diagonal terms decay exponentially leading to the loss of coherence of the qubit. As a result, the phase of the qubit becomes randomized and the quantum information stored in it is eventually lost.

We model the random dephasing by continuously concatenating pieces of fiber with randomly generated lengths $\triangle L$. The total propagation length thus can be split into segments of length ΔL with constant $\Delta n(x)$. The phase difference for the i-th segment is equal to the sum of $(2\pi/\lambda)\Delta L_i \Delta n_i$. These segments constitute a single phase profile associated with a particular instance of birefringent noise and corresponding changes in the refractive index difference $\triangle n$. Ensemble averaging over profiles gives the density matrix for the output state depicting the random dephasing in the fiber.

3.3 Dynamical decoupling to combat birefringent dephasing

Our aim is to preserve input polarization qubits against dephasing effects in an optical fiber, so we intend to implement the most suitable DD sequence to suppress dephasing for a given length of the fiber. In the following, we first illustrate how the dephasing effects in a single qubit can be suppressed with DD techniques when the DD pulses are implemented with half-wave plates along the long-distance optical fiber.

In order to do, we discuss the decoherence function formalism presented in References [73, 82] and show that with the DD pulse sequences it is possible to preserve the coherence of photon polarization qubit in a long-distance optical fiber. We first note that the decoherence function for the propagating photon qubit can be written as the ratio of the off-diagonal terms of the diagonal matrix (say ρ_{12}) at $x = L$ and $x = 0$ for an optical fiber of length L, i.e.

at the two ends of the fiber. The decoherence function for our noise model, i.e. dephasing in the fiber (without pulses) is then

$$W\left(x=L\right)=\exp\left(-\int_{0}^{\infty}\frac{dk}{2\pi}S\left(k\right)\frac{\sin^{2}(kL)/2}{k^{2}}\right), \tag{3.22}$$

where $S(k)$ is the Fourier transform of the autocorrelation function for the random spatial fluctuation of the birefringence [73]. Upon application of a DD pulse sequence with filter function $F(kL)$ [73, 82] in the space domain, the decoherence function can then be shown to be

$$W\left(x=L\right)=\exp\left(-\int_{0}^{\infty}\frac{dk}{\pi}S\left(k\right)\frac{F\left(kL\right)}{k^{2}}\right), \tag{3.23}$$

where the filter function $F(kL)$ is given by $F(kL)=\frac{1}{2}\left|\sum_{m=0}^{n}\left(-1\right)^{m}\left(e^{ikx_{m+1}}-e^{ikx_{m}}\right)\right|^{2}$, corresponding to a pulse sequence having specific set of x_m with x_0=0 and $x_{n+1}=L$. This filter function encapsulates the influence of the pulse sequence applied. For the CPMG sequence (described below), for instance, we take $F(kL)=8\sin^{4}(kL/4M)\sin^{2}(kL/2)/\cos^{2}(kL/2M)$ [73] (M is the number of waveplates in one cycle)

Equation (3.23) indicates that the decay rate of the quantum state is determined by the overlap between the spectral density and the filter function $F(kL)$. Moreover, this equation upon comparison with Equation (3.22) shows that by choosing suitable $F(kL)$ and hence DD pulse-sequence, one can expect to reduce decoherence effects introduced during the free propagation of the qubit. We assume that the waveplates are very thin (width of the waveplate $\delta \ll L_\tau$) such that the phase difference during the propagation of the photons through the waveplates is negligible (See Section 3.5 for analysis and results with finite width of the waveplates in the fiber).

In order to preserve the input polarization qubits in polarization maintaining optical fibers, we simulate the CPMG sequence by placing spatially separated half-wave plates along the fiber. Each wave plate effects a π rotation in the qubit state, equivalent to the π pulses in typical DD schemes. The multi-pulse CPMG sequence is defined by $x_k = L\frac{(k-\frac{1}{2})}{M}$ [66, 73] where the first and the last free propagation periods are half the inter-waveplate separation, effectively refocusing the Bloch vector at the conclusion of the sequence. We take the number of waveplates in one cycle, M, to be 2. With such sequence the input state remains very well-preserved after propagation through any given length of the fiber.

Each cycle of the two-pulse CPMG is implemented in the following steps:

1. Feed a single photon qubit polarized in the $+45^\circ$ or -45° state into the channel we modeled above.

2. Allow the input qubits to propagate through a segment of the fiber for a length of L_τ.

3. Implement the first π-pulse of the CPMG sequence with half-wave plates in the diagonal basis.

4. Allow a free propagation as before but this time for the length $2L_\tau$.

5. Finally, the second pulse is implemented with a half-wave plate followed by a free propagation of length L_τ.

At the end of the above cycle of length $4L_\tau$, the unitary operator corresponding to the propagation of the polarization qubit through the fiber can be written as

$$\hat{U}_{\text{cycle}} == \hat{U}_{\text{free}}(L_\tau)\hat{\sigma}_x\hat{U}_{\text{free}}(2L_\tau)\hat{\sigma}_x\hat{U}_{\text{free}}(L_\tau), \tag{3.24}$$

where $\hat{\sigma}_x$ is the Pauli X operator and $\hat{U}_{\text{free}}(L_\tau)$ are the propagators corresponding to the free propagations along distances L_τ and $2L_\tau$, respectively.

The CPMG sequence with $2N$ pulses is obtained by repeating the above cycle N times, and the propagator for such a sequence is $\hat{U}_{\text{CPMG}} = \hat{U}^N_{\text{cycle}}$ where $\hat{U}_{\text{cycle}}$ is defined above. For the CPMG sequence with $M = 2$ pulses in one cycle, the filter function is given by [73]

$$F(kL) = 8\sin^4(kL/8)\sin^2(kL/2)/\cos^2(kL/4). \tag{3.25}$$

The decoherence functions $W(x)$ without CPMG and with CPMG are plotted in Figure 3.3. We can theoretically predict that CPMG should preserve the coherence of the input polarized qubit for a longer length than the fiber without the wave plates.

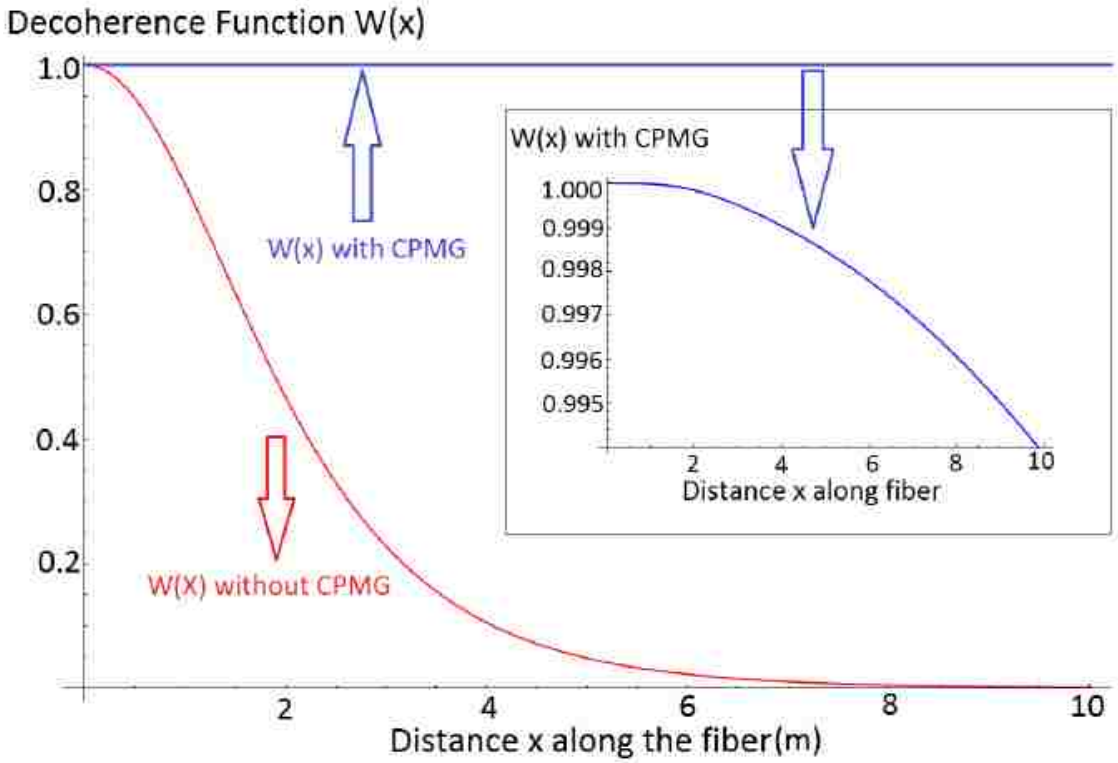

Figure 3.3: Decoherence function $W(x)$ without CPMG and with CPMG. We plot the decoherence function $W(x)$ as a function of the distance along the fiber. Inset: $W(x)$ for CPMG with M=2 is shown (zoomed in) with the filter function $F(kL) = 8\sin^4(kL/8)\sin^2(kL/2)/\cos^2(kL/4)$ and $S(k) = \exp(-\frac{k^2\sigma_n^2}{2})$. Distance along the fiber is plotted in meters in the figure.

3.4 Numerical Results

To characterize the effectiveness of our scheme, we use the fidelity $\mathcal{F}$ between the input state $|\psi_{\text{in}}\rangle$ and ρ_{out} as

$$\mathcal{F} = \langle\psi_{\text{in}}|\rho_{\text{out}}|\psi_{\text{in}}\rangle, \tag{3.26}$$

where $\rho_{\text{out}} = \frac{1}{n}\sum_{i=1}^{n}|\psi_i\rangle\langle\psi_i|$. Here n is the total number of randomly generated phase profiles, corresponding to the propagation operator $\hat{u}_i$ so that $|\psi_i\rangle = \hat{u}_i|\psi_{\text{in}}\rangle$ represents the simulated birefringent noise. Therefore, fidelity being close to one implies that the input state is well-preserved against dephasing.

For an arbitrary polarization state $\alpha|H\rangle + \beta|V\rangle$, our calculations show that after n randomly generated phase profiles, the average fidelity between the input and output states is

$$\mathcal{F}_{Avg} = \left\langle \cos^2(\theta) + \left(\frac{|\alpha|^2 - |\beta|^2}{|\alpha|^2 + |\beta|^2}\right)\sin^2(\theta)\right\rangle. \tag{3.27}$$

Here θ is the total phase introduced by the birefringent fiber as well as by the waveplates. States which minimize the fidelity are given by $\frac{1}{\sqrt{2}}\left(|H\rangle + e^{i\phi}|V\rangle\right)$ and lie on the equator of the Poincaré sphere. We observe that fidelity drastically improves when we used the waveplates even for a large variation of the parameters of the random dephasing $\Delta\phi$. This is shown in Figure 3.4.

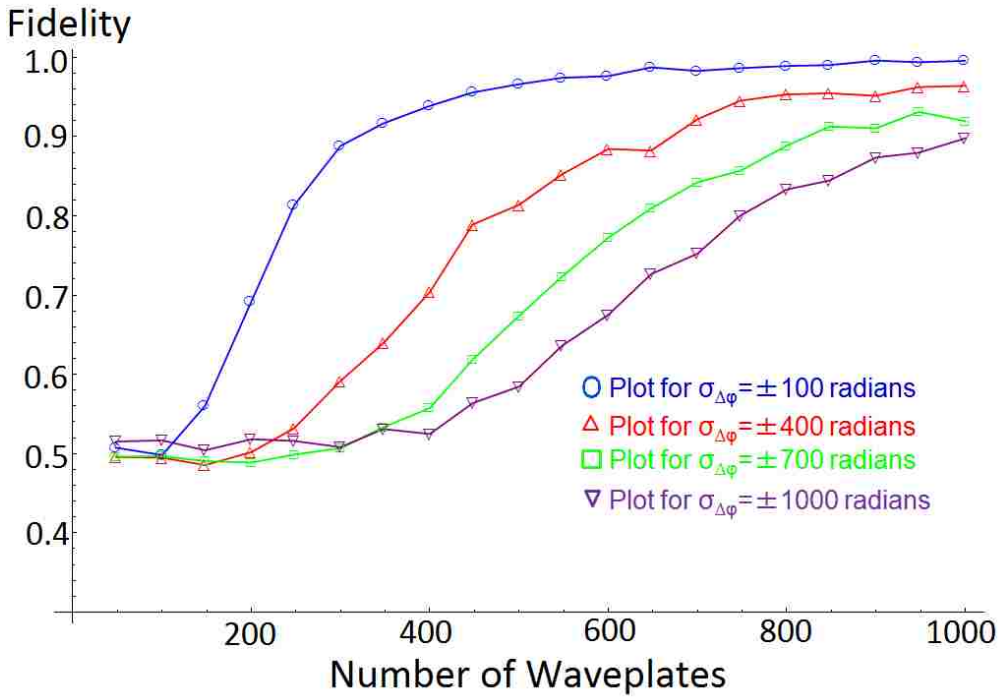

Figure 3.4: Fidelity with CPMG waveplates with variation of the number of waveplates. We show the fidelity with variation of the number of waveplates for different standard deviations of the randomly generated dephasing $\triangle\phi$ and fixed $L = 10\text{km}$, $\langle\triangle L\rangle = 10\text{m}$ and $\sigma_{\triangle L} = 3\text{m}$.

For a given length of the fiber, we can estimate the minimum number of waveplates or the distance between the waveplates required to achieve high fidelity. For instance, for a total fiber length of L=10 km, the estimated number of wave plates from Figure 3.4 is 610 to obtain a fidelity of 0.98. Using this, the rough estimate of the inter-waveplate distance L_τ is 8.2 m when we considered birefringence fluctuations Δn on a length scale of 10 m (which is fairly realistic for the long-distance communication purposes) along the fiber.

The variation of fidelity for different fiber lengths is plotted in Figure 3.5, which shows that polarization qubits can be preserved up to an excellent fidelity using the CPMG sequence for a wide range of the total fiber length.

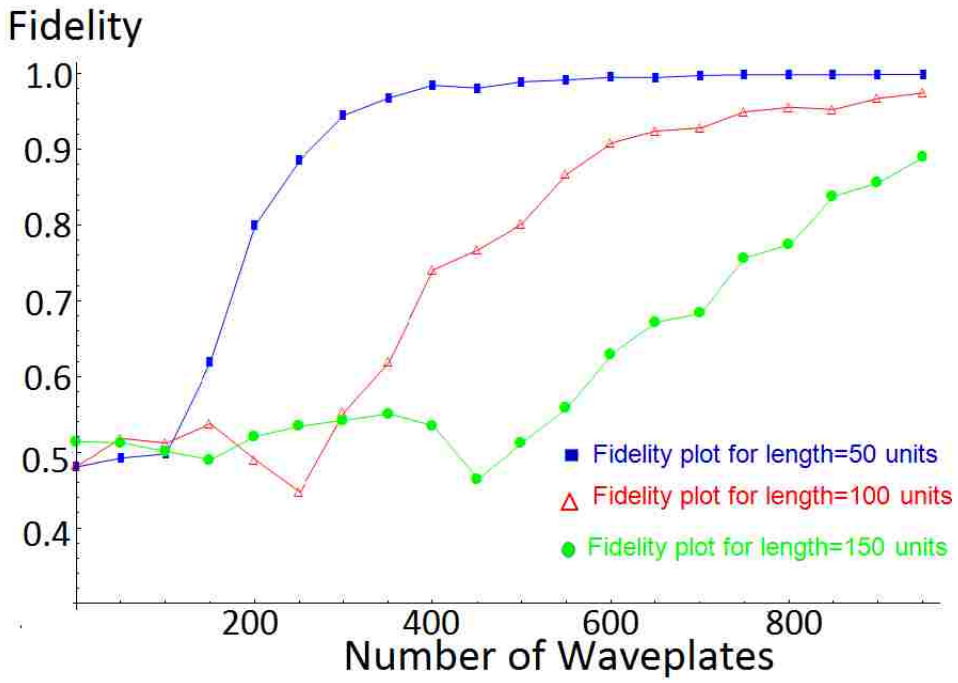

Figure 3.5: Fidelity variation for different lengths of the fiber. The parameters used are $\langle \triangle L \rangle = 10\text{m}, \sigma_{\triangle L} = 3\text{m}$ and $\sigma_{\triangle \phi} = \pm 100$ radians.

In Figure 3.6, the contour plot of the fidelity is shown with respect to the standard deviations $\triangle L$ and $\triangle \phi$. This plot illustrates that high fidelity can be obtained for a reasonably large range of random fluctuations. Therefore, we show how to preserve polarization qubits against dephasing over realistic lengths of optical fiber.

3.5 Dynamical decoupling with tailored waveplates for polarization qubits

In this section, we address the issue of the finite width of the waveplates which are likely to cause some additional errors, apart from the random birefringent dephasing noise. Finite widths of the birefringent waveplates directly affect the phase of the photon transmitted through the waveplates leading to further loss of coherence. Introducing tailored refractive index profiles within the waveplates, we show that it is possible to address such detrimental effects with DD techniques when implemented with waveplates at the prescribed locations along the fiber.

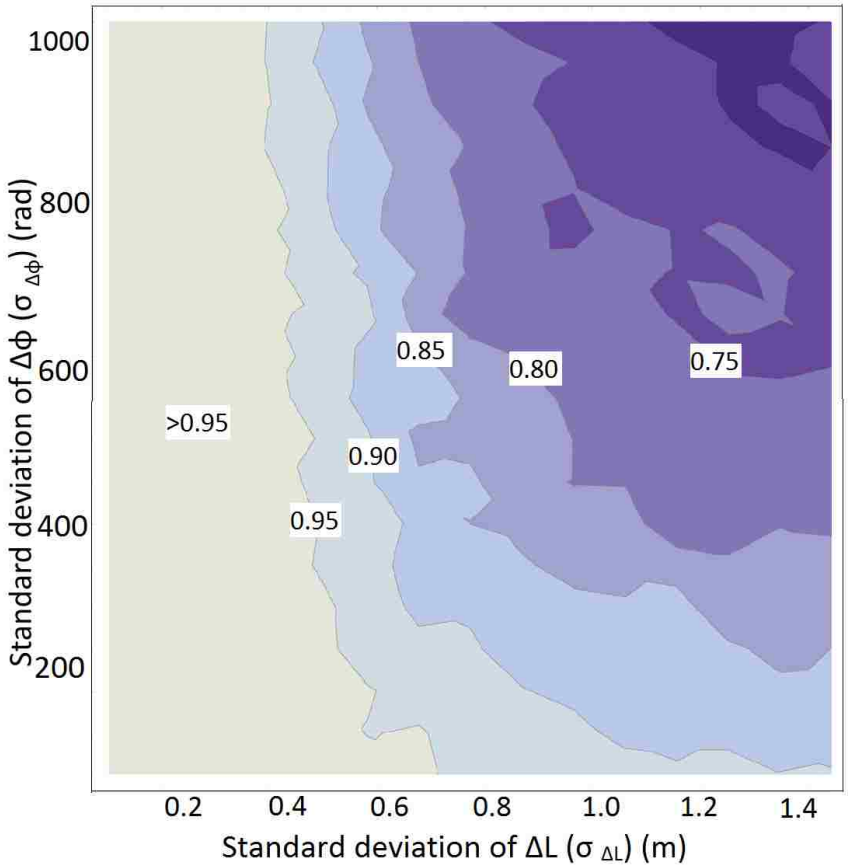

Figure 3.6: Contour plot of the fidelity with the variations of the dephasing parameter. We show the contour plot of the fidelity with the variations of the standard deviations of $\triangle L$ and $\triangle\phi$. Lighter regions show higher values of the fidelity. The simulation is done with fixed $L = 10\text{km}, \langle\triangle L\rangle = 10\text{m}$.

3.5.1 Ideal vs Real Pulses

Ideally, DD pulses are assumed to be strong and instantaneous pulses applied fast enough compared to the internal dynamics of the environment. We can follow a similar method as in Section 3.1 to analyze the evolution of the qubit. Consider a single cycle of a DD sequence with pulses of duration τ_p having a period T. The evolution operator describing the evolution of the system from time $t = 0$ to $t = T$, in the rotating frame, can be written as [106]

$$U(T) = U_f(\tau_{N+1}) \prod_{i=1}^{N} U_C^i(\tau_p) U_f(\tau_i), \tag{3.28}$$

where the free evolution operator $U_{\text{f}}(\tau)$ is given by

$$U_{\text{f}}(\tau) = \exp[-i\tilde{H}(\tau)]. \tag{3.29}$$

The time-dependent Hamiltonian $\tilde{H}(t)$ is given by Equation (3.6). Therefore, the evolution operator acting during the application of pulses is given by

$$U_C^i(\tau_p) = \mathcal{T} \exp\left[-i \int_0^{\tau_p} dt' (\tilde{H}(t') + H_C^i(t')\right]. \tag{3.30}$$

Since the evolution described in Equation (3.6) is necessarily a unitary one, it can be written as the exponential of a Hermitian operator H_{eff}

$$U(T) = \exp[-iH_{\text{eff}}T], \tag{3.31}$$

where H_{eff} can be written as a series expansion using the average Hamiltonian theory [107]

$$H_{\text{eff}} = H^{(0)} + H^{(1)} + ... = \sum_{n=0}^{\infty} H^{(n)}. \tag{3.32}$$

An ideal DD sequence, i.e. a DD sequence with instantaneous pulses, makes $H_{\text{eff}} = H^{(0)}$ by suppressing the system-bath interaction H_{I}, and better performance of a DD sequence usually corresponds to progressively eliminating the higher order terms in such an expansion [86, 82, 59] (e.g. Magnus expansion [85]).

Under the assumption of weak coupling to the environment, the evolution operator in Equation (3.30) (in the rotating frame) simplifies to

$$U_C^i(\tau_p) = \exp[-i\sigma_\alpha\theta_p/2]. \tag{3.33}$$

Here $\alpha = x, y, z$ and $\theta_p = \omega_p\tau_p$ (ω_p being the frequency of the pulses) is the rotation around the α axis. For ideal instantaneous pulses which implement π rotations, the angle θ_p will be π.

However, imperfect pulses can result in errors in the rotation axis as well as in the angle of rotation. We can write the resulting propagator as the product of the ideal pulse propagator and a rotational error $\exp[-i\sigma_{e_i}\theta_{e_i}/2]$ [106], due to the i th waveplate,

$$U_C^i(\tau_p) = \exp[-i\sigma_{e_i}\theta_{e_i}/2]\exp[-i\sigma_\alpha\theta_p/2]. \tag{3.34}$$

The modified free evolution operator in the presence of the pulse errors can be written as

$$U_f(\tau_i, \tau_p) = U_f(\tau_i)\exp[-i\sigma_{e_i}\theta_{e_i}/2]. \tag{3.35}$$

The total evolution operation from Equation (3.28) then reads

$$U(T) = U'_{f_{N+1}}(\tau_{N+1}, \tau_p)\prod_{i=1}^{N} U_C^i(0)U'_f(\tau_i, \tau_p). \tag{3.36}$$

The evolution operator in the above expression can then be written as a series expansion similar to Equation (3.31), and a good choice of DD sequence should make $U(T) \approx \exp(-iH_{\text{B}}T)\,\mathbb{I}$, (where $\mathbb{I}$ is the identity) in the presence of the pulse errors defined above. Note that the initial system is then preserved against decoherence along with the rotational imperfections, since the factor $\exp(-iH_{\text{B}}T)$ merely acts as a background noise that does not get coupled with the system.

Khodjasteh and Lidar analyzed the cumulative effects in pulse sequences and provided an optimum pulse interval for realistic pulses with a fixed minimal pulse width $\tau_{\text{p},min}$ [61]. Uhrig and Pasini showed the optimized performance of the DD sequences for considering realistic control pulses of finite duration and amplitude [95, 108]. Composite pulse sequences such as BB1, CORPSE, and SCORPSE, have been shown to correct systematic pulse errors (which might include pulse amplitude, phase and frequency errors) [109, 110, 111, 112, 113]. Pulse shaping is another method that is used to counteract environmental noise effects during the finite duration of the real pulses [114, 115, 112, 116].

3.5.2 Choice of DD to preserve the polarization qubit

The fact that the DD pulses are implemented with waveplates in our scheme, and the axis of rotation is fixed by the orientation of the optical axis of the birefringent waveplates, highly restricts our choice of DD methods. It is a technically formidable task to have precise control of the varied orientations of the optic axes as required in each sequence of the composite pulse sequences such as BB1, CORPSE, SCORPSE, or KDD (although all of them generally provide robust performance against pulse errors). Moreover, these sequences typically require a large number of pulses in each cycle, which in our case of long-distance fibers affects scalability.

In general, a judicial choice of the DD sequence is decided according to the noise spectral density of the environment. In our case, we have to choose DD sequences which provide robust performance in the presence of our dephasing model, which has randomly distributed noise with Gaussian spectral density. An optimized sequence such as UDD is not a good choice in this case as UDD works best when the noise has a sharp high-frequency cut-off [117, 90, 91, 92]). In the case of UDD, with single or multi-axis control, pulse errors generally accumulate with higher orders. A few recent studies also indicate that high-order UDD or concatenated DD sequences in general lose their advantage when the pulse intervals are strongly constrained [118, 95].

In order to preserve polarization states in a fiber, the CPMG sequence has been shown to work best in such Gaussian-distributed random birefringent noise [117, 73, 80]. Another motivation for using CPMG is that this sequence is extremely robust against all pulse imperfections, when used with the longitudinal states, while giving marginally better results to preserve the transverse components of polarization [113, 119, 72, 106, 120, 121, 117, 80]. It requires π rotations around a fixed axis which can be easily set by orienting the optical axis within half-wave plates.

For very similar reasons, we then consider the XY-4 sequence (which requires alternating π rotations around X and Y axes), and is known to provide excellent performance in the presence of pulse errors by preserving both the longitudinal and transverse components of polarization [113, 106, 122, 123]. These sequences act as high-pass filters that effectively filter out the components of the H_{I} which vary slowly compared to τ. In both sequences, the total evolution operator after one cycle, defined in Equation (3.36), is $U_T \approx \mathbb{I} + \mathcal{O}(\omega_c^2 \tau^2)$ ($\tau_c = 1/\omega_c$ is the correlation time of the environment). Hence, the errors (due to both dephasing and pulse imperfections) resulting in the randomization of the phase of the polarization state coming out of the fiber at the end, can be reduced with CPMG and XY-4 up to the first order in $\omega_c \tau$ for each cycle.

3.5.3 Numerical Results

We first model birefringent dephasing in the optical fiber in the same way as in Section 3.2 by approximating the communication channel as continuously connected fiber elements. The fluctuating random birefringence noise $\Delta n(x)$ in the fiber is simulated as a Gaussian zero mean random process with $\langle \Delta n \rangle = 0$ and standard deviation $\sigma_{\Delta n}$. Since the magnitude of the local birefringence at any point along a birefringent optical fiber is typically of the order of 10^{-4} to 10^{-7} [100, 101], the standard deviation $\sigma_{\Delta n}$ is chosen to have this range of values to mimic realistic fluctuations in the birefringence.

For simulating the effect of the finite widths of the waveplates when the polarization qubits are fed into the fiber, we first note that the total propagation operator in Equation

(3.34) after one cycle in the presence of such additional error can be written as $U_C^i(\tau_p) = \exp[-i(\theta_{p_i} + \Delta\theta_{p_i})\sigma_\alpha]$. In our model with finite-width waveplates, the angle error term $\Delta\theta_p$ is the practical deviation from the intended rotation θ_p, and is due to the refractive index profile $\Delta N(x)$ within the waveplates (which have width Δl). We can define the flip angle error corresponding to $\Delta\theta_p$ as $\Delta\theta_p/\theta_p$. [2] The angle error term $\Delta\theta_p$ can be written as

$$\Delta\theta_p = (2\pi/\lambda)\int_0^{\Delta l} \Delta N(x)dx. \tag{3.37}$$

We consider the following refractive index profiles, as shown in Figure 3.7, for simulating realistic pulse effects:

$$\Delta N(x) = \begin{cases} \exp\left[-\frac{(x-x_0)^2}{2\sigma^2}\right]; 0 < x_0 < \Delta l & \text{(Gaussian)} \\ 1; 0 < x < \Delta l \text{ and } 0 \text{ elsewhere} & \text{(Rectangular)} \\ \tanh[a(x+1)+1]\tanh[-a(x-1)+1] & \text{(Hyperbolic Tangent)} \end{cases} \tag{3.38}$$

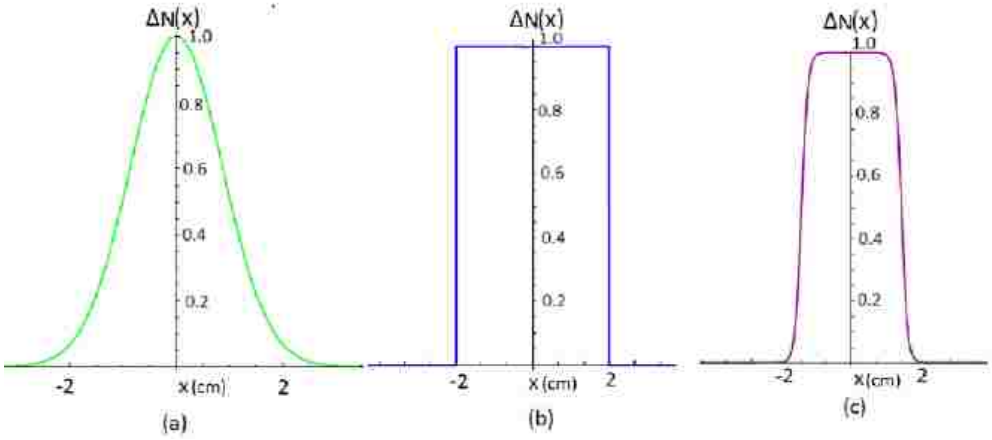

Figure 3.7: Refractive index profiles generating the effects of finite widths of waveplates. We show the refractive index profiles $\Delta N(x)$ generating the phase error due to the finite widths of the pulses, where x represents the distance within the waveplate: (a) Gaussian, (b) Rectangular, and (c) Hyperbolic tangent [as defined in the text and in Equation (3.37)].

For the Gaussian profile, x_0 and σ denote the mean and the standard deviation of the refractive index distribution within the wave plate, and for the hyperbolic tangent profile the parameter a can be used to adjust the slope of the distribution inside the waveplates. In our simulation, we first consider the flip-angle error of 5%, which is approximately generated by using the parameters $a = 8, x_0 = 1, \sigma = 1.8$, from Equations (3.37) and (3.38).

We now aim to investigate two DD sequences: CPMG and XY-4 applied to the flying polarization qubits propagating through optical fiber. The basic cycles of these two sequences are $f_\tau X f_{2\tau} X f_\tau$ and $f_\tau X f_\tau Y f_\tau X f_\tau Y$, respectively, both with cycle period of 4τ. The free evolution periods correspond to the phase error accumulated during free propagation along the fiber for a length f_τ, and the X and Y rotations correspond to the π rotations implemented

[2] This flip angle error is not to be confused with the terminology of the flip angle in the context of T_1-relaxation (for instance in Reference [124]).

with half waveplates, as shown in Figure 3.8. We make a comparative analysis of these sequences for the following refractive index profiles that are used to generate the errors due to the finite widths of the waveplates.

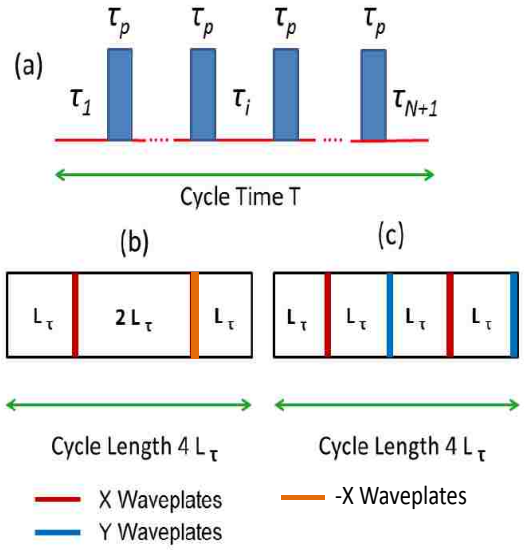

Figure 3.8: A cycle of DD pulse sequence to supress phase error: (a) Schematic representation of a cycle of general dynamical decoupling pulse sequence with pulses of duration τ_p, (b) CPMG sequence with two pulses in a cycle, and (c) XY-4 sequence with alternated X and Y waveplates. Here X, -X, an Y waveplates implement the π-rotations around $x, -x$, and y axes, respectively.

The π rotations required for CPMG and XY-4 sequences are implemented with suitably oriented half waveplates, and the effects of their finite widths on the relative random phase are generated from the refractive index profiles of Equation (3.38). In Figure 3.9, we show how the fidelity (we use the same definition of the fidelity as in Equation (3.26)) varies and improves with the XY-4 sequence being applied for a realistic fiber length of 10 km, even for a large variation of the parameters of the random dephasing $\Delta\phi$ for the chosen refractive index profiles.

Fidelity decay without the waveplates (free decays) is also shown in the inset for comparison. In this free decay plot, we note that the fidelity quickly drops to 0.5 even for a small distance (such as 20 m). The reason for this is that the random dephasing in the fiber results in complete phase-randomization, and the initial pure state rapidly decays to the fully mixed state (fidelity equal to 0.5 [125, 71]).

Figure 3.10 illustrates the results for the CPMG sequence for the same length of fiber. In both Figures 3.9 and 3.10, we considered 5% flip-angle error to make the numerical results comparable. The required number of wave plates to achieve a given fidelity can also be easily estimated from the above figures. For instance, for the hyperbolic tangent refractive index profiles, the required number of wave plates to achieve a 99.9% fidelity, are 840 and 860 for the CPMG and XY-4 sequences, respectively. Fewer wave plates are required for hyperbolic tangent refractive index profiles (for both the sequences) to achieve the same high fidelity.

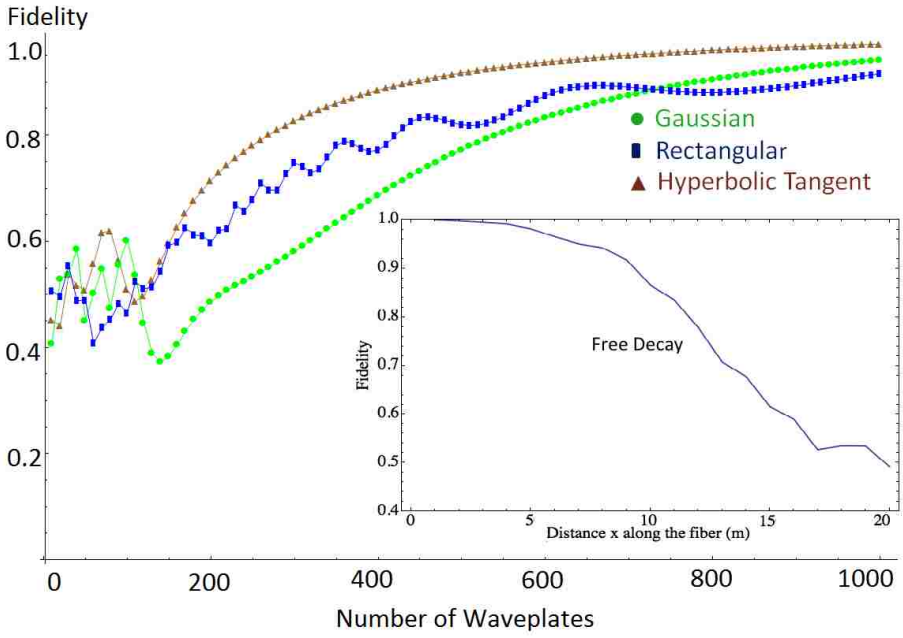

Figure 3.9: Fidelity with XY-4 sequence for different refractive index profiles. Total length of the optical fiber is 10 km.

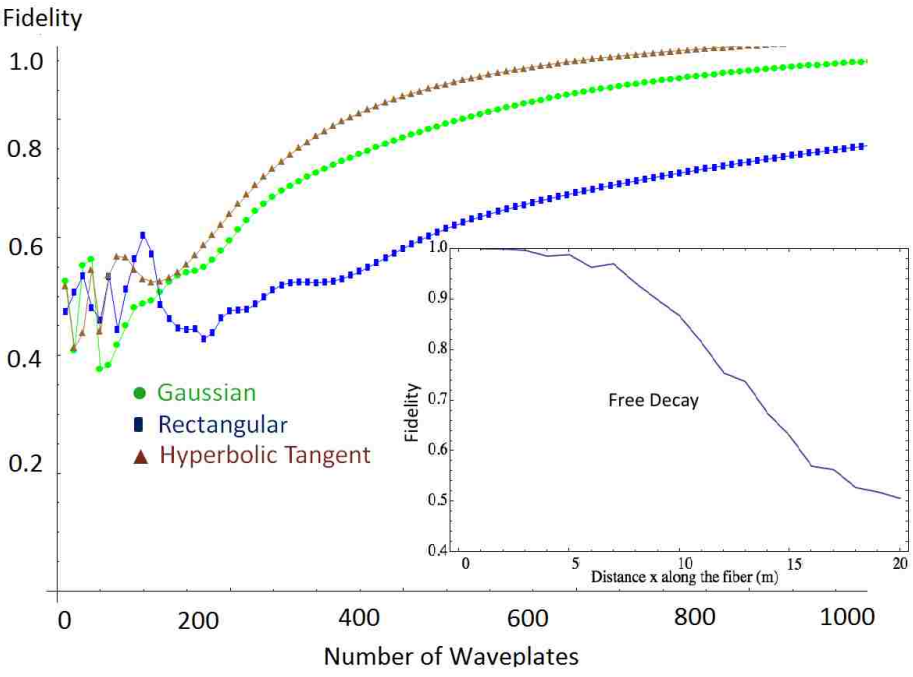

Figure 3.10: Fidelity with CPMG sequence for different refractive index profiles. Total length of the optical fiber is 10 km.

From these figures, we find that while both the sequences work reasonably well to preserve the input polarization states for both the Gaussian and hyperbolic tangent refractive index profiles, the rectangular refractive index profile gives the worst fidelity in both the cases. In fact, this profile *never* gives perfect fidelity with the CPMG sequence. In general, the fidelity is preserved better for the case of XY-4 sequence (Figure 3.9) than CPMG (Figure 3.10). This is due to the fact that the phase errors due to the finite width of the waveplates get partially cancelled due to the alternating π rotations around two orthogonal optic axes (X and Y) in a XY-4 sequence. It is also interesting to note that the fidelity in general improves with increasing number of pulses (waveplates) in both cases showing the robustness of these schemes in the sense that the pulse errors tend to cancel each other instead of getting added up.

Due to finite widths of the wave plates, the actual angle of rotation deviates from π, and this constitutes the flip angle error in the polarization state of the photon. In Figure 3.11, we plot the variations of fidelity with respect to the standard deviation of the birefringent dephasing $\Delta\phi$ and flip angle errors for both the sequences. Here large flip angle errors up to 50% are considered, and the contour plot shows that the input state is preserved up to fidelity close to one for a large variation of the dephasing error as well as for flip angle errors.

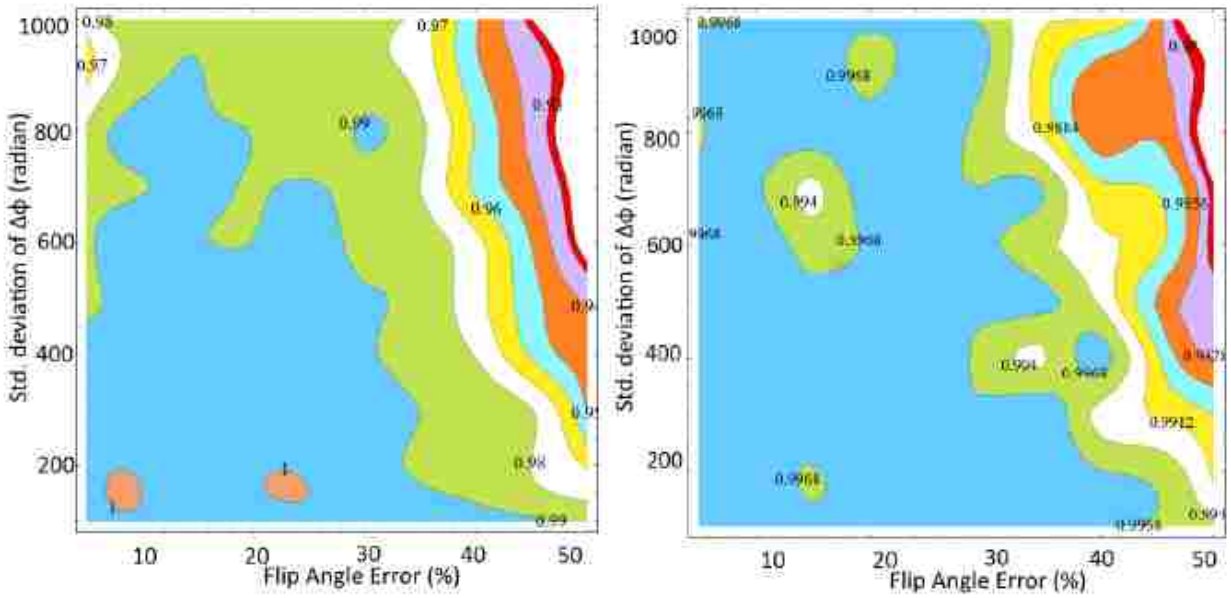

Figure 3.11: Contour plots of the fidelity in presence of finite width errors. We show the contour plots of the fidelity with the variations of the standard deviations of the random birefringent dephasing $\Delta\phi$ and the flip angle error for CPMG (Left) and XY-4 (Right). The simulations are done with fixed number of waveplates (1000) and total length of the fiber $L = 10$ km, and the average fidelity is obtained by taking 500 randomly generated phase profiles.

3.6 Conclusion

A quantum system is susceptible to inevitable interactions with its surrounding environment, and in quantum information processing it is important to have robust control on the quantum system such that it is effectively isolated from the environment. Dynamical decoupling is a technique that can be used to suppress such effects of the environment by applying a sequence of control pulses to the system. We considered the polarization photon qubits propagating through optical fibers, and demonstrated that dephasing errors, contributed by both the fiber birefringence and the finite widths of the waveplates implementing the pulse sequence, could be suppressed by suitable dynamical decoupling methods. For a large range of rotational error and random birefringent dephasing, our scheme provides a practical way to tackle them as long as appropriate wave plate separations are maintained.

As we have dealt with noises due to random fluctuations caused by any possible source such as temperature, stress, etc., the prescribed DD methods can be applied without an experimentalist having a detailed, quantitative knowledge of the decohering environment. To implement our proposed method experimentally to preserve the polarization qubits, several familiar techniques could be suitable depending on the range of fiber lengths one wishes to use. The wave plates may be directly incorporated into the fiber during the manufacturing process. Other methods include writing a Bragg transmission grating periodically into the fiber [76, 77], or twisting the fiber in controlled ways causing suitable mechanical stress [78]. Periodic modulations or perturbations in the refractive index in the graded index optical fiber, implementing the desired profiles, can be generated by the techniques described in the References [126, 127, 128].

Chapter 4
Amplification and attenuation of Gaussian entangled states

Quantum entanglement is one of the most fundamental quantum mechanical resources, and it has wide range of applications in teleportation, cryptography, and super-sensitive and super-resolving precision measurement. In this chapter, we will see that the propagation of entangled light through an absorbing or amplifying medium significantly affects the non-classical properties of the field. In particular, we consider the two-mode squeezed vacuum state which is a well-studied entangled Gaussian state. This entangled state is easy to produce and has been widely used in continuous-variable quantum information processing including quantum metrology, quantum teleportation, quantum cryptography, quantum illumination, etc. We study how the entanglement properties of an input field represented by such entangled Gaussian states are affected by optical amplifiers and attenuators.

As an application of the above study, we present our work where we seek to exploit the loss of the entanglement of the two-mode squeezed vacuum state in a lossy and noisy medium to provide an estimate of the tolerable noise present in the medium for a given entanglement to be preserved, and also to determine whether a target is present in the noisy medium. The noisy environment, through which the signal mode is transmitted, is modeled as an attenuator, and the optical amplifier is used to compensate the loss of the signal amplitude in the attenuator.

In this chapter, we first briefly discuss the two-mode Gaussian states, particularly the two-mode squeezed vacuum state, and their entanglement properties. We then provide an overview of the models for an optical phase-insensitive amplifier and an attenuator and their effects on the entanglement of the two-mode squeezed vacuum states in Section 4.2. In Section 4.3, we present the model describing the propagation of the signal mode of a two-mode squeezed vacuum state through a noisy medium (that may or may not contain a weakly reflecting target) while the ancilla mode is retained. Section 4.4 contains our results with the loss of entanglement where we use the covariance matrix formalism to characterize the two-mode squeezed vacuum state, and the logarithmic negativity as a measure of the entanglement present in the entangled system. We also discuss how the loss of entanglement can be used as a direct signature of the presence or absence of a target in the noisy medium.

4.1 Gaussian States

Gaussian states are widely used in both quantum optics and quantum information theory. They can be described by simple analytical formulas and their entanglement criteria are well-developed [129, 130, 131]. A two-mode Gaussian state ρ with modes a and b is completely characterized by its first and second statistical moments.

4.1.1 Covariance matrix formalism

Let us first define the set of quadrature operators $\{x_a, y_a, x_b, y_b\}$ as

$$x_j = (a_j + a_j^\dagger)/\sqrt{2},\ y_j = (a_j - a_j^\dagger)/\sqrt{2}i, \tag{4.1}$$

where $j = a, b$ is the index for denoting the modes a and b. Let X denote a row vector with elements (x_a, y_a, x_b, y_b) defined above. The first moment of the state ρ is called the displacement vector (or the mean value)

$$\bar{X} = \langle X \rangle = \mathrm{Tr}(X\rho), \tag{4.2}$$

while the second moment is given by the covariance matrix σ of the normalized Wigner distribution [132]

$$W(X) = \frac{e^{-(X-\langle X\rangle)\sigma^{-1}(X-\langle X\rangle)^T/2}}{(2\pi)^n\sqrt{\det(\sigma)}}, \tag{4.3}$$

whose elements can be written as

$$\sigma_{ij} = \frac{1}{2}\langle (X_iX_j + X_jX_i)\rangle - \langle X_i\rangle\langle X_j\rangle. \tag{4.4}$$

The expression in Equation (4.3) is valid for any n-mode Gaussian state.

The covariance matrix for an n-mode Gaussian state is, by definition, a real positive symmetric matrix, and therefore one can make use of Williamson's theorem [134]. This theorem states that any real positive matrix of even dimension can be expressed in diagonal form by using a symplectic transformation. By this theorem, for the n-mode covariance matrix σ, there exists a symplectic matrix S such that

$$\sigma = S\sigma^\oplus S^T, \sigma^\oplus = \oplus_{k=1}^n \nu_k \hat{I}, \tag{4.5}$$

where the diagonal matrix $\sigma^\oplus$ is known as the Williamson form of the covariance matrix σ, and its diagonal entries ν_k $(k = 1, \ldots, n)$ are the symplectic eigenvalues of σ.

4.1.2 Entanglement measures from the covariance matrix

From the symplectic eigenvalue spectra $\{\nu_k\}$ defined in Equation (4.5), one can define the von Neumann entropy $H(\rho)$ of the n-mode Gaussian state ρ as

$$H(\rho) = \sum_{k=1}^{n} g(\nu_k), \tag{4.6}$$

where $g(x) \equiv \left(\frac{x+1}{2}\right)\log\left(\frac{x+1}{2}\right) - \left(\frac{x-1}{2}\right)\log\left(\frac{x-1}{2}\right)$. The von Neumann entropy of the reduced state, for a bipartite state $\rho^{A,B}$, defines the *entropy of entanglement* which serves as a measure of the entanglement [135].

The symplectic eigenvalues, when evaluated for the partially transposed density matrix, can be used to characterize the conditions for separability (or rather the signature of the entanglement) for bipartite Gaussian quantum states [129, 130, 136, 137]. In fact, if a quantum state is separable, then its partial transpose is positive, and the positivity of the partial transpose serves as a necessary condition for its separability.

In the following, we discuss another quantitative measure of the entanglement known as the *logarithmic negativity* that can also be evaluated from the symplectic eigenvalues of the covariance matrix. For the sake of simplicity, let us consider the two-mode Gaussian state case ($n = 2$). In this case, the covariance matrix has the following form

$$\sigma = \begin{pmatrix} \alpha & \gamma \\ \gamma^T & \beta \end{pmatrix},$$

where $\alpha = \alpha^T, \beta = \beta^T$ and γ are all 2×2 real matrices. In this case, the two symplectic eigenvalues of the covariance matrix associated with its partial transpose $\tilde{\rho}$ are given by,

$$\nu_{\pm} = \sqrt{\frac{\tilde{\Delta}(\sigma) \pm \sqrt{\tilde{\Delta}(\sigma)^2 - 4\det(\sigma)}}{2}}, \tag{4.7}$$

where $\tilde{\Delta}(\sigma) = \det(\alpha) + \det(\beta) - 2\det(\gamma)$. If $\nu_<$ denotes the smaller of the two symplectic eigenvalues, then the necessary and sufficient condition for the corresponding quantum to be entangled is

$$\nu_< < \frac{1}{2}. \tag{4.8}$$

The associated quantitative measure of entanglement, the *logarithmic negativity* is given by $E_N = \max[0, -\ln(2\nu_<)]$ [138, 131].

4.1.3 Two-mode squeezed vacuum state

We now consider the *two-mode squeezed vacuum state* $|\xi\rangle$ that can be generated by applying the unitary two-mode squeezing operator

$$\hat{S}(\xi) = \exp\left(\xi \hat{a}^\dagger \hat{b}^\dagger - \xi^* \hat{a}\hat{b}\right), \tag{4.9}$$

on the two-mode vacuum state, i.e

$$|\xi\rangle = \hat{S}(\xi)|0,0\rangle, \tag{4.10}$$

where $\hat{a}$ and $\hat{b}$ denote the annihilation operators corresponding to the modes a and b, respectively.

The density matrix corresponding to this state can be written as $\rho = \hat{S}(\xi)|0,0\rangle\langle 0,0|\hat{S}^\dagger(\xi)$, where $\xi = re^{i\theta}$. The parameter r is called the squeezing parameter. The two symplectic eigenvalues are evaluated to be $\nu_{\pm} = e^{\pm 2r}/2$, and thus the quantum entanglement as quantified by the logarithmic negativity $E_N = 2r$ is proportional to the squeezing parameter r.

4.2 Optical amplifier and attenuator models

An optical amplifier can be modeled as a bath containing N two-level atoms where N_1 atoms are in the excited state while N_2 are in the ground state. Here $N_1 + N_2 = N$, and $N_1 > N_2$. Consider a single mode a of radiation (with annihilation and creation operators $\hat{a}$ and $\hat{a}^\dagger$, respectively) incident on the amplifier and in resonance with the atomic transition. We assume that width of the atomic transition is large, and also the bath of N atoms is maintained at the steady state [132, 139].

In the interaction picture, the evolution of the density operator ρ for the mode a can be described by the following master equation [132, 139, 140]

$$\frac{\partial \rho}{\partial t} = -\kappa N_1(\hat{a}\hat{a}^\dagger\rho - 2\hat{a}^\dagger\rho\hat{a} + \rho\hat{a}\hat{a}^\dagger) - \kappa N_2(\hat{a}^\dagger\hat{a}\rho - 2\hat{a}\rho\hat{a}^\dagger + \rho\hat{a}^\dagger\hat{a}). \tag{4.11}$$

In the above master equation, an input Gaussian state evolves into a Gaussian state, preserving its Gaussian character. The gain of the amplifier is written as $|G|^2 = \exp[2\kappa t(N_1 - N_2)]$. Moreover, it has been shown that under the condition $|G|^2 < \frac{2N_1}{N_1+N_2}$, both the squeezing and sub-Poisonnian statistics of an input state are preserved [141].

The optical amplifier described above adds quantum noise to the input field. As a result, the Heisenberg-like evolution equation for the mode a can be written as

$$a(t) = Ga(0) + f^\dagger, \tag{4.12}$$

where $f^\dagger$ represents the noise added by the amplifier with the noise correlations $\langle ff^\dagger\rangle = (1+\eta)(|G|^2 - 1)$ and $\langle f^\dagger f\rangle = \eta(|G|^2 - 1)$ that follow from the commutation-preserving relations. Here $\eta = \frac{N_2}{N_1 - N_2}$.

Let us now consider the two-mode case, for instance, the two-mode squeezed vacuum state $\hat{S}(\xi) = \exp\left(\xi\hat{a}^\dagger\hat{b}^\dagger - \xi^*\hat{a}\hat{b}\right)$, and subject *both* modes a and b to the optical amplifier with gain G. The associated mode transformation equations are

$$a \longrightarrow Ga + c^\dagger,\ b \longrightarrow Gb + d^\dagger. \tag{4.13}$$

The elements of the covariance matrix, as defined in Equation (4.4), can be obtained as [139]

$$\alpha = \beta = \frac{|G|^2\cosh 2r + (1+2\eta)(|G|^2 - 1)}{2}\begin{pmatrix} 1 & 0 \\ 0 & 1 \end{pmatrix}, \tag{4.14}$$

$$\gamma = \frac{1}{2}|G|^2\sinh 2r\begin{pmatrix} \cos\theta & \sin\theta \\ -\sin\theta & \cos\theta \end{pmatrix}. \tag{4.15}$$

which gives

$$\nu_< = \frac{|G|^2(e^{-2r} + (1+2\eta)) - (1+2\eta)}{2}. \tag{4.16}$$

For the output state to be an entangled state, i.e. $\nu_< < 1/2$, the gain of the amplifier must satisfy

$$|G|^2 < \frac{2}{(1+e^{-2r})} = \frac{2}{(1+e^{-E_N})}. \tag{4.17}$$

Note that in the limit $r \to \infty$, the above condition becomes $|G|^2 < 2$.

We now consider the case when *only one* mode (say a) is amplified, i.e. $a \longrightarrow Ga + c^\dagger,\ b \longrightarrow b$. In this case, the elements of the covariance matrix are given by

$$\alpha = \frac{|G|^2\cosh 2r + (1+2\eta)(|G|^2 - 1)}{2}\begin{pmatrix} 1 & 0 \\ 0 & 1 \end{pmatrix}, \tag{4.18}$$

$$\beta = \frac{\cosh 2r}{2}\begin{pmatrix} 1 & 0 \\ 0 & 1 \end{pmatrix}, \tag{4.19}$$

$$\gamma = \frac{1}{2}|G|^2\sinh 2r\begin{pmatrix} \cos\theta & \sin\theta \\ -\sin\theta & \cos\theta \end{pmatrix}. \tag{4.20}$$

We can then obtain the following lowest symplectic eigenvalue

$$\nu_< = \frac{1}{4}(|G|^2+1)\cosh 2r + (1+2\eta)(|G|^2-1) \\ -\sqrt{(|G|^2-1)^2(\cosh 2r+1+2\eta)^2 + 4|G|^2\sinh^2 2r}), \tag{4.21}$$

and find that $\nu_< < 1/2$ is satisfied for $\eta = 0$ (ideal amplification), i.e. the entanglement survives regardless of the value of the gain. For $\eta \neq 0$, however, there exists a threshold gain, and above this value of the gain, the entanglement disappears.

An attenuator which results in absorption of the radiation field can be described using the same model as above but with $N_2 > N_1$ in the master equation in Equation (4.11). The ideal attenuation corresponds to the case when $N_2 = N, N_1 = 0$. The Heisenberg-like evolution equation for the mode a can be written as

$$a(t) = Ta(0) + g,\ T(t) = e^{-i\omega t-\kappa t}, \tag{4.22}$$

where g represents the noise added by the amplifier with the noise correlation $\langle g(t)g^\dagger(t)\rangle = 1-|T(t)|^2$.

In this case, the elements of the covariance matrix can be obtained as

$$\alpha = \beta = \left(e^{-2\kappa t}\sinh^2 r + \frac{1}{2}\right)\begin{pmatrix}1 & 0\\ 0 & 1\end{pmatrix}, \tag{4.23}$$

$$\gamma = \frac{1}{2}e^{-2\kappa t}\sinh 2r\begin{pmatrix}-1 & 0\\ 0 & 1\end{pmatrix}, \tag{4.24}$$

which gives

$$\nu_< = \frac{1}{2}e^{-2\kappa t}(e^{-2r}+e^{2\kappa t}-1). \tag{4.25}$$

Here the eigenvalues $\nu_<$ are always less than $1/2$, implying that although both the amplifier and the attenuator add noise to the modes of the entangled light, the effect of the attenuator is less severe on the entanglement (or other non-classical properties) than is the amplifier's effect.

4.3 Propagation of Gaussian entangled state through noisy, lossy medium

4.3.1 Initial state—two mode squeezed vacuum

We consider quantum entanglement between different optical modes of radiation field, and denote the two modes of the field by a_0 and b_0. An optical parametric amplifier (OPA) produces two-mode squeezed vacuum states of the two modes a_0 and b_0, a prominent example of Gaussian entangled continuous-variable states.

After the two-mode squeezed vacuum state $|\xi\rangle = \exp\left(\xi\hat{a}_0^\dagger\hat{b}_0^\dagger - \xi^*\hat{a}_0\hat{b}_0\right)$ (where $|\xi\rangle = re^{i\theta}$) is generated by the OPA, one of the modes (say b_0) is retained, and we transmit the signal mode a_0 through a noisy environment (or atmosphere) toward a spatial region that may or may not contain a weakly reflecting target.

4.3.2 Propagation through noisy environment

We model the noisy environment as an attenuator with attenuation factor T, along with a classical noise A that represents the overall noise or turbulence in the atmosphere. When the signal mode a_0 is transmitted through an atmosphere, the signal mode is attenuated by the factor T, as shown in Figure 4.1.

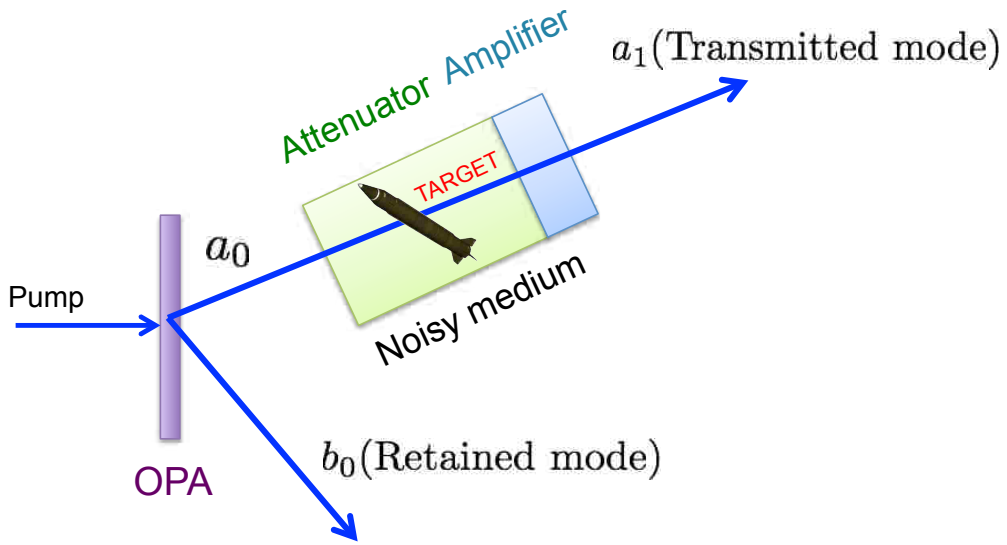

Figure 4.1: Schematic diagram of propagation of the signal mode through noisy medium. The signal mode a_0 propagates through through the noisy medium which is modeled by an attenuator, and to compensate the loss a phase-insensitive amplifier is used. The entanglement is calculated between the retained mode b_0 and the mode a_1 after propagation.

For such an attenuator with attenuation factor T and intrinsic noise g, we can write a Heisenberg-like evolution equation for the mode a_0 as

$$a_0(t) = Ta_0(0) + g(t), T(t) = e^{-i\omega t - \kappa t}, \tag{4.26}$$

$$\langle g(t)\rangle = 0, \langle g^\dagger(t)g(t)\rangle = 0, \langle g(t)g^\dagger(t)\rangle = 1 - |T(t)|^2. \tag{4.27}$$

If there is some additional ambient noise present in the medium, that further aggravates the loss of entanglement when an initially entangled state propagates through the medium. Let us denote such classical noise, which can represent the turbulence noise in atmosphere for instance, by A and assume that this noise is Gaussian in nature. Adding this noise to Equation (4.26), we can write

$$a_0'(t) = Ta_0(0) + g(t) + A. \tag{4.28}$$

The signal-to-noise ratio for the mode at the output of the attenuator further decreases due to this added noise. We will see in the next section (see Section 4.4) that it also degrades the entanglement of the quantum state being transmitted, and it is possible to provide a range of the tolerable noise from the information of the entanglement calculated between the transmitted mode and the retained mode.

As we model the atmosphere or the noisy environment with the attenuator, the input signal consisting of the two-mode squeezed vacuum $|\xi\rangle$ is affected by the loss and attenuation and eventually the signal itself is lost. For the sake of practical applications, one therefore needs to preserve the amplitude of the signal by employing optical amplifiers.

An optical amplifier, as the name suggests, amplifies the optical mode in the signal but also adds quantum noise to the signal. As a matter of fact, the optical amplifier adds more noise photons to the signal than the attenuator, affecting its non-classical characteristics in a more severe way than the attenuator. Hence, the amplifier with a gain G can be used to compensate the attenuation effects T (with $TG \approx 1$) to preserve the signal amplitude with the trade-off of having a more rapid decay of entanglement.

In the previous section (see Section 4.2), we have discussed the effects of such optical amplifiers on the entanglement of the Gaussian entangled states. Here in order to quantify the degradation of the entanglement affected by an optical amplifier (adding the quantum noise denoted by f) in conjunction with the attenuator, we first write the expression for the output mode

$$a_1 = G(Ta_0 + g + A) + f = TGa_0 + G(g + A) + f. \tag{4.29}$$

We use the logarithmic negativity (see Section 4.2) as the measure of the entanglement for the two-mode squeezed vacuum, and calculate the symplectic eigenvalues of the covariance matrix using Equation (4.29).

4.4 Covariance matrix and entanglement calculation

In the following, we calculate the entanglement (or the loss thereof) between the modes a_0 after propagation and the retained mode b_0 that will depend on the noise terms, depicting the loss of entanglement due to such propagation. In other words, the loss of entanglement (quantified by the logarithmic negativity) due to the propagation through the attenuator followed by the amplifier will have the signature of the noise present in the medium.

The signal mode a_0 that is propagated through the noisy medium satisfies the commutation relation $[a_0, a_0^\dagger] = 1$. The mean photon number in this mode is given by

$$\langle a_0^\dagger a_0 \rangle = \sinh^2 r, \tag{4.30}$$

while the correlation between the modes a_0 and b_0 is

$$\langle a_0 b_0 \rangle = \cosh r \sinh r e^{i\theta}, \tag{4.31}$$

r being the squeezing parameter.

The covariance matrix σ in the present case is a 4×4 real symmetric matrix which can be written as [132]

$$\sigma = \begin{pmatrix} A & 0 & B & C \\ 0 & A & C & -B \\ B & C & A' & 0 \\ C & -B & 0 & A' \end{pmatrix}, \tag{4.32}$$

where the lowest symplectic eigenvalue $\nu_<$ can be written as

$$\nu_< = \frac{1}{2}\left[(A + A') - \sqrt{(A - A')^2 + 4(B^2 + C^2)}\right]. \tag{4.33}$$

In order to evaluate the elements of the covariance matrix shown above, we first calculate $\langle a_1^\dagger a_1\rangle$ and $\langle a_1 a_1^\dagger\rangle$ for the transmitted mode a_1. From Equation (4.29), we obtain

$$\langle a_1^\dagger a_1\rangle = T^2G^2\langle a_0^\dagger a_0\rangle + (|G|^2-1) + |G|^2|A|^2, \tag{4.34}$$

$$\langle a_1 a_1^\dagger\rangle = T^2G^2\langle a_0 a_0^\dagger\rangle + (1-|T|^2) + |G|^2|A|^2, \tag{4.35}$$

which gives the elements of the covariance matrix as

$$\sigma_{11} = \frac{1}{2}\left[T^2G^2\cosh 2r + |G|^2(1+2|A|^2) - |T|^2\right] = \sigma_{22}, \tag{4.36}$$

$$\sigma_{12} = \sigma_{21} = \sigma_{34} = \sigma_{43} = 0, \tag{4.37}$$

$$\sigma_{13} = \sigma_{31} = \frac{TG\sinh 2r\cos\theta}{2}, \tag{4.38}$$

$$\sigma_{14} = \sigma_{41} = \frac{TG\sinh 2r\sin\theta}{2}, \tag{4.39}$$

where $\sigma_{ij} = \frac{1}{2}\langle(X_iX_j + X_jX_i)\rangle - \langle X_i\rangle\langle X_j\rangle$ for the quadratures X_i and X_j (see Section 4.3) of the two modes a_1 and b_0. Thus,

$$A = \frac{1}{2}\left[T^2G^2\cosh 2r + |G|^2(1+2|A|^2) - |T|^2\right], \tag{4.40}$$

$$A' = \frac{\cosh 2r}{2}, B = \frac{TG\sinh 2r\cos\theta}{2}, C = \frac{TG\sinh 2r\sin\theta}{2}. \tag{4.41}$$

The lowest symplectic eigenvalue is $\nu_<$ is evaluated as

$$\nu_< = \frac{1}{2}\left[\frac{(T^2G^2+1)\cosh 2r + F}{2} - \sqrt{\left(\frac{(T^2G^2-1)\cosh 2r + F}{2}\right)^2 + T^2G^2\sinh^2 2r}\right], \tag{4.42}$$

where the combined effect of the noise is given by the noise term

$$F = |G|^2(1+2|A|^2) - |T|^2. \tag{4.43}$$

The expression of $\nu_<$ in Equation (4.42) serves as a measure of the entanglement between the optical modes a_1 after propagation and the retained mode b_0, and it also yields information about the noisy environment as described below. In this sense, using the entanglement calculation, we can provide a precise way of probing (or remote mapping) noisy medium.

The effect of the classical noise A on the entanglement is depicted in Figure 4.2, where one can see that the entanglement measure $\nu_<$ is plotted as a function of the gain $|G|^2$ of the amplifier for a fixed value of the attenuation $|T|^2 = 0.5$. We see that the entanglement decreases as the value of the classical noise $|A|^2$ is increased from $|A|^2 = 0$ (no classical noise) to $|A|^2 = 0.3$. The solid red line marks the value of $\nu_< = 1/2$ beyond which the entanglement between the modes a_1 and b_0 vanishes. Larger values of the noise $|A|^2$ results in more rapid decay of entanglement.

In Figure 4.3, we plot the entanglement measure $\nu_<$ as a function of the squeezing parameter r for different classical noise values keeping the attenuation factor the same $|T|^2 = 0.5$. The plots in this figure also reflects the detrimental effects of the noise $|A|^2$ on the entanglement.

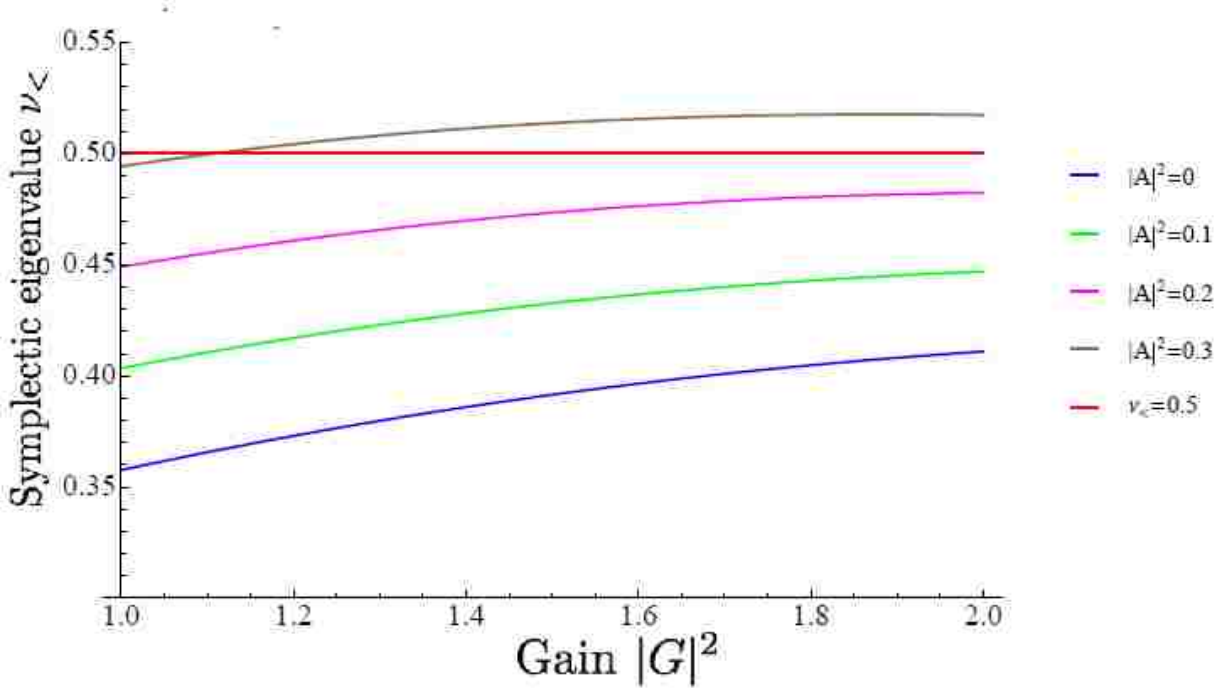

Figure 4.2: Plot of the eigenvalue $\nu_<$ as a function of the gain $|G|^2$ of the amplifier. We show the variation of $\nu_<$ for different values of the classical noise $|A|^2$. As the value of $|A|^2$ increases, the entanglement between the optical modes starts to disappear faster.

We also compare the results of the entanglement for one attenuator without any amplifier, (i.e., $|G| = 1$) and with the ones where amplifier is used to compensate the effect of the loss on the signal amplitude (by making the approximation $|T||G| = 1$). These results are plotted in Figure 4.4, where we can see that although adding an amplifier to the attenuator is important for practical purposes, it affects the entanglement between the optical modes in a more severe way than the attenuator. The solid red line marks the value of $\nu_< = 1/2$ beyond which, thus providing a reference for the comparing the plots in the figure. Note that $|T|^2 = \exp(-2\kappa t)$ can be varied from 0 to 1.

Since presence of noise, be it the intrinsic quantum noise of the amplifiers or the attenuators or the classical turbulence noise, is generally unavoidable in most practical applications, one might also be interested in determining the allowable ranges of the classical noise for a given attenuation (or vice versa) for preserving a given entanglement in order to maintain its usefulness in the presence of such noise. In other words, the entanglemenet can be regarded as a probe for the noise present in the medium. Using the contour plot in Figure 4.5, we show that it is possible to provide an estimate for the range of noises $|T|^2$ and $|A|^2$ one can allow for the transmission of the signal mode through the noisy atmosphere.

In Figure 4.6, we compare the variations of the entanglement measure $\nu_<$ for different values of the initial entanglement (i.e. different values of the squeezing parameter r). Higher values of r imply higher initial entanglement (note that $E_N = 2r$ initially, i.e. initial entanglement is proportional to r), and we find that if one starts with higher values of squeezing parameter r, a larger classical noise $|A|^2$ can be tolerated before the output state becomes

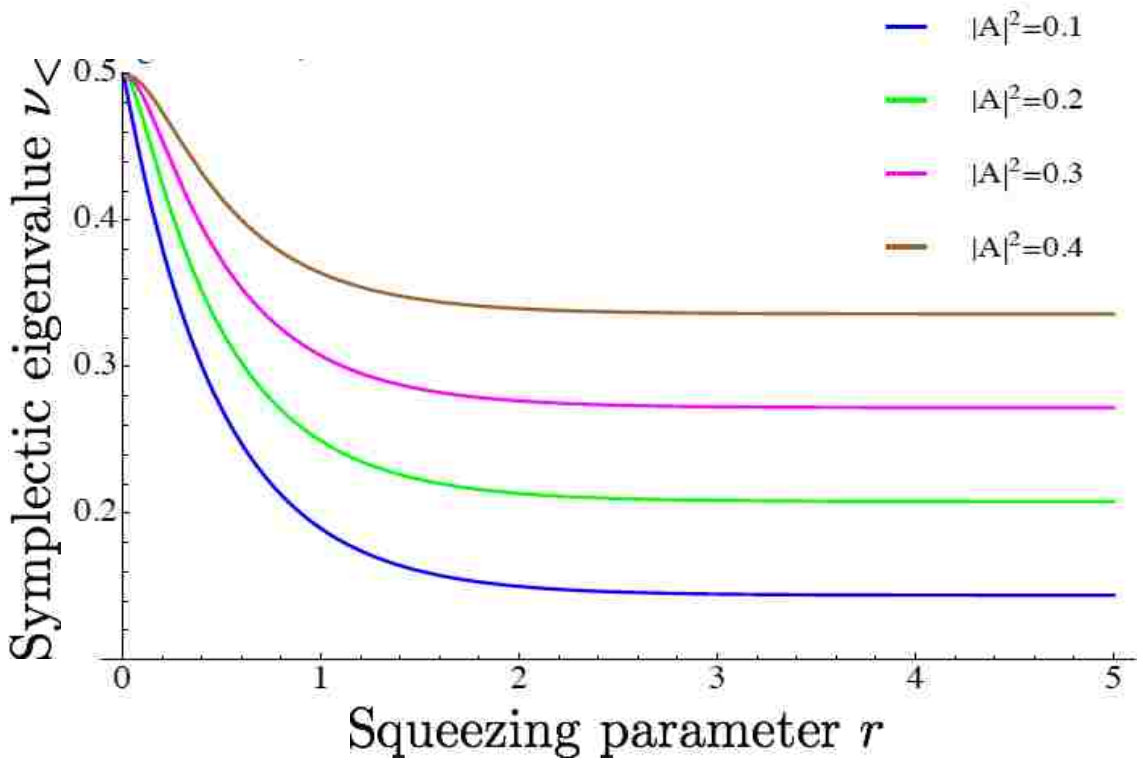

Figure 4.3: Plot of the eigenvalue $\nu_<$ for different values of the classical noise $|A|^2$. We plot $\nu_<$ as a function of the squeezing parameter r for different values of classical noise $|A|^2$ with the same $|T|^2 = 0.5$.

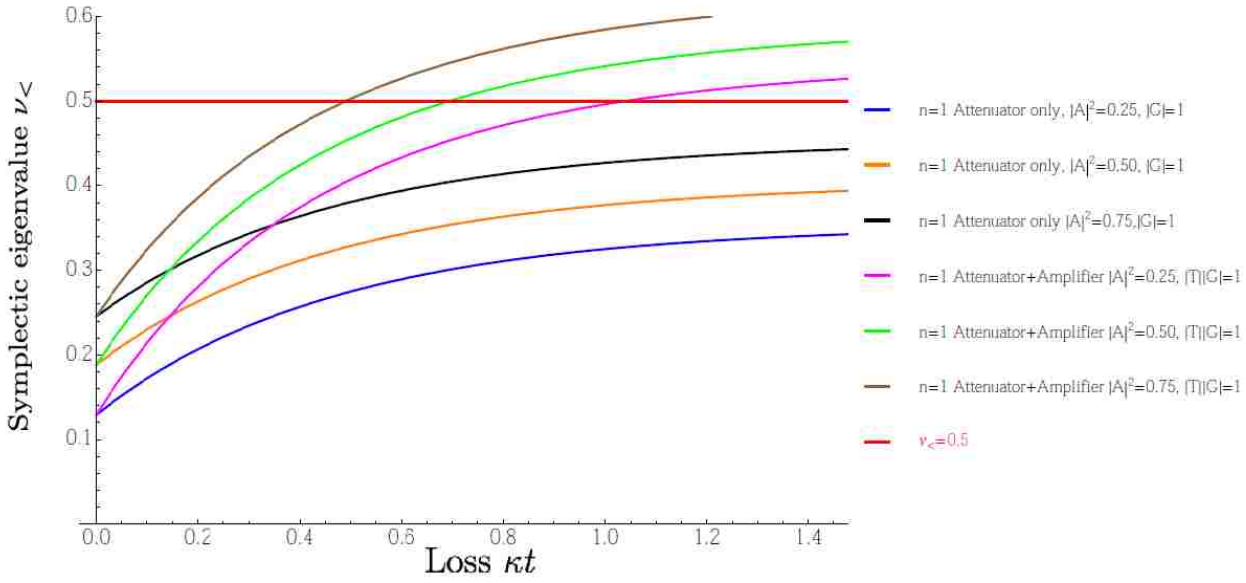

Figure 4.4: Plot of the eigenvalue $\nu_<$ without and with optical amplifier for different noise. We compare $\nu_<$ for r=1, without any amplifier and with optical amplifier for different values of the classical noise $|A|^2$.

unentangled. The solid brown line marks the $\nu_< = 1/2$, beyond which the entanglement disappears.

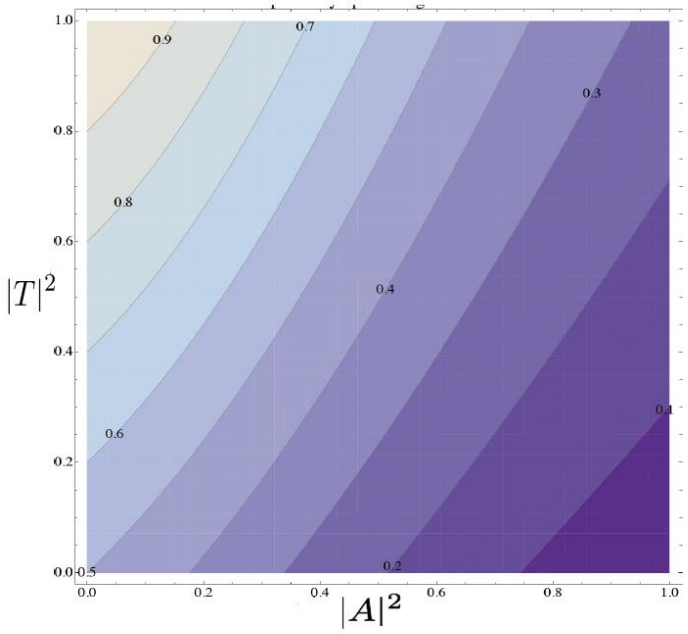

Figure 4.5: Contour plot of the eigenvalue $\nu_<$ for different noise with fixed $r = 1.5$. We plot $\nu_<$ as a function of the classical noise $|A|^2$ and the attenuation $|T|^2$ for the squeezing parameter $r = 1.5$.

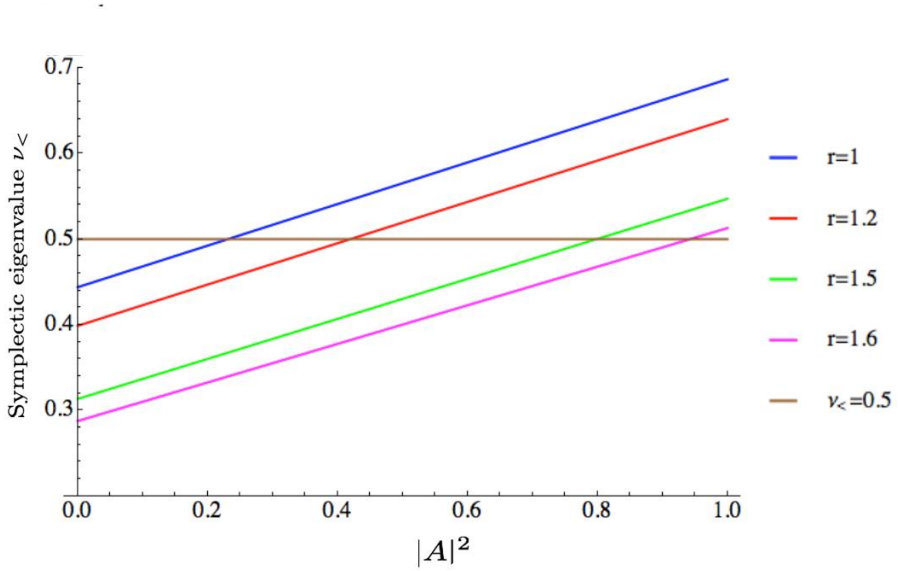

Figure 4.6: Eigenvalue $\nu_<$ for different values of the squeezing parameter r.

4.5 Entanglement as a tool for target detection

In the above we showed how the entanglement calculation can be useful for providing an estimate of the noise and losses in the medium through which the signal mode has been propagated. In the following, we show how we can exploit this information about the entanglement to detect the presence of an object. The conventional way to detect the presence of an object to shine light (coherent laser source) in the direction where the object is likely to be present and to see if any light is reflected off. Lloyd *et al.* showed that using entangled photons in such scenario can provide substantial advantage, despite the complete loss of entanglement in a highly lossy and noisy medium, over the unentangled or coherent light [142, 143]. This is also known as quantum illumination where it is possible to get significant improvement in the signal-to-background noise ratio in detecting a target embedded in the noisy medium.

In a typical setup for target detection using entangled light, an entangled state is prepared with a signal photon and an ancilla photon, and the signal photon is used only to detect the target, while the ancilla photon is retained. If the target is immersed in noise or thermal radiation, the signal photon will be affected by such noise and as a result, entanglement between the signal photon and the ancilla photon will be significantly deteriorated. When we detect the signal photon at the detector, the final entanglement between the detected signal photon and the retained ancilla photon will carry all the information about the noisy environment as well the information regarding whether the object is present or not. In this sense, entanglement can be used as a direct measure of the presence of the target, despite the presence of entanglement-destroying loss and noise.

The intuitive reason behind the enhancement of sensitivity for photon counting, according to the References [142, 143], is that if the signal is entangled with the ancilla, then it is harder for the noise to masquerade as the returning signal. This intuition turns out to be correct in our case too, as we argue in the following, with the calculation of final entanglement between the modes at the detector even though the noise and loss completely destroy the entanglement; hence it also can justify one's choice of using entangled Gaussian state over conventional light for the purpose of precise detection of the target.

After transmitting the signal mode a_0 through the noisy environment modeled by the attenuator (and followed by the amplifier to compensate the loss), the output mode a_1 given by Equation (4.29). For the attenuation factor $T = 0$, we see that the signal is lost in the noisy medium, and we get only the (amplified) noise at the output. In other words, the initial entanglement is completely lost which is also reflected in the following covariance matrix

$$\sigma_{T=0} = \frac{1}{2}\begin{pmatrix} (1+2|A|^2) & 0 & 0 & 0 \\ 0 & (1+2|A|^2) & 0 & 0 \\ 0 & 0 & \cosh 2r & 0 \\ 0 & 0 & 0 & \cosh 2r \end{pmatrix}, \tag{4.44}$$

when we consider propagation through the attenuator, without the amplifier (using amplifier merely adds one constant factor in the diagonal terms as can be seen from Equation (4.29)). Note that the off-diagonal terms in the covariance matrix disappear in this case implying the complete loss of entanglement. This corresponds to the case of the presence of the target in the medium when only the noise photons arrive at the detector. While for the $T \neq 0$ case, the non-zero off-diagonal terms effectively carry the signature of the cross-correlations present between the mode a_1 after propagation and the retained idler mode b_0. The latter

case, i.e. $T \neq 0$, corresponds to when the entanglement is still present between these two modes, and the total signal at the detector consists of the signal and the noise. For $T = 0$, however, since all the entanglement present in the initial two-mode squeezed vacuum state is lost, the output signal at the detector consists of only noise photons. Furthermore, we can expect intuitively the entanglement reduces as $|T|^2 \neq 0$ decreases.

In Figure 4.7, we plot the entanglement measure $\nu_<$ as a function of the squeezing parameter r for different values of $|T|^2$ (with same classical noise $|A|^2$). The solid red line corresponds to $|T|^2 = 0$, while the initial entanglement between the modes a_0 and b_0 is also plotted for comparison as the solid blue line. For $T = 0$, we see that $\nu_<$ is always greater than $1/2$ regardless of the value of the squeezing parameter r, i.e., the output mode is no longer entangled with the retained mode even if we start with a highly entangled initial state. In this sense, the entanglement measure $\nu_<$ can be considered to carry a signature of the absence or the presence of the target.

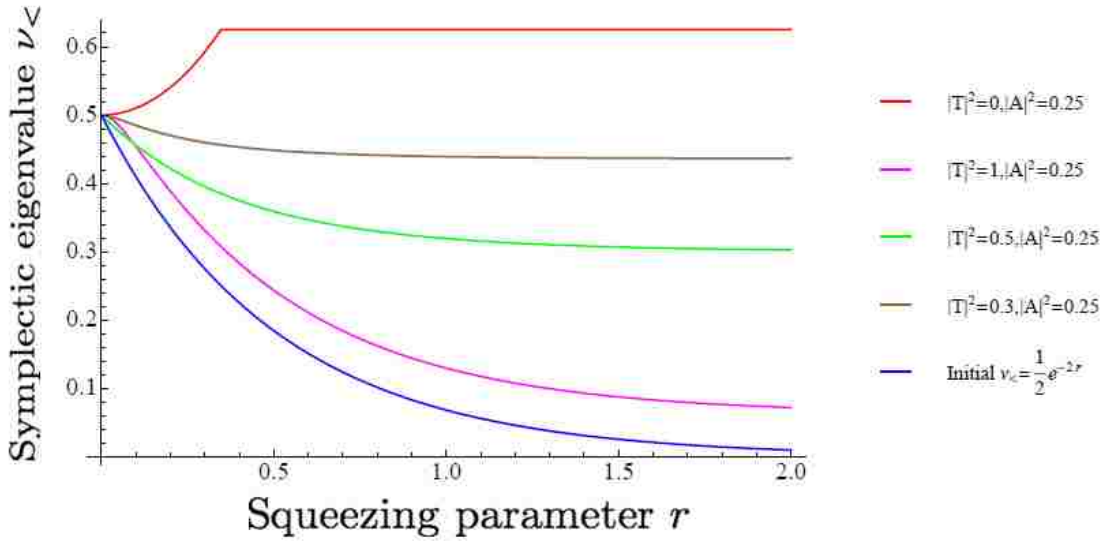

Figure 4.7: Entanglement as a tool for target detection . We plot the variation of the symplectic eigenvalue $\nu_<$ as a function of the squeezing parameter r for different $|T|^2$. The solid red line marks the $T = 0$, that corresponds to the no target case where all the entanglement has been lost, i.e. $\nu_< > 1/2$ for all values of r.

4.6 Conclusion

In this chapter, we have discussed how the optical amplifiers and attenuators affect the entanglement properties of Gaussian entangled state by adding quantum noise to the state propagating through them. The detrimental effects of the added noise is shown in terms of the entanglement measure known as the logarithmic negativity that follows from the well-studied covariance matrix (or symplectic) formalism for general Gaussian continuous variable quantum states.

We considered a noisy medium that has been modeled by an attenuator followed by an optical amplifier to compensate the loss, and analyzed the loss of entanglement for the two-mode squeezed vacuum state using a necessary and sufficient condition for the entanglement to be present. We showed how the loss of entanglement in such a noisy medium can be

used to predict the absence or presence of a target embedded in the medium. However, this proposed scheme to detect the target requires, in principle, reconstruction of the covariance matrix which can be implemented, for example, by means of a single homodyne detector [144]. This is in contrast to the case analyzed by Shapiro *et al.* where the quantum target detection problem is considered to be a quantum binary hypothesis testing problem by performing joint quantum measurement on the received states at the detector [143, 145]. In both cases, however, we note that the non-classical cross-correlation signature between the modes can effectively be exploited to distinguish between the presence or absence of such a target. Furthermore, we also showed that the entanglement calculation can be useful to provide an estimate of the tolerable noise for a given entanglement to be preserved.

Chapter 5
Noisy quantum channels and limits on the rate of communication [1]

Any communication system aims to transfer information reliably from one point to another. Such transfer of information is typically done by modulating the information into an electromagnetic wave (carrier), which is then transmitted through a noisy communication channel. The receiver, upon receiving the signal, demodulates the received state in order to recover the information sent. In reality, however, noise present in the communication channels limit the performance of such communication systems based on electromagnetic wave propagation. Hence, determining the information-carrying capacity of noisy quantum communication channels is of practical relevance.

A quantum model for optical communication systems (e.g., the ones that are based on fiber or free-space communication) is provided by the lossy bosonic channels, where the modes of the electromagnetic field are used as the information carrier interacting with thermal-like noisy environments. Gaussian bosonic channels are used to represent realistic models of noise in many communication protocols [146, 6, 147], and in this chapter we will consider the transmission of classical messages through such channels.

For the last few decades, extensive efforts have been put in the field of quantum information theory to investigate the ultimate limits on reliable communication through noisy quantum communication channels. In quantum information theory, the classical capacity of a quantum channel is the maximum rate at which a sender can transmit classical messages over the quantum channel such that the error probability decreases to zero in the limit of many independent uses of the channel. This notion of the classical capacity is inspired by the Shannon's seminal work [5] that established the capacity theorem for a classical channel. Holevo, Schumacher, and Westmoreland (HSW) later proved that a quantum generalization of Shannon's formula characterizes the capacity of a quantum channel [6, 7]. Many of the open questions in quantum information, quantum communication, and quantum optics communities revolve around identifying a tractable formula for the capacity of quantum communication channels.

The above definition of the classical capacity suggests that (a) for any rate below capacity, one can communicate error free in the limit of many channel uses, and (b) there cannot exist an error-free communication scheme in the limit of many channel uses when the rate of communication exceeds the capacity. However, this definition leaves open the possibility to increase the communication rate R by allowing for some error $\varepsilon > 0$, whenever the rate R exceeds the capacity. Leaving room for the possibility of such a trade-off between the rate R and the error ε is the hallmark of a "weak converse," and the corresponding capacity is some-

[1] Parts of this chapter previously appeared as B. Roy Bardhan and M. M. Wilde, Physical Review A **89**, 022302 (2014) (Copyright(2014) American Physical Society) [158] and B. Roy Bardhan, R. Garcia-Patron, M. M. Wilde, and A. Winter, Proceedings of IEEE International Symposium on Information Theory (ISIT), pages 726-730 (2014)(Copyright(2014) IEEE) [159]. They are reprinted by permission from the publishers See Appendix C for details.

times called the weak capacity. A *strong converse*, on the contrary, establishes the capacity as a very sharp threshold, so that there is no such room for a trade-off between rate and error in the limit of many independent uses of the channel. The strong converse thus guarantees that the error probability of any communication scheme asymptotically converges to one if its rate exceeds the classical capacity. A conceptual illustration of this idea is provided in Figure 5.1, where we also demonstrate the achievability of the rate of communication and the weak converse part. Note that this plot should be interpreted in the limit of large n where n is the number of channel uses.

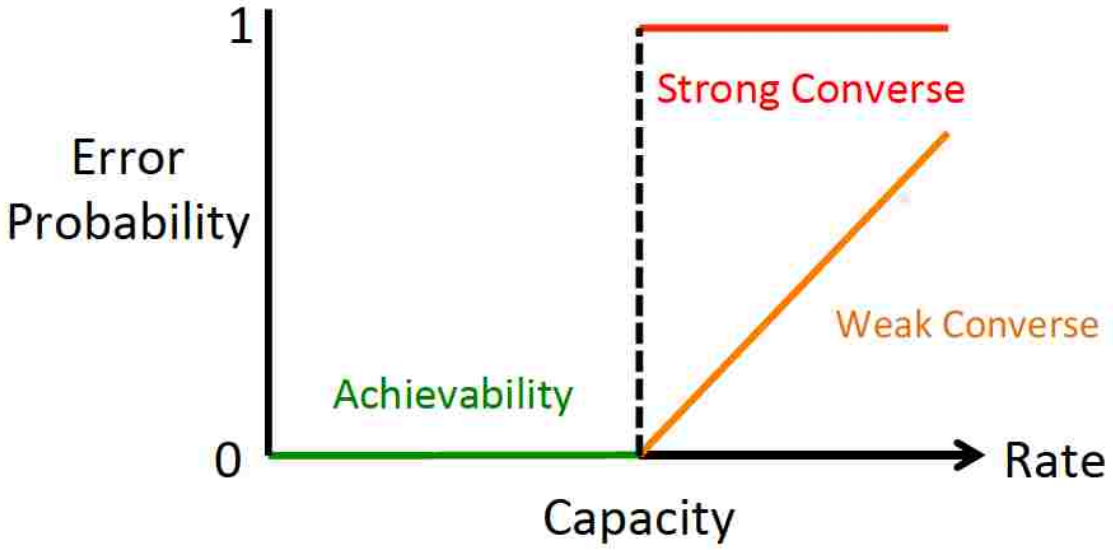

Figure 5.1: Weak versus strong converse for communication through quantum channels. Here, we illustrate the idea that the error probability converges to one in the limit of many channel uses if a communication rate corresponds to a strong converse rate, whereas establishing a communication rate as a weak converse rate suggests that there exists room for a trade-off between communication rate and error proability. Achievable rates are such that there exists a communication scheme whose error probability converges to zero in the limit of many channel uses.

Despite their significance in understanding the ultimate information-carrying capacity of noisy communication channels, strong converse theorems are known to hold only for a handful of quantum channels [148, 149, 150]. Strong converse theorems have been shown to hold for quantum memoryless channels with classical inputs and quantum outputs [151, 152]. Recently, a strong converse theorem has been proved to hold for the classical capacity of the pure-loss bosonic channel [153]. These studies have provided an estimate of the communication rate for the respective channels above which it is not possible to transmit reliably the messages from the sender to the receiver of the channel. The strong converse results are also helpful in establishing the security for particular models of cryptography in which the eavesdropper is limited to having noisy storage [154].

In this chapter, we consider the transmission of classical messages through phase-insensitive Gaussian channels. These channels are considered to be the most practically relevant models to describe free space or optical fiber transmission, or transmission of classical messages through dielectric media, etc. The recent works in References [155, 156] have established the exact expressions of the classical capacities of these channels under the constraint on the

mean photon number of the input signal states. For instance, consider the thermal noise channel represented by a beamsplitter with transmissivity $\eta \in [0,1]$ mixing signaling photons (with mean photon number N_S) with a thermal state of mean photon number N_B. The results in References [155, 157, 156] imply that the classical capacity of this channel is

$$g(\eta N_S + (1-\eta)N_B) - g((1-\eta)N_B), \tag{5.1}$$

where $g(x) \equiv (x+1)\log_2(x+1) - x\log_2 x$ is the entropy of a bosonic thermal state with mean photon number x. However, the corresponding converse theorem, which can be inferred as a further implication of their work, is only a weak converse, in the sense that the upper bound on the communication rate R of any coding scheme for the thermal noise channel can be written as

$$R \leq \frac{1}{1-\varepsilon}[g(\eta N_S + (1-\eta)N_B) - g((1-\eta)N_B) + h_2(\varepsilon)],$$

where ε is the error probability, and $h_2(\varepsilon)$ is the binary entropy with the property that $\lim_{\varepsilon\to 0} h_2(\varepsilon) = 0$. That is, only in the limit $\varepsilon \to 0$ the above expression serves as the classical capacity of the channel, leaving room for a possible trade-off between rate and error probability. We prove a strong converse theorem for the classical capacity of all phase-insensitive Gaussian channels that completely rules out such possibility of trade-off guaranteeing that the success probability of correctly decoding the transmitted message asymptotically converges to zero when the rate of communication exceeds the capacity of such channels.

This chapter is structured as follows. First, we present a brief review of bosonic Gaussian channels, and specify the capacities of a few canonical bosonic Gaussian channels in Section 5.1. In Section 5.2, we review some preliminary ideas and notations on the classical capacity of noisy bosonic quantum channels. Section 5.3 contains our main result that the strong converse property holds for the capacity of noisy bosonic Gaussian channels when imposing a maximum photon number constraint on the signal photon states. We then conclude this chapter with a brief summary and a few potential applications of our results.

5.1 Noisy Bosonic Channel Models

Bosonic Gaussian channels play a very significant role in modeling optical communication channels that rely on optical fibers or free space transmission. In general, an N mode bosonic channel can be represented by N quantized modes of the electromagnetic field in a tensor-product Hilbert space $\mathcal{H}^{\otimes N} = \otimes_{k=1}^{N}\mathcal{H}_k$ with N pairs of bosonic field operators $\{\hat{a}_k, \hat{a}_k^\dagger\}$ $(k = 1, \ldots, N)$. These bosonic field operators $\hat{a}_k$ and $\hat{a}_k^\dagger$ are known as the annihilation and the creation operators of the k th mode of the field, respectively.

In the following discussion, we will restrict ourselves to memoryless Gaussian channels, in which each mode of the field transmitted through the noisy channel is affected independently and identically with respect to each other. This simplifies the description of the channel in the sense that it is now sufficient to consider the individual modes of the field resulting in a single-mode description of the noisy communication channel. However, the corresponding multi-mode descriptions of the same channel can be constructed from tensor-product structures using the single-mode channels.

Bosonic Gaussian channels are represented by completely positive and trace preserving (CPTP) maps and they evolve Gaussian input states into Gaussian output states [160, 146, 161]. We note that a Gaussian state (e.g., the vacuum state or the thermal state) is completely characterized by a mean vector and a covariance matrix [160]), which are necessarily the first

and second moments of the quantum state $\hat{\rho}$ representing the Gaussian state. Since it is easy to characterize the Gaussian states in this manner, it turns out that the action of the Gaussian channels on such states are also easy to describe. Single-mode Gaussian channels are characterized by two matrices X and Y acting on the covariance matrix Γ of a single-mode Gaussian state in the following way:

$$\Gamma \longrightarrow \Gamma' = X\Gamma X^T + Y, \tag{5.2}$$

where X^T is the transpose of the matrix X. Here X and Y are both 2×2 real matrices, and in order for the map to be a CPTP map, they must satisfy

$$Y \geq 0, \qquad \det Y \geq (\det X - 1)^2.$$

A bosonic Gaussian quantum channel is said to be 'quantum-limited' if the above inequality (involving $\det X$ and $\det Y$) is saturated [162, 163, 155, 156].

Phase-insensitive Gaussian channels are invariant with respect to phase space rotations [164, 161, 147, 163], and they are considered to be one of the most practically relevant models to describe free space or optical fiber transmission, or transmission of classical messages through dielectric media, etc. In fact, phase-insensitive Gaussian channels constitute a broad class of noisy bosonic channels, encompassing all of the following: thermal noise channels, additive noise channels , and noisy amplifier channels [164, 155, 156, 165]. In general, the phase-insensitive channels can be characterized by the following matrices

$$\begin{aligned} X &= \mathrm{diag}\left(\sqrt{\tau}, \sqrt{\tau}\right), \\ Y &= \mathrm{diag}\left(\nu, \nu\right), \end{aligned} \tag{5.3}$$

with $\tau, \nu \geq 0$ obeying the constraint above. The action of such phase-insensitive channels on an input signal mode can be uniquely described by their transformation of the symmetrically ordered characteristic function, defined as

$$\chi(\mu) \equiv \mathrm{Tr}[\rho D(\mu)], \tag{5.4}$$

where $D(\mu) \equiv \exp(\mu\hat{a}^\dagger - \mu^*\hat{a})$ is the displacement operator for the input signal mode $\hat{a}$ [160]. For the Gaussian channels, the transformed characteristic function at the output is given by $\chi'(\mu) = \chi(\sqrt{\tau}\mu)\exp(-\nu\left|\mu\right|^2/2)$ [156, 155, 146].

In the following, we discuss some examples of phase-insensitive Gaussian channels.

5.1.1 Thermal noise channel

For the thermal noise channel, the environmental mode $\hat{b}$ is in the thermal state, i.e., an isotropic Gaussian mixture of coherent states with average photon number $N_B > 0$. In the number state representation, the density matrix of the thermal state ρ_b can be written as

$$\rho_b = \int d^2\alpha \frac{\exp(-|\alpha|^2/N_B)}{\pi N_B} |\alpha\rangle\langle\alpha| = \frac{1}{(N_B+1)} \sum_{l=0}^{\infty} \left(\frac{N_B}{N_B+1}\right)^l |l\rangle\langle l|. \tag{5.5}$$

The interaction of signal photons with the thermal channel $\mathcal{E}_{\eta,N_B}$ can be modeled by a beamsplitter of transmissivity η coupling the signal with a thermal state with mean photon number N_B. The parameter $\eta \in [0,1]$ of the beamsplitter characterizes the fraction of input

photons that make it to the output on average. The special case $N_B = 0$ (zero-temperature reservoir) corresponds to the pure-loss bosonic channel $\mathcal{E}_{\eta,0}$, in which each input photon has probability η of reaching the output.

The beamsplitter transformation corresponding to the thermal channel can be written as the following Heisenberg-like evolution of the signal mode $\hat{a}$ and the environmental mode $\hat{b}$:

$$\begin{aligned} \hat{a} &\longrightarrow \sqrt{\eta}\hat{a} + \sqrt{1-\eta}\hat{b} \\ \hat{b} &\longrightarrow \sqrt{\eta}\hat{b} - \sqrt{1-\eta}\hat{a}. \end{aligned} \tag{5.6}$$

The unitary evolution operator U for the above transformation is given by the following matrix $U := \begin{pmatrix} \sqrt{\eta} & \sqrt{1-\eta} \\ -\sqrt{1-\eta} & \sqrt{\eta} \end{pmatrix}$. Tracing out the environmental mode $\hat{b}$ from it yields the CP map $\mathcal{E}_{\eta,N_B}$ for the thermal noise channel

$$\mathcal{E}_{\eta,N_B} = \mathrm{Tr}_{\hat{b}}\left[U(\rho_a \otimes \rho_b)U^\dagger\right], \tag{5.7}$$

where ρ_a and ρ_b correspond to the input state and the environmental thermal state, respectively, and ρ_b is given by Equation (5.5).

The vacuum state at the input of the thermal channel produces a thermal output state given by

$$\mathcal{E}_{\eta,N_B}(|0\rangle\langle 0|) = \frac{1}{((1-\eta)N_B + 1)}\left(\frac{(1-\eta)N_B}{(1-\eta)N_B + 1}\right)^{\hat{a}^\dagger\hat{a}}. \tag{5.8}$$

5.1.2 Additive noise channel

The additive noise channel is another example of a noisy bosonic channel, which is given by the following completely-positive (CP) map:

$$\mathcal{N}_{\bar{n}}(\rho) = \int d^2\alpha P_{\bar{n}}(\alpha) D(\alpha)\rho D^\dagger(\alpha), \tag{5.9}$$

where $P_{\bar{n}}(\alpha) = \frac{\exp\left(-|\alpha|^2/\bar{n}\right)}{\pi\bar{n}}$, and $D(\alpha) = \exp(\alpha\hat{a}^\dagger - \alpha^*\hat{a})$ is the displacement operator for the input signal mode $\hat{a}$. $P_{\bar{n}}(\alpha)$ the Gaussian probability distribution representing a random displacement of the signal mode $\hat{a}$ in phase space. For this channel, a classical Gaussian noise is superimposed on the signal mode, resulting in the displacement in phase space.

The variance $\bar{n}$ of this distribution, that characterizes the additive noise channel $\mathcal{N}_{\bar{n}}$, represents the number of noise photons added to the mode $\hat{a}$ by the channel [166]. For $\bar{n} = 0$, the CP map in Equation (5.9) becomes the identity channel, while for $\bar{n} > 0$, noise photons are injected into the channel.

The additive noise channel $\mathcal{N}_{\bar{n}}$ on a vacuum-state input $|0\rangle$ produces a thermal-state output

$$\mathcal{N}_{\bar{n}}(|0\rangle\langle 0|) = \frac{1}{\bar{n}+1}\left(\frac{\bar{n}}{\bar{n}+1}\right)^{\hat{a}^\dagger\hat{a}}. \tag{5.10}$$

Note that the additive noise channel can be obtained from the thermal noise channel in the limit $\eta \to 1$ and $N_B \to \infty$, with $(1-\eta)N_B \to \bar{n}$ [167].

5.1.3 Noisy amplifier channel

The noisy amplifier channel is a widely used model in optical communication— it is not only extensively used to model noisy communication when the channel provides gain to the signal amplitude at the cost of added quantum noise, but also to model the optical parametric amplifier used in various practical receivers.

The amplifier channel $\mathcal{A}_G^N$ is characterized by its gain $G \geq 1$ and the mean number of photons N in the associated ancilla input mode (which is in a thermal state). The corresponding CPTP map for this channel can be obtained from the following commutator-preserving phase-insensitive amplifier mode transformation relation [162]

$$\hat{c} = \sqrt{G}\hat{a} + \sqrt{G-1}\hat{b}^\dagger, \tag{5.11}$$

where $\hat{b}$ is the modal annihilation operator for the noise injected by the amplifier. The amplifier channel $\mathcal{A}_G^N$ is called quantum-limited when the environment is in its vacuum state (we will denote such a quantum-limited amplifier by $\mathcal{A}_G^0$). This is the case when the minimum possible noise is introduced by the amplifier to the signal since the environment mode is in the vacuum state.

The transformed characteristic functions for the above Gaussian channels in phase-space are given by the following expressions [157, 167, 165]

$$\chi'(\mu) = \begin{cases} \chi(\sqrt{\eta}\mu)e^{-(1-\eta)(N_B+1/2)|\mu|^2} & \text{for } \mathcal{E}_{\eta,N_B} \\ \chi(\mu)e^{-\bar{n}|\mu|^2} & \text{for } \mathcal{N}_{\bar{n}} \\ \chi(\sqrt{G}\mu)e^{-(G-1)(N+1/2)|\mu|^2} & \text{for } \mathcal{A}_G^N. \end{cases} \tag{5.12}$$

5.1.4 Structural decompositions

Any phase-insensitive Gaussian bosonic channel $\mathcal{P}$ can be written as a concatenation of a pure-loss channel followed by a quantum-limited amplifier channel [168, 164],

$$\mathcal{P} = \mathcal{A}_G^0 \circ \mathcal{E}_{\eta,0}, \tag{5.13}$$

where $\mathcal{E}_{\eta,0}$ is a pure-loss channel with parameter $\eta \in [0,1]$ and $\mathcal{A}_G^0$ is a quantum-limited amplifier whose gain $G \geq 1$. We can note that for the above decomposition rule, $\tau = \eta G$ and $\nu = G(1-\eta) + G - 1$ (with τ and ν defined in (5.3)).

For instance, the additive noise channel $\mathcal{N}_{\bar{n}}$ can be viewed as a cascade of a pure-loss channel with transmissivity $\eta = 1/(\bar{n}+1)$ followed by a quantum-limited amplifier channel whose gain $G = \bar{n}+1$ exactly compensates for the loss, i.e.

$$\mathcal{N}_{\bar{n}}(\rho) = (\mathcal{A}^0_{\bar{n}+1} \circ \mathcal{E}_{\frac{1}{\bar{n}+1},0})(\rho), \tag{5.14}$$

Also, we can consider the thermal noise channel $\mathcal{E}_{\eta,N_B}$ as a cascade of a pure-loss channel with transmissivity $\eta' = \eta/G'$ followed by a quantum-limited amplifier channel with gain $G' = (1-\eta)N_B + 1$, i.e.

$$\mathcal{E}_{\eta,N_B}(\rho) = (\mathcal{A}^0_{(1-\eta)N_B+1} \circ \mathcal{E}_{\eta',0})(\rho). \tag{5.15}$$

Appendix B contains details on how the above structural decompositions can be obtained by considering the action of the channels on the covariance matrix Γ.

5.1.5 Capacitiies of noisy phase-insensitive Gaussian channels

For a single-mode pure-loss bosonic channel (where the environmental mode is in the vacuum state) when the sender is constrained to use at most N_S photons on average per use of the channel, the capacity is given by $g(\eta N_S)$ [169], where

$$g(x) \equiv (x+1)\log_2(x+1) - x\log_2(x) \tag{5.16}$$

denotes the entropy of a bosonic thermal state with average photon number x. The above capacity has shown to be achievable with coherent-state encoding with a constraint on the mean number of photons per use of the channel [169].

The recent breakthrough works in References [155, 156] have provided a solution to the long-standing minimum output entropy conjecture [147, 167] for all phase-insensitive Gaussian channels, showing that the minimum output entropy for such channels is indeed achieved by the vacuum input state, i.e., $H[\mathcal{P}(|0\rangle\langle 0|)] \leq H[\mathcal{P}(\rho)]$ for every ρ, where $H(.)$ is the von Neumann entropy. As a major implication of this work, the expressions for the classical capacities of various phase-insensitive channels are known exactly, and are given by,

$$C(\mathcal{E}_{\eta,N_B}) = g(\eta N_S + (1-\eta)N_B) - g((1-\eta)N_B), \tag{5.17}$$

$$C(\mathcal{N}_{\bar{n}}) = g(N_S + \bar{n}) - g(\bar{n})\,, \tag{5.18}$$

$$C(\mathcal{A}_G^N) = g(GN_S + (G-1)(N+1)) - g((G-1)(N+1)), \tag{5.19}$$

where N_S is the mean input photon number. In general, the classical capacity of *any* phase-insensitive Gaussian channel can be expressed as

$$g(N_S') - g(N_B'), \tag{5.20}$$

where $N_S' = \tau N_S + (\tau + \nu - 1)/2$ and $N_B' = (\tau + \nu - 1)/2$, with τ and ν defined in (5.3). In the above, N_S' is equal to the mean number of photons at the output when a thermal state of mean photon number N_S is input, and N_B' is equal to the mean number of noise photons when the vacuum state is transmitted. Note that the capacities in (5.17), (5.18), and (5.19) all have this particular form as in Equation (5.20). The classical capacities specified above can be achieved by using coherent-state encoding for the respective channels [147].

5.2 Notations and Definitions

In this section, we present a brief review of the notations and the preliminary ideas that we will use in the next section to prove our strong converse theorems for the capacity of phase-insensitive channels.

5.2.1 Quantum Rényi entropy and smooth min-entropy

The quantum Rényi entropy $H_\alpha(\rho)$ of a density operator ρ is defined for $0 < \alpha < \infty$, $\alpha \neq 1$ as

$$H_\alpha(\rho) \equiv \frac{1}{1-\alpha}\log_2 \mathrm{Tr}[\rho^\alpha]\,. \tag{5.21}$$

It is a monotonic function of the "α-purity" $\mathrm{Tr}[\rho^\alpha]$, and the von Neumann entropy $H(\rho)$ is recovered from it in the limit $\alpha \to 1$:

$$\lim_{\alpha\to 1} H_\alpha(\rho) = H(\rho) \equiv -\mathrm{Tr}[\rho\log_2\rho]\,.$$

The min-entropy of ρ, which is the negative logarithm of its maximum eigenvalue, can also be recovered from it in the limit as $\alpha \to \infty$:

$$\lim_{\alpha\to\infty} H_\alpha(\rho) = H_{\min}(\rho) \equiv -\log_2 \|\rho\|_\infty ,$$

where $\|\rho\|_\infty$ is the infinity norm of ρ defined as

$$\|\rho\|_\infty := \max_i\{|\lambda_i|\}, \tag{5.22}$$

λ_i being the eigenvalues of the density operator ρ.

The quantum Rényi entropy of order $\alpha > 1$ of a thermal state with mean photon number N_B can be written as [170]

$$\frac{\log_2\left[(N_B+1)^\alpha - N_B^\alpha\right]}{\alpha-1}.$$

For an additive noise channel $\mathcal{N}_{\bar{n}}$, the Rényi entropy $H_\alpha(\mathcal{N}_{\bar{n}}(\rho))$ for $\alpha > 1$ achieves its minimum value when the input ρ is the vacuum state $|0\rangle\langle 0|$ [157]:

$$\min_\rho H_\alpha(\mathcal{N}_{\bar{n}}(\rho)) = H_\alpha(\mathcal{N}_{\bar{n}}(|0\rangle\langle 0|)) = \frac{\log_2[(\bar{n}+1)^\alpha - \bar{n}^\alpha]}{\alpha-1} \text{ for } \alpha > 1. \tag{5.23}$$

Similarly, for the thermal noise channel $\mathcal{E}_{\eta,N_B}$, the Rényi entropy $H_\alpha(\mathcal{E}_{\eta,N_B}(\rho))$ for $\alpha > 1$ achieves its minimum value when the input ρ is the vacuum state $|0\rangle\langle 0|$ [157]:

$$\min_\rho H_\alpha(\mathcal{E}_{\eta,N_B}(\rho)) = H_\alpha(\mathcal{E}_{\eta,N_B}(|0\rangle\langle 0|)) = \frac{\log_2[((1-\eta)N_B+1)^\alpha - ((1-\eta)N_B)^\alpha]}{\alpha-1} \text{ for } \alpha > 1. \tag{5.24}$$

Furthermore, using the main result of [157] we can say that the *minimum output Rényi entropy* of any phase-insensitive Gaussian channel $\mathcal{P}$ is achieved by the vacuum state:

$$\min_{\rho^{(n)}} H_\alpha(\mathcal{P}^{\otimes n}(\rho^{(n)})) = nH_\alpha(\mathcal{P}(|0\rangle\langle 0|). \tag{5.25}$$

An elegant generalization of the above Rényi entropy is the *smooth Rényi entropy*. The smoothed Rényi entropy was first introduced by Renner and Wolf for classical information sources [171], while it was later generalized to the quantum case by considering the set $\mathcal{B}^\varepsilon(\rho)$ of density matrices $\tilde{\rho}$ that are ε-close in trace distance to ρ for $\varepsilon \geq 0$. The ε-smooth quantum Rényi entropy of order α of a density matrix ρ is defined as [172]

$$H_\alpha^\varepsilon(\rho) = \inf_{\tilde{\rho}\in\mathcal{B}^\varepsilon(\rho)} H_\alpha(\tilde{\rho}) \text{ for } 0 \leq \alpha < 1,$$
$$H_\alpha^\varepsilon(\rho) = \sup_{\tilde{\rho}\in\mathcal{B}^\varepsilon(\rho)} H_\alpha(\tilde{\rho}) \text{ for } 1 < \alpha < \infty.$$

In the limit as $\alpha \to \infty$, we recover the smooth min-entropy of ρ [172, 173]:

$$H_{\min}^\varepsilon(\rho) \equiv \sup_{\tilde{\rho}\in\mathcal{B}^\varepsilon(\rho)} \left[-\log_2 \|\widetilde{\rho}\|_\infty\right] . \tag{5.26}$$

From the above, we see that the following relation holds

$$\inf_{\widetilde{\rho}\in\mathcal{B}^\varepsilon(\rho)} \|\widetilde{\rho}\|_\infty = 2^{-H_{\min}^\varepsilon(\rho)} . \tag{5.27}$$

This relation gives the definition of the smooth min-entropy $H_{\min}^{\varepsilon}$, and we will show in Section 5.3 that it leads to a strong converse theorem for the capacity of noisy bosonic channels. A relation between the smooth min-entropy and the Rényi entropy of order $\alpha > 1$ is given by the following inequality [174]

$$H_{\min}^{\varepsilon}(\rho) \geq H_{\alpha}(\rho) - \frac{1}{\alpha - 1} \log_2 \left(\frac{1}{\varepsilon} \right). \tag{5.28}$$

We will exploit this relation, along with the minimum output entropy results from [157], to prove the strong converse theorem for the classical capacity of all phase-insensitive Gaussian channels.

5.3 Strong converse for all phase-insensitive Gaussian channels

In the following, we prove that a strong converse theorem holds for the capacity of all phase-insensitive Gaussian channels when imposing a maximum photon-number constraint. This means that if we demand that the average code density operator for the codewords, which are used for transmission of classical messages, is constrained to have a large shadow onto a subspace with photon number no larger than some fixed amount, then the probability of successfully decoding the message converges to zero in the limit of many channel uses if the rate R of communication exceeds the classical capacity of these channels.

We first present the arguments to prove the strong converse theorem for a *noiseless qubit channel* [175, 176], illustrating a simple approach for establishing the strong converse property of classical capacity.

Suppose that any scheme for classical communication over n noiseless qubit channels consists of an encoding of the message m as a quantum state on n qubits, followed by a decoding POVM $\{\Lambda_m\}$. The rate of the code is $R = (\log_2 M)/n$, and the success probability for correctly recovering the message by a receiver is given by

$$\begin{aligned} \frac{1}{M} \sum_m \mathrm{Tr}\{\Lambda_m \rho_m\} &\leq \frac{1}{M} \sum_m \mathrm{Tr}\{\Lambda_m\} \|\rho_m\|_{\infty} && (5.29) \\ &\leq \frac{1}{M} \sum_m \mathrm{Tr}\{\Lambda_m\} && (5.30) \\ &= M^{-1} 2^n && (5.31) \\ &= 2^{-n(R-1)}, && (5.32) \end{aligned}$$

where $\|\rho_m\|_{\infty}$ is the infinity norm of ρ_m. We have used the facts that the maximum eigenvalue corresponding to $\|\rho_m\|_{\infty}$ is one, and $\sum_m \Lambda_m = I^{\otimes n}$ for the POVM measurements $\{\Lambda_m\}$. The above argument suggests that for a rate $R > 1$, the average success probability of any communication scheme decreases exponentially fast to zero with increasing n.

The above proof for the noiseless qubit channel highlights an interplay of the success probability of decoding with the strong converse rate, dimension of the encoding space, and the purity of the channel in terms of the infinity-norm of the output states of the channel. Our proof of the strong converse theorem for the phase-insensitive channels can be regarded as a generalization of these arguments but also invites comparison with the proof of the strong converse for covariant channels with additive minimum output Rényi-entropy [175].

5.3.1 Strong converse under the maximum photon number constraint

In the context of optical communication, suppose that the sender and receiver are allowed access to many independent uses of a quantum channel. If we allow the signal states at the input of the channel to have an arbitrarily large number of photons, then the classical capacity of the channel would be infinite, which makes this case practically uninteresting. Therefore, it is essential to restrict the average number of photons of the signal states per channel use such that the mean number of photons in any codeword transmitted through the channel should be no larger than some number $N_S \in [0, \infty)$. This is known as the mean photon number constraint and is commonly used in establishing the information-carrying capacity of a given channel [147, 169, 155, 156].

However, following the same arguments as in [153] (and later in [158]), we can show that the strong converse need not hold under such a mean photon number constraint for a phase-insensitive Gaussian channel. So instead, we prove that the strong converse theorem holds under a maximum photon number constraint on the number of photons in the input states.

Let ρ_m denote a codeword of any code for communication over a phase-insensitive Gaussian channel $\mathcal{P}$. The *maximum photon number constraint* that we impose on the codebook is to require that the average code density operator $\frac{1}{M}\sum_m \rho_m$ (M is the total number of messages) has a large shadow onto a subspace with photon number no larger than some fixed amount nN_S. Such a constraint on the channel inputs can be defined by introducing a photon number cutoff projector Π_L that projects onto a subspace of n bosonic modes such that the total photon number is no larger than L:

$$\Pi_L \equiv \sum_{a_1,\ldots,a_n:\sum_i a_i \leq L} |a_1\rangle\langle a_1| \otimes \ldots \otimes |a_n\rangle\langle a_n|, \tag{5.33}$$

where $|a_i\rangle$ is a photon number state of photon number a_i. The rank of the above projector $\Pi_{\lceil nN_S \rceil}$ has been shown to be never larger than $2^{n[g(N_S)+\delta_0]}$ (Lemma 3 in [153]), i.e.,

$$\mathrm{Tr}\left\{\Pi_{\lceil nN_S \rceil}\right\} \leq 2^{n[g(N_S)+\delta_0]}, \tag{5.34}$$

where $\delta_0 \geq \frac{1}{n}(\log_2 e + \log_2(1 + \frac{1}{N_S}))$, so that δ_0 can be chosen arbitrarily small by taking n large enough.

Mathematically, the maximum photon number constraint can then be written as

$$\frac{1}{M}\sum_m \mathrm{Tr}\left\{\Pi_{\lceil nN_S \rceil}\rho_m\right\} \geq 1 - \delta_1(n), \tag{5.35}$$

where $\delta_1(n)$ is a function that decreases to zero as n increases. In fact, the coherent-state encodings that attain the known capacities of the phase-insensitive channels do indeed satisfy the maximum photon number constraint, with an exponentially decreasing $\delta_1(n)$, if coherent states with mean photon number per mode $< N_S - \delta$ are used, with δ being a small positive number (see Reference [153] for an argument along these lines).

The first important step in proving the strong converse is to show that if most of the probability mass of the input state of the phase-insensitive channel $\mathcal{P}$ is in a subspace with photon number no larger than nN_S, then most of the probability mass of the channel output is in a subspace with photon number no larger than nN'_S, where N'_S is the mean energy of the output state.

Lemma 3 *Let $\rho^{(n)}$ denote a density operator on n modes that satisfies*

$$\mathrm{Tr}\{\Pi_{\lceil nN_S\rceil}\rho^{(n)}\} \geq 1-\delta_1(n),$$

where $\delta_1(n)$ is defined in (5.35)*. Let $\mathcal{P}$ be a phase-insensitive Gaussian channel with parameters τ and ν as defined in* (5.3)*. Then*

$$\mathrm{Tr}\{\Pi_{\lceil nN'_S+\delta_2)\rceil}\mathcal{P}^{\otimes n}(\rho^{(n)})\} \geq 1-\delta_1(n)-2\sqrt{\delta_1(n)}-\delta_3(n),$$

where $N'_S = \tau N_S + (\tau+\nu-1)/2$, $\mathcal{P}^{\otimes n}$ represents n instances of $\mathcal{P}$ that act on the density operator $\rho^{(n)}$, δ_2 is an arbitrarily small positive constant, and $\delta_3(n)$ is a function of n decreasing to zero as $n\to\infty$.

Proof. The proof of this lemma is essentially the same as the proof of Lemma 1 of [158], with some minor modifications. We include the details of it for completeness. We first recall the structural decomposition in (5.13) for any phase-insensitive channel:

$$\mathcal{P}(\rho) = \left(\mathcal{A}^0_G \circ \mathcal{E}_T\right)(\rho),$$

i.e., that any phase-insensitive Gaussian channel can be realized as a concatenation of a pure-loss channel $\mathcal{E}_T$ of transmissivity T followed by a quantum-limited amplifier channel $\mathcal{A}_G$ with gain G, with $\tau = TG$ and $\nu = G(1-T)+G-1$. Thus, a photon number state $|k\rangle\langle k|$ input to the phase-insensitive noise channel leads to an output of the following form:

$$\mathcal{P}(|k\rangle\langle k|) = \sum_{m=0}^{k} p(m)\,\mathcal{A}^0_G(|m\rangle\langle m|), \tag{5.36}$$

where

$$p(m) = \binom{k}{m} T^m (1-T)^{k-m}.$$

The quantum-limited amplifier channel has the following action on a photon number state $|m\rangle$ [164]:

$$\mathcal{A}^0_G(|m\rangle\langle m|) = \sum_{l=0}^{\infty} q(l|m)\,|l\rangle\langle l|,$$

where the conditional probabilities $q(l|m)$ are given by:

$$q(l|m) = \begin{cases} 0 & l<m \\ (1-\mu^2)^{m+1}\mu^{2(l-m)}\binom{l}{l-m} & l\geq m \end{cases},$$

where $\mu = \tanh r \in [0,1]$, with r chosen such that $G = \cosh^2(r)$.

The conditional distribution $q(l|m)$ has the two important properties of having finite second moment and exponential decay with increasing photon number. The property of exponential decay with increasing l follows from

$$\begin{aligned}(1-\mu^2)^{m+1}\mu^{2(l-m)}\binom{l}{l-m} &= (1-\mu^2)^{m+1}\mu^{-2m}2^{-2\log_2\left(\frac{1}{\mu}\right)l}\binom{l}{l-m} \\ &\leq (1-\mu^2)^{m+1}\mu^{-2m}2^{-2\log_2\left(\frac{1}{\mu}\right)l}2^{lh_2\left(\frac{l-m}{l}\right)} \\ &= (1-\mu^2)^{m+1}\mu^{-2m}2^{-l\left[2\log_2\left(\frac{1}{\mu}\right)-h_2\left(\frac{l-m}{l}\right)\right]}.\end{aligned}$$

The inequality applies the bound $\binom{n}{k} \leq 2^{nh_2(k/n)}$ (see (11.40) of [177]), where $h_2(x)$ is the binary entropy with the property that $\lim_{x\to 1} h_2(x) = 0$. Thus, for large enough l, it will be the case that $2\log\left(\frac{1}{\mu}\right) - h_2\left(\frac{l-m}{l}\right) > 0$, so that the conditional distribution $q(l|m)$ has exponential decay with increasing l. We can also then conclude that this distribution has a finite second moment. It follows from (5.36) that

$$\mathcal{P}(|k\rangle\langle k|) = \sum_{l=0}^{\infty}\left[\sum_{m=0}^{k} p(m)\, q(l|m)\right]|l\rangle\langle l|. \tag{5.37}$$

The eigenvalues above (i.e., $\sum_{m=0}^{k} p(m)\, q(l|m)$) represent a distribution over photon number states at the output of the phase-insensitive channel $\mathcal{P}$, which we can write as a conditional probability distribution $p(l|k)$ over l given the input with definite photon number k. This probability distribution has its mean equal to $\tau k + (\tau+\nu-1)/2$, since the mean energy of the input state is k. Furthermore, this distribution inherits the properties of having a finite second moment and an exponential decay to zero as $l \to \infty$.

For example, we can consider the thermal noise channel $\mathcal{E}_{\eta,N_B}$ with the structural decomposition given by (5.15)

$$\mathcal{E}_{\eta,N_B}(\rho) = (\mathcal{A}^0_{(1-\eta)N_B+1} \circ \mathcal{E}_{\eta/((1-\eta)N_B+1)})(\rho).$$

The mean of the corresponding distribution for this channel when a state of definite photon number k is input, following the above arguments, is equal to $\eta k + (1-\eta)N_B$.

We now suppose that the input state satisfies the maximum photon-number constraint in (5.35), and apply the Gentle Measurement Lemma [149, 148] to obtain the following inequality

$$\mathrm{Tr}\left\{\Pi_{\lceil nN'_S+\delta_2\rceil}\mathcal{P}^{\otimes n}\left(\rho^{(n)}\right)\right\} \geq \mathrm{Tr}\left\{\Pi_{\lceil nN'_S+\delta_2\rceil}\mathcal{P}^{\otimes n}\left(\Pi_{\lceil nN_S\rceil}\rho^{(n)}\Pi_{\lceil nN_S\rceil}\right)\right\} - 2\sqrt{\delta_1(n)}, \tag{5.38}$$

where $N'_S = \tau N_S + (\tau+\nu-1)/2$. Since there is photodetection at the output (i.e., the projector $\Pi_{\lceil n\eta N'_S+\delta_2\rceil}$ is diagonal in the number basis), it suffices for us to consider the input $\Pi_{\lceil nN_S\rceil}\rho^{(n)}\Pi_{\lceil nN_S\rceil}$ to be diagonal in the photon-number basis, and we write this as

$$\rho^{(n)} = \sum_{a^n:\sum_i a_i \leq \lceil nN_S\rceil} p(a^n)\,|a^n\rangle\langle a^n|,$$

where $|a^n\rangle$ represents strings of photon number states. We then find that (5.38) is equal to

$$\begin{aligned}
&\sum_{a^n:\sum_i a_i\leq\lceil nN_S\rceil} p(a^n)\,\mathrm{Tr}\left\{\left(\Pi_{\lceil nN'_S+\delta_2\rceil}\right)\mathcal{P}^{\otimes n}\left(|a^n\rangle\langle a^n|\right)\right\} - 2\sqrt{\delta_1(n)}\\
&= \sum_{a^n:\sum_i a_i\leq\lceil nN_S\rceil} p(a^n) \sum_{l^n:\sum_i l_i\leq\left\lceil nN'_S+\delta_2\right\rceil} p(l^n|a^n) - 2\sqrt{\delta_1(n)},
\end{aligned} \tag{5.39}$$

where the distribution $p(l^n|a^n) \equiv \prod_{i=1}^{n} p(l_i|a_i)$ with $p(l_i|a_i)$ coming from (5.37). In order to obtain a lower bound on the expression in (5.39), we analyze the term

$$\sum_{l^n:\sum_i l_i\leq\left\lceil nN'_S+\delta_2\right\rceil} p(l^n|a^n) \tag{5.40}$$

on its own under the assumption that $\sum_i a_i \leq \lceil nN_S \rceil$. Let $L_i|a_i$ denote a conditional random variable with distribution $p\left(l_i|a_i\right)$, and let $\overline{L^n}|a^n$ denote the sum random variable:

$$\overline{L^n}|a^n \equiv \sum_i L_i|a_i,$$

so that the term $\sum_{l^n:\sum_i l_i \leq \lceil nN_S' + \delta_2 \rceil} p\left(l^n|a^n\right)$ becomes

$$\begin{aligned}
\sum_{l^n:\sum_i l_i \leq \lceil nN_S' + \delta_2 \rceil} p\left(l^n|a^n\right) &= \Pr\left\{\overline{L^n}|a^n \leq n(N_S' + \delta_2)\right\} \\
&= \Pr\left\{\overline{L^n}|a^n \leq n\left(\tau N_S + \left(\tau + \nu - 1\right)/2 + \delta_2\right)\right\} \quad (5.41) \\
&\geq \Pr\left\{\overline{L^n}|a^n \leq n\left(\tau \frac{1}{n}\sum_i a_i + \left(\tau + \nu - 1\right)/2 + \delta_2\right)\right\}, \quad (5.42)
\end{aligned}$$

where $\left(\tau + \nu - 1\right)/2$ represents the mean number of noise photons injected by the channel, and the inequality follows from the constraint $\sum_i a_i \leq \lceil nN_S \rceil$. Since

$$\mathbb{E}\left\{L_i|a_i\right\} = \tau a_i + \left(\tau + \nu - 1\right)/2,$$

it follows that

$$\mathbb{E}\left\{\overline{L^n}|a^n\right\} = n\left(\tau \frac{1}{n}\sum_i a_i + \left(\tau + \nu - 1\right)/2\right),$$

and so the expression in (5.42) is the probability that a sum of independent random variables deviates from its mean by no more than δ_2. To obtain a bound on the probability in (5.42) from below, we now follow the approach in [158] employing the truncation method (see Section 2.1 of [178] for more details), in which each random variable $L_i|a_i$ is split into two parts:

$$\begin{aligned}
\left(L_i|a_i\right)_{>T_0} &\equiv \left(L_i|a_i\right)\mathcal{I}\left(\left(L_i|a_i\right) > T_0\right), \\
\left(L_i|a_i\right)_{\leq T_0} &\equiv \left(L_i|a_i\right)\mathcal{I}\left(\left(L_i|a_i\right) \leq T_0\right),
\end{aligned}$$

where $\mathcal{I}\left(\cdot\right)$ is the indicator function and T_0 is a truncation parameter taken to be very large (much larger than $\max_i a_i$, for example). We can then split the sum random variable into two parts as well:

$$\begin{aligned}
\overline{L^n}|a^n &= \left(\overline{L^n}|a^n\right)_{>T_0} + \left(\overline{L^n}|a^n\right)_{\leq T_0} \\
&\equiv \sum_i \left(L_i|a_i\right)_{>T_0} + \sum_i \left(L_i|a_i\right)_{\leq T_0}.
\end{aligned}$$

We can use the union bound to argue that

$$\begin{aligned}
\Pr\left\{\overline{L^n}|a^n \geq \mathbb{E}\left\{\overline{L^n}|a^n\right\} + n\delta_2\right\} \leq{}& \Pr\left\{\left(\overline{L^n}|a^n\right)_{>T_0} \geq \mathbb{E}\left\{\left(\overline{L^n}|a^n\right)_{>T_0}\right\} + n\delta_2/2\right\} \\
&+ \Pr\left\{\left(\overline{L^n}|a^n\right)_{\leq T_0} \geq \mathbb{E}\left\{\left(\overline{L^n}|a^n\right)_{\leq T_0}\right\} + n\delta_2/2\right\}. \quad (5.43)
\end{aligned}$$

The idea from here is that for a random variable $L_i|a_i$ with sufficient decay for large values, we can bound the first probability for $\left(\overline{L^n}|a^n\right)_{>T_0}$ from above by ε/δ_2 for ε an arbitrarily small

positive constant (made small by taking T_0 larger) by employing the Markov inequality. We then bound the second probability for $\left(\overline{L^n}|a^n\right)_{\leq T_0}$ using a Chernoff bound, since these random variables are bounded. This latter bound has an exponential decay with increasing n due to the use of a Chernoff bound. So, the argument is just to make ε arbitrarily small by increasing the truncation parameter T_0, and for n large enough, we obtain an exponential convergence to zero. We point the reader to Section 2.1 of [178] for more details. By using either approach, we arrive at the following bound:

$$\sum_{l^n:\sum_i l_i \leq \left\lceil nN_S'+\delta_2 \right\rceil} p\left(l^n|a^n\right) \geq 1-\delta_3(n),$$

where $\delta_3(n)$ is a function decreasing to zero as $n \to \infty$. Finally, we put this together with Equation (5.39) to obtain

$$\begin{aligned}
&\operatorname{Tr}\left\{\Pi_{\left\lceil nN_S'+\delta_2 \right\rceil}\mathcal{P}^{\otimes n}\left(\rho^{(n)}\right)\right\} \\
&\geq \sum_{a^n:\sum_i a_i \leq \lceil nN_S \rceil} p\left(a^n\right) \sum_{l^n:\sum_i l_i \leq \left\lceil nN_S'+\delta_2 \right\rceil} p\left(l^n|a^n\right) - 2\sqrt{\delta_1(n)} \\
&\geq \left(1-\delta_1(n)\right)\left(1-\delta_3(n)\right) - 2\sqrt{\delta_1(n)} \\
&\geq 1-\delta_1(n)-\delta_3(n)-2\sqrt{\delta_1(n)},
\end{aligned}$$

which completes the proof. ■

Let Λ_m denote a decoding POVM acting on the output space of n instances of the phase-insensitive channel. In what follows, we prove the strong converse theorem for the classical capacity of all phase-insensitive Gaussian channels.

Theorem 1 *Let $\mathcal{P}$ be a phase-insensitive Gaussian channel with parameters τ and ν as defined in* (5.3)*. The average success probability p_{succ} of any code for this channel satisfying* (5.35) *is bounded as*

$$p_{\text{succ}} = \frac{1}{M}\sum_m \operatorname{Tr}\{\Lambda_m \mathcal{P}^{\otimes n}(\rho_m)\} \leq 2^{-nR}2^{n\left[g\left(N_S'\right)-H_\alpha(\mathcal{P}(|0\rangle\langle 0|))+\delta_2+\frac{1}{n(\alpha-1)}\log_2(1/\varepsilon)\right]} + \varepsilon + \delta_6(n), \tag{5.44}$$

where $\alpha > 1$, $\varepsilon \in (0,1)$, $N_S' = \tau N_S + (\tau+\nu-1)/2$, $\mathcal{P}^{\otimes n}$ denotes n instances of $\mathcal{P}$, and $\delta_6(n) = 2\sqrt{\delta_1(n)+2\sqrt{\delta_1(n)}+\delta_3(n)}$. $\delta_1(n)$ is defined in (5.35)*, δ_2 is an arbitrarily small positive constant and $\delta_3(n)$ is a function decreasing with n (both defined in Lemma 3).*

Proof. This proof is very similar to the proof of Theorem 2 of [158], with the exception that we can now invoke the main result of [157] (that the minimum output entropy for Rényi entropies of arbitrary order is attained by the vacuum state input for any phase-insensitive Gaussian channel).

Let us consider the success probability of any code satisfying the maximum photon-number constraint (5.35). The average success probability can be written as:

$$\begin{aligned}\frac{1}{M}\sum_m \mathrm{Tr}\{\Lambda_m \mathcal{P}^{\otimes n}(\rho_m)\} &\leq \frac{1}{M}\sum_m \mathrm{Tr}\{\Lambda_m \Pi_{\lceil nN'_S\rceil}\mathcal{P}^{\otimes n}(\rho_m)\Pi_{\lceil nN'_S\rceil}\} \\ &\quad + \frac{1}{M}\sum_m \left\|\Pi_{\lceil nN'_S\rceil}\mathcal{P}^{\otimes n}(\rho_m)\Pi_{\lceil nN'_S\rceil} - \mathcal{P}^{\otimes n}(\rho_m)\right\|_1 \\ &\leq \frac{1}{M}\sum_m \mathrm{Tr}\{\Lambda_m \Pi_{\lceil nN'_S\rceil}\mathcal{P}^{\otimes n}(\rho_m)\Pi_{\lceil nN'_S\rceil}\} \\ &\quad + 2\sqrt{\delta_1(n) + 2\sqrt{\delta_1(n)} + \delta_3(n)}.\end{aligned}$$

The first inequality is a special case of the inequality

$$\mathrm{Tr}\{\Lambda\sigma\} \leq \mathrm{Tr}\{\Lambda\rho\} + \left\|\rho - \sigma\right\|_1, \tag{5.45}$$

which holds for $0 \leq \Lambda \leq I$, $\rho, \sigma \geq 0$, and $\mathrm{Tr}\{\rho\}, \mathrm{Tr}\{\sigma\} \leq 1$. The second inequality is obtained by invoking Lemma 3 and the Gentle Measurement Lemma [149, 148] for ensembles.

Note that in the above, the second term vanishes as $n \to \infty$; hence it suffices to focus on the first term, which by cyclicity of trace yields

$$\frac{1}{M}\sum_m \mathrm{Tr}\{\Lambda_m \Pi_{\lceil nN'_S\rceil}\mathcal{P}^{\otimes n}(\rho_m)\Pi_{\lceil nN'_S\rceil}\} = \frac{1}{M}\sum_m \mathrm{Tr}\{\Pi_{\lceil nN'_S\rceil}\Lambda_m \Pi_{\lceil nN'_S\rceil}\mathcal{P}^{\otimes n}(\rho_m)\}. \tag{5.46}$$

At this point, we consider the set of all states $\widetilde{\sigma}_m$ that are ε-close in trace distance to each output of the phase-insensitive channel $\mathcal{P}^{\otimes n}(\rho_m)$ (let us denote this set by $\mathcal{B}^{\varepsilon}(\mathcal{P}^{\otimes n}(\rho_m))$. This consideration will allow us to relate the success probability to the smooth min-entropy. We find the following upper bound on (5.46):

$$\begin{aligned}\frac{1}{M}\sum_m \mathrm{Tr}\{\Pi_{\lceil nN'_S\rceil}\Lambda_m \Pi_{\lceil nN'_S\rceil}\mathcal{P}^{\otimes n}(\rho_m)\} &\leq \frac{1}{M}\sum_m \mathrm{Tr}\{\Pi_{\lceil nN'_S\rceil}\Lambda_m \Pi_{\lceil nN'_S\rceil}\widetilde{\sigma}_m\} + \varepsilon \\ &\leq \frac{1}{M}\sum_m \mathrm{Tr}\{\Pi_{\lceil nN'_S\rceil}\Lambda_m \Pi_{\lceil nN'_S\rceil}\}\left\|\widetilde{\sigma}_m\right\|_\infty + \varepsilon.\end{aligned}$$

We can now optimize over all of the states $\widetilde{\sigma}_m$ that are ε-close to $\mathcal{P}^{\otimes n}(\rho_m)$, leading to the tightest upper bound on the success probability

$$\frac{1}{M}\sum_m \mathrm{Tr}\{\Pi_{\lceil nN'_S\rceil}\Lambda_m \Pi_{\lceil nN'_S\rceil}\mathcal{P}^{\otimes n}(\rho_m)\} \tag{5.47}$$

$$\leq \frac{1}{M}\sum_m \mathrm{Tr}\{\Pi_{\lceil nN'_S\rceil}\Lambda_m \Pi_{\lceil nN'_S\rceil}\} \inf_{\widetilde{\sigma}_m \in \mathcal{B}^{\varepsilon}(\mathcal{P}^{\otimes n}(\rho_m))} \left\|\widetilde{\sigma}_m\right\|_\infty + \varepsilon. \tag{5.48}$$

Since the quantity $\inf_{\widetilde{\sigma}_m \in \mathcal{B}^{\varepsilon}(\mathcal{P}^{\otimes n}(\rho_m))} \left\|\widetilde{\sigma}_m\right\|_\infty$ is related to the smooth min-entropy via

$$\inf_{\widetilde{\sigma}_m \in \mathcal{B}^{\varepsilon}(\mathcal{P}^{\otimes n}(\rho_m))} \left\|\widetilde{\sigma}_m\right\|_\infty = 2^{-H_{\min}^{\varepsilon}\left(\mathcal{P}^{\otimes n}(\rho_m)\right)},$$

we can get from the upper bound in (5.48)

$$\begin{aligned}
&\frac{1}{M}\sum_m \mathrm{Tr}\{\Pi_{\lceil nN_S'\rceil}\Lambda_m\Pi_{\lceil nN_S'\rceil}\}2^{-H_{\min}^{\varepsilon}\left(\mathcal{P}^{\otimes n}(\rho_m)\right)}+\varepsilon\\
&\leq \frac{1}{M}\sum_m \mathrm{Tr}\{\Pi_{\lceil nN_S'\rceil}\Lambda_m\Pi_{\lceil nN_S'\rceil}\}\sup_\rho 2^{-H_{\min}^{\varepsilon}\left(\mathcal{P}^{\otimes n}(\rho)\right)}+\varepsilon\\
&= \frac{1}{M}2^{-\inf_\rho H_{\min}^{\varepsilon}\left(\mathcal{P}^{\otimes n}(\rho)\right)}\mathrm{Tr}\{\Pi_{\lceil nN_S'\rceil}\}+\varepsilon\\
&\leq 2^{-nR}2^{-\inf_\rho H_{\min}^{\varepsilon}\left(\mathcal{P}^{\otimes n}(\rho)\right)}2^{n\left[g\left(N_S'\right)+\delta\right]}+\varepsilon. \qquad (5.49)
\end{aligned}$$

The first inequality follows by taking a supremum over all input states. The first equality follows because $\sum_m \Lambda_m = I$ for the set of decoding POVM measurements $\{\Lambda_m\}$, and the second inequality is a result of the upper bound on the rank of the photon number cutoff projector in (5.34). We have also used the fact that the rate of the channel is expressed as $R = (\log_2 M)/n$, where M is the number of messages.

Observe that the success probability is now related to the smooth min-entropy, and we can exploit the following relation between smooth min-entropy and the Rényi entropies for $\alpha > 1$ [174]:

$$H_{\min}^{\varepsilon}(\omega) \geq H_\alpha(\omega) - \frac{1}{\alpha-1}\log_2\left(\frac{1}{\varepsilon}\right).$$

Using the above inequality and the fact that the "strong" Gaussian optimizer conjecture has been proven for the Rényi entropies of all orders [157] (recall (5.25)), we get that

$$\inf_\rho H_{\min}^{\varepsilon}\left(\mathcal{P}^{\otimes n}(\rho)\right) \geq n\left[H_\alpha\left(\mathcal{P}(|0\rangle\langle 0|)\right) - \frac{1}{n(\alpha-1)}\log_2\left(\frac{1}{\varepsilon}\right)\right]. \qquad (5.50)$$

The first term on the right hand side is a result of the fact that the vacuum state minimizes the Rényi entropy of all orders at the output of a phase-insensitive Gaussian channel. ■

By tuning the parameters α and ε appropriately, we recover the strong converse theorem:

Corollary 1 (Strong converse) *Let $\mathcal{P}$ be a phase-insensitive Gaussian channel with parameters τ and ν as defined in* (5.3)*. The average success probability p_{succ} of any code for this channel satisfying* (5.35) *is bounded as*

$$p_{\mathrm{succ}} = \frac{1}{M}\sum_m \mathrm{Tr}\{\Lambda_m\mathcal{P}^{\otimes n}(\rho_m)\} \leq 2^{-nR}2^{n\left[g\left(N_S'\right)-g\left(N_B'\right)+\delta_2+\delta_5/\delta_4+\delta_4 C\left(N_B'\right)\right]}+2^{-n\delta_5}+\delta_6(n), \qquad (5.51)$$

where $N_S' = \tau N_S + (\tau+\nu-1)/2$, $N_B' \equiv (\tau+\nu-1)/2$, $\mathcal{P}^{\otimes n}$ denotes n instances of $\mathcal{P}$, and $\delta_6(n) = 2\sqrt{\delta_1(n)+2\sqrt{\delta_1(n)}+\delta_3(n)}$. $\delta_1(n)$ is defined in (5.35)*, δ_2 is an arbitrarily small positive constant and $\delta_3(n)$ is a function decreasing with n (both defined in Lemma 3), δ_4 and δ_5 are arbitrarily small positive constants such that δ_5/δ_4 is arbitrarily small, and $C(N_B')$ is a function of N_B' only. Thus, for any rate $R > g(N_S') - g(N_B')$, it is possible to choose the parameters such that the success probability of any family of codes satisfying* (5.35) *decreases to zero in the limit of large n.*

Proof. In Theorem 1, we can pick $\alpha = 1 + \delta_4$ and $\varepsilon = 2^{-n\delta_5}$, with $\delta_5 > 0$ much smaller than $\delta_4 > 0$ such that δ_5/δ_4 is arbitrarily small, and the terms on the right hand side in (5.50) simplify to

$$n\left[H_{1+\delta_4}\left(\mathcal{P}(|0\rangle\langle 0|)\right) - \frac{\delta_5}{\delta_4}\right].$$

The output state $\mathcal{P}(|0\rangle\langle 0|)$ for the phase-insensitive channel with the vacuum state as the input is a thermal state with mean photon number $N_B' \equiv (\tau + \nu - 1)/2$. The quantum Rényi entropy of order $\alpha > 1$ of a thermal state with mean photon number N_B' is given by [167]

$$\frac{\log_2\left[(N_B'+1)^\alpha - N_B'^\alpha\right]}{\alpha - 1}. \tag{5.52}$$

Lemma 6.3 of [173] gives us the following inequality for a general state (for α close enough to one):

$$H_\alpha(\rho) \geq H(\rho) - 4(\alpha - 1)\left(\log_2 v\right)^2,$$

where

$$v \equiv 2^{-\frac{1}{2}H_{3/2}(\rho)} + 2^{\frac{1}{2}H_{1/2}(\rho)} + 1.$$

For a thermal state, we find using (5.52) that

$$H_{3/2}(\rho) = 2\log_2\left[(N_B'+1)^{3/2} - N_B'^{3/2}\right],$$
$$H_{1/2}(\rho) = -2\log_2\left[(N_B'+1)^{1/2} - N_B'^{1/2}\right],$$

so that

$$v(N_B') = \left[(N_B'+1)^{3/2} - N_B'^{3/2}\right]^2 + \left[(N_B'+1)^{1/2} - N_B'^{1/2}\right]^{-2} + 1.$$

We then find that

$$\begin{aligned} H_{1+\delta_4}\left(\mathcal{P}(|0\rangle\langle 0|)\right) &\geq H\left(\mathcal{P}(|0\rangle\langle 0|)\right) - \delta_4 C(N_B') \\ &= g(N_B') - \delta_4 C(N_B'), \end{aligned}$$

where

$$C(N_B') \equiv 4\left[\log_2 v(N_B')\right]^2.$$

We now recover the bound in the statement of the corollary. ■

Finally, we recall the capacities of the phase-insensitive channels in (5.17), (5.18), and (5.19). Comparing them with the statement of Corollary 1, we can conclude that these expressions indeed represent strong converse rates for these respective channels, since the success probability when communicating above these rates decreases to zero in the limit $n \to \infty$.

Our results proving the strong converse of all phase-insensitive channels thus establishes the capacity as a sharp transition between two regimes—one which is an error-free regime for communication rates below the capacity, and the other in which the probability of correctly decoding a classical message converges exponentially fast to zero if the communication rate exceeds the classical capacity.

5.4 Conclusion

In this chapter, we discussed various phase-insensitive Gaussian channels that represent physical noise models which are relevant for optical quantum communication, including lossy optical fibers, amplifier and free-space communication. In the context of transmission of the classical messages through these noisy quantum channels, we established a proof of the strong converse theorem for these channels by relating the success probability of any code with its rate of data transmission, the effective dimension of the channel output space, and the purity of the channel as quantified by the minimum output entropy. For the communication rate exceeding the capacity, the success probability of correctly decoding classical information has been shown to asymptotically converge to zero in the limit of many channel uses.

Our result thus establishes the capacity of these channels as a very sharp dividing line between possible and impossible communication rates through these channels and opens up the path to applications, one of which could be to prove security of the noisy bounded storage model of cryptography for optical links [154] for continuous-variable systems. The results presented in this chapter can also be easily extended to the more general case of multimode bosonic Gaussian channels [155]. Another area of research where our result might be extended is in the setting of network information theory—for example, one might consider establishing a strong converse for the classical capacity of the multiple-access bosonic channels, in which two or more senders communicate to a common receiver over a shared communication channel [179].

Bibliography

[1] C. M. Caves, "Quantum-mechanical noise in an interferometer", *Physical Review D* **23** (1981), no. 8, 1693–1708.

[2] H. Cramér, "Mathematical methods of statistics", Princeton University, Princeton, 1946.

[3] S. Boixo, S. Flammia, C. M. Caves, and J. Geremia, "Generalized Limits for Single-Parameter Quantum Estimation", *Physical Review Letters* **98** (2007), no. 9, 090401.

[4] J. P. Dowling, "Quantum optical metrology the lowdown on high-N00N states", *Contemporary Physics* **49** (2008), no. 2, 125–143.

[5] C. E. Shannon, "A mathematical theory of communication", *Bell System Technical Journal* **27** (1948) 379–423.

[6] A. S. Holevo, "The Capacity of the Quantum Channel with General Signal States.", *IEEE Transactions on Information Theory* **44** (1998) 269–273.

[7] B. Schumacher and M. D. Westmoreland, "Sending classical information via noisy quantum channels", *Physical Review A* **56** Jul (1997) 131–138.

[8] M. M. Wilde, "Quantum Information Theory", Cambridge University Press, Cambridge, 2013.

[9] A. Boto, P. Kok, D. Abrams, S. Braunstein, C. Williams, and J. P. Dowling, "Quantum Interferometric Optical Lithography: Exploiting Entanglement to Beat the Diffraction Limit", *Physical Review Letters* **85** (2000), no. 13, 2733–2736.

[10] G. Durkin and J. Dowling, "Local and Global Distinguishability in Quantum Interferometry", *Physical Review Letters* **99** (2007), no. 7, 070801.

[11] G. Gilbert, M. Hamrick, and Y. S. Weinstein, "Use of maximally entangled N-photon states for practical quantum interferometry", *Journal of the Optical Society of America B* **25** (2008), no. 8, 1336.

[12] M. Rubin and S. Kaushik, "Loss-induced limits to phase measurement precision with maximally entangled states", *Physical Review A* **75** (2007), no. 5, 053805.

[13] A. D. Parks, S. E. Spence, J. E. Troupe, and N. J. Rodecap, "Tripartite loss model for Mach-Zehnder interferometers with application to phase sensitivity", *Review of Scientific Instruments* **76** (2005), no. 4, 043103.

[14] S. Huver, C. Wildfeuer, and J. P. Dowling, "Entangled Fock states for robust quantum optical metrology, imaging, and sensing", *Physical Review A* **78** (2008), no. 6, 063828.

[15] K. Jiang, C. J. Brignac, Y. Weng, M. B. Kim, H. Lee, and J. P. Dowling, "Strategies for choosing path-entangled number states for optimal robust quantum-optical metrology in the presence of loss", *Physical Review A* **86** (2012), no. 1, 013826.

[16] C. Gerry, "Heisenberg-limit interferometry with four-wave mixers operating in a nonlinear regime", *Physical Review A* **61** (2000), no. 4, 043811.

[17] R. Campos, C. Gerry, and A. Benmoussa, "Optical interferometry at the Heisenberg limit with twin Fock states and parity measurements", *Physical Review A* **68** (2003), no. 2, 023810.

[18] C. C. Gerry and J. Mimih, "The parity operator in quantum optical metrology", *Contemporary Physics* **51** (2010), no. 6, 497–511.

[19] K. P. Seshadreesan, S. Kim, J. P. Dowling, and H. Lee, "Phase estimation at the quantum Cramér-Rao bound via parity detection", *Physical Review A* **87** (2013), no. 4, 043833.

[20] S. Braunstein and C. M. Caves, "Statistical distance and the geometry of quantum states", *Physical Review Letters* **72** (1994), no. 22, 3439–3443.

[21] S. L. Braunstein, C. M. Caves, and G. Milburn, "Generalized Uncertainty Relations: Theory, Examples, and Lorentz Invariance", *Annals of Physics* **247** (1996), no. 1, 135–173.

[22] B. Roy Bardhan, K. Jiang, and J. P. Dowling, "Effects of phase fluctuations on phase sensitivity and visibility of path-entangled photon Fock states", *Physical Review A* **88** (2013), no. 2, 023857.

[23] K. T. Kapale, L. D. Didomenico, H. Lee, P. Kok, and J. P. Dowling, "Quantum Interferometric Sensors", *Concepts of Physics* **2** (2005), no. 225, arXiv:0507150.

[24] V. Giovannetti, S. Lloyd, and L. Maccone, "Quantum-enhanced measurements: beating the standard quantum limit.", *Science (New York, N.Y.)* **306** (2004), no. 5700, 1330–6.

[25] P. Kok, K. Nemoto, T. C. Ralph, J. P. Dowling, and G. J. Milburn, "Linear optical quantum computing with photonic qubits", *Reviews of Modern Physics* **79** (2007), no. 1, 135–174.

[26] B. Sanders, "Quantum dynamics of the nonlinear rotator and the effects of continual spin measurement", *Physical Review A* **40** (1989), no. 5, 2417–2427.

[27] C. Wildfeuer, A. Lund, and J. P. Dowling, "Strong violations of Bell-type inequalities for path-entangled number states", *Physical Review A* **76** (2007), no. 5, 052101.

[28] M. W. Mitchell, J. S. Lundeen, and A. M. Steinberg, "Super-resolving phase measurements with a multiphoton entangled state", *Nature* **429** (2004), no. 6988, 161–4.

[29] P. Walther, J.-W. Pan, M. Aspelmeyer, R. Ursin, S. Gasparoni, and A. Zeilinger, "De Broglie wavelength of a non-local four-photon state", *Nature* **429** (2004), no. 6988, 158–61.

[30] A. Nielsen and K. Mø lmer, "Conditional generation of path-entangled optical N00N states", *Physical Review A* **75** (2007), no. 6, 063803.

[31] T. Nagata, R. Okamoto, J. L. O'brien, K. Sasaki, and S. Takeuchi, "Beating the standard quantum limit with four-entangled photons", *Science (New York, N.Y.)* **316** (2007), no. 5825, 726–9.

[32] C. Vitelli, N. Spagnolo, F. Sciarrino, and F. De Martini, "Amplification of polarization NOON states", *Journal of the Optical Society of America B* **26** (2009), no. 5, 892.

[33] N. Spagnolo, C. Vitelli, T. De Angelis, F. Sciarrino, and F. De Martini, "Wigner-function theory and decoherence of the quantum-injected optical parametric amplifier", *Physical Review A* **80** (2009), no. 3, 032318.

[34] J. A. Jones, S. D. Karlen, J. Fitzsimons, A. Ardavan, S. C. Benjamin, G. A. D. Briggs, and J. J. L. Morton, "Magnetic field sensing beyond the standard quantum limit using 10-spin NOON states", *Science (New York, N.Y.)* **324** (2009), no. 5931, 1166–8.

[35] R. Glasser, H. Cable, J. Dowling, F. De Martini, F. Sciarrino, and C. Vitelli, "Entanglement-seeded, dual, optical parametric amplification: Applications to quantum imaging and metrology", *Physical Review A* **78** (2008), no. 1, 012339.

[36] A. Al-Qasimi and D. F. James, "Nonexistence of entanglement sudden death in dephasing of high NOON states", *Optics Letters* **34** (2009), no. 3, 268.

[37] J. Bollinger, W. Itano, D. Wineland, and D. Heinzen, "Optimal frequency measurements with maximally correlated states", *Physical Review A* **54** (1996), no. 6, R4649–R4652.

[38] A. Chiruvelli and H. Lee, "Parity measurements in quantum optical metrology", *Journal of Modern Optics* **58** (2011), no. 11, 945–953.

[39] P. R. Bevington, "Data reduction and error analysis for the physical sciences", McGraw-Hill, New York, 1969.

[40] C. Helstrom, "Quantum detection and estimation theory", Academic Press, New York, 1976.

[41] A. Holevo, "Probabilistic and statistical aspects of quantum theory", North-Holland, Amsterdam, 1982.

[42] B. M. Escher, R. L. de Matos Filho, and L. Davidovich, "General framework for estimating the ultimate precision limit in noisy quantum-enhanced metrology", *Nature Physics* **7** (2011), no. 5, 406–411.

[43] M. G. Genoni, S. Olivares, and M. G. A. Paris, "Optical Phase Estimation in the Presence of Phase Diffusion", *Physical Review Letters* **106** (2011), no. 15, 153603.

[44] M. G. A. Paris, "Quantum Estimation for Quantum Technology", *International Journal of Quantum Information* **07** (2009), no. supp01, 125–137.

[45] C. Wildfeuer, A. Pearlman, J. Chen, J. Fan, A. Migdall, and J. P. Dowling, "Resolution and sensitivity of a Fabry-Perot interferometer with a photon-number-resolving detector", *Physical Review A* **80** (2009), no. 4, 043822.

[46] C. C. Gerry and T. Bui, "Quantum non-demolition measurement of photon number using weak nonlinearities", *Physics Letters A* **372** (2008), no. 48, 7101–7104.

[47] W. N. Plick, P. M. Anisimov, J. P. Dowling, H. Lee, and G. S. Agarwal, "Parity detection in quantum optical metrology without number-resolving detectors", *New Journal of Physics* **12** (2010), no. 11, 113025.

[48] K. Jiang, H. Lee, C. C. Gerry, and J. P. Dowling, "Super-resolving quantum radar: Coherent-state sources with homodyne detection suffice to beat the diffraction limit", *Journal of Applied Physics* **114** (2013), no. 19, 193102.

[49] P. W. Shor, "Polynomial-Time Algorithms for Prime Factorization and Discrete Logarithms on a Quantum Computer", *SIAM Review* **41** (1999), no. 2, 303–332.

[50] L. Grover, "Quantum Mechanics Helps in Searching for a Needle in a Haystack", *Physical Review Letters* **79** (1997), no. 2, 325–328.

[51] R. P. Feynman, "Simulating Physics with Computers", *International Journal of Theoretical Physics* **21** (1982), no. 6/7, 467–488.

[52] S. Somaroo, C. Tseng, T. Havel, R. Laflamme, and D. Cory, "Quantum Simulations on a Quantum Computer", *Physical Review Letters* **82** (1999), no. 26, 5381–5384.

[53] D. Lidar, I. Chuang, and K. Whaley, "Decoherence-Free Subspaces for Quantum Computation", *Physical Review Letters* **81** (1998), no. 12, 2594–2597.

[54] P. G. Kwiat, "Experimental Verification of Decoherence-Free Subspaces", *Science* **290** (2000), no. 5491, 498–501.

[55] P. W. Shor, "Scheme for reducing decoherence in quantum computer memory", *Physical Review A* **52** (1995), no. 4, R2493–R2496.

[56] A. Steane, "Error Correcting Codes in Quantum Theory", *Physical Review Letters* **77** (1996), no. 5, 793–797.

[57] D. DiVincenzo and P. Shor, "Fault-Tolerant Error Correction with Efficient Quantum Codes", *Physical Review Letters* **77** (1996), no. 15, 3260–3263.

[58] L. Viola and S. Lloyd, "Dynamical suppression of decoherence in two-state quantum systems", *Physical Review A* **58** (1998), no. 4, 2733–2744.

[59] K. Khodjasteh and D. Lidar, "Fault-Tolerant Quantum Dynamical Decoupling", *Physical Review Letters* **95** (2005), no. 18, 180501.

[60] G. Uhrig, "Keeping a Quantum Bit Alive by Optimized π-Pulse Sequences", *Physical Review Letters* **98** (2007), no. 10, 100504.

[61] K. Khodjasteh and D. Lidar, "Performance of deterministic dynamical decoupling schemes: Concatenated and periodic pulse sequences", *Physical Review A* **75** (2007), no. 6, 062310.

[62] W.-J. Kuo and D. A. Lidar, "Quadratic dynamical decoupling: Universality proof and error analysis", *Physical Review A* **84** (2011), no. 4, 042329.

[63] E. Hahn, "Spin Echoes", *Physical Review* **80** (1950), no. 4, 580–594.

[64] L. Viola, E. Knill, and S. Lloyd, "Dynamical Decoupling of Open Quantum Systems", *Physical Review Letters* **82** (1999), no. 12, 2417–2421.

[65] H. Carr and E. Purcell, "Effects of Diffusion on Free Precession in Nuclear Magnetic Resonance Experiments", *Physical Review* **94** (1954), no. 3, 630–638.

[66] S. Meiboom and D. Gill, "Modified Spin-Echo Method for Measuring Nuclear Relaxation Times", *Review of Scientific Instruments* **29** (1958), no. 8, 688.

[67] L.-A. Wu and D. Lidar, "Overcoming quantum noise in optical fibers", *Physical Review A* **70** (2004), no. 6, 062310.

[68] M. Lucamarini, G. Di Giuseppe, S. Damodarakurup, D. Vitali, and P. Tombesi, "Suppression of polarization decoherence for traveling light pulses via bang-bang dynamical decoupling", *Physical Review A* **83** (2011), no. 032320, 1101.3739.

[69] S. Massar and S. Popescu, "Reducing polarization mode dispersion with controlled polarization rotations", *New Journal of Physics* **9** (2007), no. 6, 158–158.

[70] W. Rosenfeld, F. Hocke, F. Henkel, M. Krug, J. Volz, M. Weber, and H. Weinfurter, "Towards Long-Distance Atom-Photon Entanglement", *Physical Review Letters* **101** (2008), no. 26, 260403.

[71] S. Damodarakurup, M. Lucamarini, G. Di Giuseppe, D. Vitali, and P. Tombesi, "Experimental Inhibition of Decoherence on Flying Qubits via Bang-Bang Control", *Physical Review Letters* **103** (2009), no. 4, 040502.

[72] J. Morton, A. Tyryshkin, A. Ardavan, K. Porfyrakis, S. Lyon, and G. Briggs, "Measuring errors in single-qubit rotations by pulsed electron paramagnetic resonance", *Physical Review A* **71** (2005), no. 1, 012332.

[73] L. Cywiński, R. Lutchyn, C. Nave, and S. Das Sarma, "How to enhance dephasing time in superconducting qubits", *Physical Review B* **77** (2008), no. 17, 174509.

[74] C. H. Bennett and G. Brassard, "Quantum cryptography: Public key distribution and coin tossing", *Proceedings of IEEE International Conference on Computers, Systems and Signal Processing*, 1984 175–179.

[75] J. P. Dowling and G. J. Milburn, "Quantum technology: the second quantum revolution.", *Philosophical transactions. Series A, Mathematical, physical, and engineering sciences* **361** (2003), no. 1809, 1655–74.

[76] M. Scalora, R. Flynn, S. Reinhardt, R. Fork, M. Bloemer, M. Tocci, C. Bowden, H. Ledbetter, J. Bendickson, J. P. Dowling, and R. Leavitt, "Ultrashort pulse propagation at the photonic band edge: Large tunable group delay with minimal distortion and loss", *Physical Review E* **54** (1996), no. 2, R1078–R1081.

[77] K. O. Hill and G. Meltz, "Fiber Bragg Grating Technology Fundamentals and Overview", *Journal of Lightwave Technology* **15** (1997), no. 8,.

[78] R. Ulrich, S. C. Rashleigh, and W. Eickhoff, "Bending-induced birefringence in single-mode fibers", *Optics Letters* **5** (1980), no. 6, 273.

[79] B. Roy Bardhan, K. L. Brown, and J. P. Dowling, "Dynamical decoupling with tailored wave plates for long-distance communication using polarization qubits", *Physical Review A* **88** (2013), no. 5, 052311.

[80] B. Roy Bardhan, P. M. Anisimov, M. K. Gupta, K. L. Brown, N. C. Jones, H. Lee, and J. P. Dowling, "Dynamical decoupling in optical fibers: Preserving polarization qubits from birefringent dephasing", *Physical Review A* **85** (2012), no. 2, 022340.

[81] J. R. West, B. H. Fong, and D. A. Lidar, "Near-Optimal Dynamical Decoupling of a Qubit", *Physical Review Letters* **104** (2010), no. 13, 130501.

[82] M. J. Biercuk, A. C. Doherty, and H. Uys, "Dynamical decoupling sequence construction as a filter-design problem", *Journal of Physics B: Atomic, Molecular and Optical Physics* **44** (2011), no. 15, 154002.

[83] U. Haeberlen and J. Waugh, "Coherent Averaging Effects in Magnetic Resonance", *Physical Review* **175** (1968), no. 2, 453–467.

[84] P. Zanardi, "Symmetrizing evolutions", *Physics Letters A* **258** (1999), no. 2-3, 77–82.

[85] S. Blanes, F. Casas, J. Oteo, and J. Ros, "The Magnus expansion and some of its applications", *Physics Reports* **470** (2009), no. 5-6, 151–238.

[86] W. Yang, Z.-Y. Wang, and R.-B. Liu, "Preserving qubit coherence by dynamical decoupling", *Frontiers of Physics* **6** (2010), no. 1, 2–14.

[87] L. Vandersypen and I. Chuang, "NMR techniques for quantum control and computation", *Reviews of Modern Physics* **76** (2005), no. 4, 1037–1069.

[88] G. S. Uhrig and S. Pasini, "Efficient coherent control by sequences of pulses of finite duration", *New Journal of Physics* **12** (2010), no. 4, 045001.

[89] K. Khodjasteh, T. Erdélyi, and L. Viola, "Limits on preserving quantum coherence using multipulse control", *Physical Review A* **83** (2011), no. 2, 020305.

[90] M. J. Biercuk, H. Uys, A. P. VanDevender, N. Shiga, W. M. Itano, and J. J. Bollinger, "Optimized dynamical decoupling in a model quantum memory.", *Nature* **458** (2009), no. 7241, 996–1000.

[91] E. R. Jenista, A. M. Stokes, R. T. Branca, and W. S. Warren, "Optimized, unequal pulse spacing in multiple echo sequences improves refocusing in magnetic resonance.", *The Journal of Chemical Physics* **131** (2009), no. 20, 204510.

[92] J. Du, X. Rong, N. Zhao, Y. Wang, J. Yang, and R. B. Liu, "Preserving electron spin coherence in solids by optimal dynamical decoupling.", *Nature* **461** (2009), no. 7268, 1265–8.

[93] B. Lee, W. Witzel, and S. Das Sarma, "Universal Pulse Sequence to Minimize Spin Dephasing in the Central Spin Decoherence Problem", *Physical Review Letters* **100** (2008), no. 16, 160505.

[94] A. Abragam, "Principles of Nuclear Magnetism", Oxford University Press, 1983.

[95] S. Pasini and G. S. Uhrig, "Optimized dynamical decoupling for power-law noise spectra", *Physical Review A* **81** (2010), no. 1, 012309.

[96] R. Gingrich, P. Kok, H. Lee, F. Vatan, and J. P. Dowling, "All Linear Optical Quantum Memory Based on Quantum Error Correction", *Physical Review Letters* **91** (2003), no. 21, 217901.

[97] A. I. Lvovsky, B. C. Sanders, and W. Tittel, "Optical quantum memory", *Nature Photonics* **3** (2009), no. 12, 706–714.

[98] H. J. Kimble, "The quantum internet.", *Nature* **453** (2008), no. 7198, 1023–30.

[99] D. Bouwmeester, A. K. Ekert, and A. Zeilinger, "The physics of quantum information: Quantum cryptography, quantum teleportation, quantum computation:", Springer, 2000.

[100] G. D. VanWiggeren and R. Roy, "Transmission of Linearly Polarized Light through a Single-Mode Fiber with Random Fluctuations of Birefringence", *Applied Optics* **38** (1999), no. 18, 3888.

[101] S. C. Rashleigh, W. K. Burns, R. P. Moeller, and R. Ulrich, "Polarization holding in birefringent single-mode fibers", *Optics Letters* **7** (1982), no. 1, 40.

[102] P. Shor and J. Preskill, "Simple Proof of Security of the BB84 Quantum Key Distribution Protocol", *Physical Review Letters* **85** (2000), no. 2, 441–444.

[103] P. A. Hiskett, D. Rosenberg, C. G. Peterson, R. J. Hughes, S. Nam, A. E. Lita, A. J. Miller, and J. E. Nordholt, "Long-distance quantum key distribution in optical fibre", *New Journal of Physics* **8** (2006), no. 9, 193–193.

[104] R. H. Hadfield, J. L. Habif, J. Schlafer, R. E. Schwall, and S. W. Nam, "Quantum key distribution at 1550 nm with twin superconducting single-photon detectors", *Applied Physics Letters* **89** (2006), no. 24, 241129.

[105] A. Galtarossa, L. Palmieri, M. Schiano, and T. Tambosso, "Measurements of beat length and perturbation length in long single-mode fibers", *Optics Letters* **25** (2000), no. 6, 384.

[106] G. A. Álvarez, A. Ajoy, X. Peng, and D. Suter, "Performance comparison of dynamical decoupling sequences for a qubit in a rapidly fluctuating spin bath", *Physical Review A* **82** (2010), no. 4, 042306.

[107] U. Haeberlen, "High Resolution NMR in Solids: Selective Averaging", Academic Press, New York, 1976.

[108] G. S. Uhrig and S. Pasini, "Efficient coherent control by sequences of pulses of finite duration", *New Journal of Physics* **12** (2010), no. 4, 045001.

[109] K. Brown, A. Harrow, and I. Chuang, "Arbitrarily accurate composite pulse sequences", *Physical Review A* **70** (2004), no. 5, 052318.

[110] H. K. Cummins and J. A. Jones, "Use of composite rotations to correct systematic errors in NMR quantum computation", *New Journal of Physics* **2** (2000), no. 1, 6–6.

[111] H. Cummins, G. Llewellyn, and J. Jones, "Tackling systematic errors in quantum logic gates with composite rotations", *Physical Review A* **67** (2003), no. 4, 042308.

[112] M. Möttönen, R. de Sousa, J. Zhang, and K. Whaley, "High-fidelity one-qubit operations under random telegraph noise", *Physical Review A* **73** (2006), no. 2, 022332.

[113] A. M. Souza, G. A. Álvarez, and D. Suter, "Robust dynamical decoupling.", *Philosophical transactions. Series A, Mathematical, physical, and engineering sciences* **370** (2012), no. 1976, 4748–69.

[114] S. Pasini, T. Fischer, P. Karbach, and G. Uhrig, "Optimization of short coherent control pulses", *Physical Review A* **77** (2008), no. 3, 032315.

[115] L. Pryadko and G. Quiroz, "Soft-pulse dynamical decoupling in a cavity", *Physical Review A* **77** (2008), no. 1, 012330.

[116] P. Sengupta and L. Pryadko, "Scalable Design of Tailored Soft Pulses for Coherent Control", *Physical Review Letters* **95** (2005), no. 3, 037202.

[117] A. Ajoy, G. A. Álvarez, and D. Suter, "Optimal pulse spacing for dynamical decoupling in the presence of a purely dephasing spin bath", *Physical Review A* **83** (2011), no. 3, 032303.

[118] G. A. Álvarez, A. M. Souza, and D. Suter, "Iterative rotation scheme for robust dynamical decoupling", *Physical Review A* **85** (2012), no. 5, 052324.

[119] R. Freeman, "Spin Choreography: Basic Steps in High Resolution NMR", Oxford University Press, London, 1998.

[120] W. Witzel and S. Das Sarma, "Multiple-Pulse Coherence Enhancement of Solid State Spin Qubits", *Physical Review Letters* **98** (2007), no. 7, 077601.

[121] W. Yao, R.-B. Liu, and L. Sham, "Restoring Coherence Lost to a Slow Interacting Mesoscopic Spin Bath", *Physical Review Letters* **98** (2007), no. 7, 077602.

[122] A. A. Maudsley and J. Magn, "Modified Carr-Purcell-Meiboom-Gill Sequence for NMR Fourier Imaging Applications", *Journal of Magnetic Resonance* **69** (1986) 488–491.

[123] T. Gullion, D. B. Baker, and J. M. M. S. Conradi, "New, Compensated Carr-Purcell Sequences", *Journal of Magnetic Resonance* **89** (1990) 479–484.

[124] R. G. Spencer and K. W. Fishbein, "Measurement of spin-lattice relaxation times and concentrations in systems with chemical exchange using the one-pulse sequence: breakdown of the ernst model for partial saturation in nuclear magnetic resonance spectroscopy", *Journal of Magnetic Resonance* **142** January (2000) 120–35.

[125] K. Zyczkowski and H.-J. Sommers, "Average fidelity between random quantum states", *Physical Review A* **71** (2005), no. 3, 032313.

[126] M. Hisatomi, M. C. Parker, and S. D. Walker, "Binary multi-zoned microstructured fiber: A comparative dispersion analysis of radially chirped bragg fiber", *Journal of Lightwave Technology* **23** (2005)a, no. 11,.

[127] M. Hisatomi, M. C. Parker, and S. D. Walker, "Comparison of zoned microstructure fiber geometries for low-dispersion waveguiding", *Journal of Lightwave Technology* **23** (2005)b, no. 2,.

[128] D. Leduc, X. Chapeleau, C. Lupi, F. L. Gejo, M. Douay, R. L. Ny, and C. Boisrobert, "Experimental synthesis of fibre Bragg gratings index profiles: comparison of two inverse scattering algorithms", *Measurement Science and Technology* **18** (2007), no. 1, 12–18.

[129] R. Simon, "Peres-horodecki separability criterion for continuous variable systems", *Physical Review Letters* **84** Mar (2000) 2726–2729.

[130] L.-M. Duan, G. Giedke, J. I. Cirac, and P. Zoller, "Inseparability criterion for continuous variable systems", *Physical Review Letters* **84** Mar (2000) 2722–2725.

[131] M. B. Plenio, "Logarithmic negativity: A full entanglement monotone that is not convex", *Physical Review Letters* **95** Aug (2005) 090503.

[132] G. S. Agarwal, "Quantum Optics", Cambridge University Press, 2012.

[133] D. F. Walls and G. J. Milburn, "Quantum Optics", Springer, 2008.

[134] J. Williamson, "On the algebraic problem concerning the normal forms of linear dynamical systems", *American Journal of Mathematics* **58** (1936).

[135] C. H. Bennett, H. J. Bernstein, S. Popescu, and B. Schumacher, "Concentrating partial entanglement by local operations", *Physical Review A* **53** Apr (1996) 2046–2052.

[136] G. Giedke, B. Kraus, M. Lewenstein, and J. I. Cirac, "Entanglement criteria for all bipartite gaussian states", *Physical Review Letters* **87** Oct (2001) 167904.

[137] R. F. Werner and M. M. Wolf, "Bound entangled gaussian states", *Physical Review Letters* **86** Apr (2001) 3658–3661.

[138] G. Vidal and R. F. Werner, "Computable measure of entanglement", *Physical Review A* **65** Feb (2002) 032314.

[139] G. S. Agarwal, "How much quantum noise of amplifiers is detrimental to entanglement", *Optics Communications* **283** (2010) 839–842.

[140] V. Josse, M. Sabuncu, N. J. Cerf, G. Leuchs, and U. L. Andersen, "Universal optical amplification without nonlinearity", *Physical Review Letters* **96** Apr (2006) 163602.

[141] C. K. Hong, S. Friberg, and L. Mandel, "Conditions for nonclassical behavior in the light amplifier", *Journal of the Optical Society of America B* **2** Mar (1985) 494–496.

[142] S. Lloyd, "Enhanced sensitivity of photodetection via quantum illumination", *Science* **321** (2008) 1463–1465.

[143] S.-H. Tan, B. I. Erkmen, V. Giovannetti, S. Guha, S. Lloyd, L. Maccone, S. Pirandola, and J. H. Shapiro, "Quantum illumination with Gaussian states", *Physical Review Letters* **101** Dec (2008) 253601.

[144] D. Buono, G. Nocerino, V. DAuria, A. Porzio, S. Olivares, and M. G. A. Paris, "Quantum characterization of bipartite Gaussian states", *Journal of the Optical Society of America B* **27** (2010), no. 6, A110.

[145] S. Guha, "Receiver design to harness quantum illumination advantage", in "2009 IEEE International Symposium on Information Theory", pp. 963–967. IEEE, 2009.

[146] J. Eisert and M. M. Wolf, "Gaussian quantum channels", *Quantum Information with Continuous Variables of Atoms and Light*, 2007 23–42, arXiv:quant-ph/0505151.

[147] A. S. Holevo and R. F. Werner, "Evaluating capacities of bosonic Gaussian channels", *Physical Review A* **63** Feb (2001) 032312.

[148] A. Winter, "Coding Theorem and Strong Converse for Quantum Channels", *IEEE Transactions on Information Theory* **45** (1999), no. 7, 2481–2485.

[149] T. Ogawa and H. Nagaoka, "Making Good Codes for Classical-Quantum Channel Coding via Quantum Hypothesis Testing", *IEEE Transactions on Information Theory* **53** June (2007) 2261–2266.

[150] M. M. Wilde, A. Winter, and D. Yang, "Strong converse for the classical capacity of entanglement-breaking and Hadamard channels", *Communications in Mathematical Physics* **331** October (2014) 593–622, arXiv:1306.1586.

[151] S. Arimoto, "On the converse to the coding theorem for discrete memoryless channels", *IEEE Transactions on Information Theory* **19** May (1973) 357–359.

[152] J. Wolfowitz, "Coding theorems of information theory", Springer, 1964.

[153] M. M. Wilde and A. Winter, "Strong converse for the classical capacity of the pure-loss bosonic channel", *Problems of Information Transmission* **50** (2014), no. 2, 117–132, arXiv:1308.6732.

[154] R. Koenig, S. Wehner, and J. Wullschleger, "Unconditional security from noisy quantum storage", *IEEE Transactions on Information Theory* **58** (2012) 1962–1984, arXiv:0906.1030.

[155] V. Giovannetti, A. S. Holevo, and R. García-Patrón, "A solution of the Gaussian optimizer conjecture", December (2013), arXiv:1312.2251.

[156] V. Giovannetti, R. Garcia-Patron, N. J. Cerf, and A. S. Holevo, "Ultimate communication capacity of quantum optical channels by solving the Gaussian minimum-entropy conjecture", December (2013), arXiv:1312.6225.

[157] A. Mari, V. Giovannetti, and A. S. Holevo, "Quantum state majorization at the output of bosonic Gaussian channels", *Nature Communications* **5** May (2014), arXiv:1312.3545.

[158] B. Roy Bardhan and M. M. Wilde, "Strong converse rates for classical communication over thermal and additive noise bosonic channels", *Physical Review A* **89** (2014), no. 2, 022302, arXiv:1312.3287.

[159] B. Roy Bardhan, R. Garcia-Patron, M. M. Wilde, and A. Winter, "Strong converse for the capacity of quantum Gaussian channels", in "2014 IEEE International Symposium on Information Theory", pp. 726–730. IEEE (2014).

[160] C. Weedbrook, S. Pirandola, R. García-Patrón, N. J. Cerf, T. C. Ralph, J. H. Shapiro, and S. Lloyd, "Gaussian Quantum Information", *Reviews of Modern Physics* **84** May (2012) 621–669, arXiv:1110.3234.

[161] C. M. Caves and P. D. Drummond, "Quantum limits on bosonic communication rates", *Reviews of Modern Physics* **66** April (1994) 481–537.

[162] C. M. Caves, "Quantum limits on noise in linear amplifiers", *Physical Review D* **26** (1982), no. 8, 1817–1839.

[163] J. S. Ivan, K. K. Sabapathy, and R. Simon, "Operator-sum representation for bosonic Gaussian channels", *Physical Review A* **84** October (2011) 042311, arXiv:1012.4266.

[164] R. Garcia-Patron, C. Navarrete-Benlloch, S. Lloyd, J. H. Shapiro, and N. J. Cerf, "Majorization theory approach to the Gaussian channel minimum entropy conjecture", *Physical Review Letters* **108** March (2012) 110505, arXiv:1111.1986.

[165] V. Giovannetti, S. Lloyd, L. Maccone, and J. H. Shapiro, "Electromagnetic channel capacity for practical purposes", *Nature Photonics* **7** 10 (2013) 834–838.

[166] M. J. W. Hall, "Gaussian noise and quantum-optical communication", *Physical Review A* **50** October (1994) 3295–3303.

[167] V. Giovannetti, S. Guha, S. Lloyd, L. Maccone, and J. H. Shapiro, "Minimum output entropy of bosonic channels: A conjecture", *Physical Review A* **70** Sep (2004) 032315.

[168] F. Caruso, V. Giovannetti, and A. S. Holevo, "One-mode bosonic Gaussian channels: A full weak-degradability classification", *New Journal of Physics* **8** (2006), no. 12, 310, arXiv:quant-ph/0609013.

[169] V. Giovannetti, S. Guha, S. Lloyd, L. Maccone, J. H. Shapiro, and H. P. Yuen, "Classical Capacity of the Lossy Bosonic Channel: The Exact Solution", *Physical Review Letters* **92** January (2004) 027902, arXiv:quant-ph/0308012.

[170] V. Giovannetti, S. Lloyd, L. Maccone, J. H. Shapiro, and B. J. Yen, "Minimum Rényi and Wehrl entropies at the output of bosonic channels", *Physical Review A* **70** Aug (2004) 022328.

[171] R. Renner and R. Koenig, "Universally composable privacy amplification against quantum adversaries", Springer Berlin Heidelberg, 2005. arXiv:quant-ph/0403133.

[172] R. Renner,"Security of Quantum Key Distribution", PhD Thesis, ETH Zürich, 2005, arXiv:quant-ph/0512258.

[173] M. Tomamichel, "A Framework for Non-Asymptotic Quantum Information Theory", PhD Thesis, ETH Zürich, 2012, arXiv:1203.2142.

[174] R. Renner and S. Wolf, "Smooth Rényi entropy and applications", in "Proceedings of the 2007 International Symposium on Information Theory", p. 232. 2004.

[175] R. Koenig and S. Wehner, "A Strong Converse for Classical Channel Coding Using Entangled Inputs", *Physical Review Letters* **103** August (2009) 070504, arXiv:0903.2838.

[176] A. Nayak, "Optimal lower bounds for quantum automata and random access codes", in "Proceedings of the 40th Annual Symposium on Foundations of Computer Science", pp. 369–376. New York City, NY, USA, October 1999. arXiv:quant-ph/9904093.

[177] T. M. Cover and J. A. Thomas, "Elements of Information Theory", Wiley-Interscience, 2nd ed., 2006.

[178] T. Tao, "Topics in random matrix theory", American Mathematical Society, 2012. see also http://terrytao.wordpress.com/2010/01/03/254a-notes-1-concentration-of-measure.

[179] B. Yen and J. Shapiro, "Multiple-access bosonic communications", *Physical Review A* **72** (2005), no. 6, 062312.

Appendix A: Effects of both photon loss and phase noise on the sensitivity and visibility [2]

In this appendix, we provide detailed calculations of the phase sensitivity and the visibility using the parity detection technique when both photon loss and phase fluctuations are present in the interferometric setup discussed in Chapter 2.

We consider the N00N and mm' states, and to model photon loss from the system into the environment, we add two fictitious beam splitters are added before stage I of our previous configuration in Chapter 2 (See Fig 2.5). The two fictitious beam splitters have transmittance T_a and T_b, and reflectance $R_a = 1 - T_a$ and $R_b = 1 - T_b$, respectively. General T_a and T_b are used in the following derivation of the density matrix, but later we assume $R_a = 0$ to mimic the local path which is well-isolated from the environment. The photon loss entangles the system with the environment and leaves the system in a mixed state. For a general mm' input state, the density matrix of the system at stage II can be easily deducted from the Reference [15] as

$$\begin{aligned}\rho_{mm'}(t) = & \sum_{k=0}^{m}\sum_{k'=0}^{m'}\Big\{|\alpha|^2 d_1(t)|k,k'\rangle\langle k,k'| + |\beta|^2 d_2(t)|k',k\rangle\langle k',k|\Big\} \\ & + \sum_{k=0}^{m'}\sum_{k'=0}^{m'}\Big\{\alpha\beta^* d_3(t)|\Delta m+k,k'\rangle\langle k,\Delta m+k'| \\ & + \alpha^*\beta d_4(t)|k',\Delta m+k\rangle\langle\Delta m+k',k|\Big\}.\end{aligned} \tag{53}$$

In the above, $\alpha = e^{im'\phi}/\sqrt{2}$, $\beta = e^{im\phi}/\sqrt{2}$ as before, and the coefficients $d_i (i = 1, 2, 3, 4)$ are defined in Reference [15]. m and m' are the number of photons injected into the two modes of the interferometer.

Given the system undergoes pure dephasing after stage II, we may use previous result and show that the evolution of the density matrix $\rho_{mm'}(t)$ is

$$\begin{aligned}\dot{\rho}_{mm'}(t) = & -\Delta m^2\Gamma\times \\ & \sum_{k,k'=0}^{m'}\Big\{\alpha\beta^* d_3(t)|\Delta m+k,k'\rangle\langle k,\Delta m+k'| + \alpha^*\beta d_4(t)|k',\Delta m+k\rangle\langle\Delta m+k',k|\Big\}.\end{aligned}$$

[2] Part of this appendix previously appeared in B. Roy Bardhan, K. Jiang, and J. P. Dowling, Physical Review A **88**, 023857 (2013) (Copyright(2013) American Physical Society) [22]. It is reprinted by permission of the American Physical Society. See Appendix C for the copyright permission from the publisher.

From the above, it is then easy to see that

$$\begin{aligned} d_1(t) &= d_1(0), \\ d_2(t) &= d_2(0), \\ d_3(t) &= e^{-\Delta m^2 \Gamma L} d_3(0), \\ d_4(t) &= e^{-\Delta m^2 \Gamma L} d_4(0). \end{aligned} \tag{54}$$

Similar to Reference [15], we define

$$\begin{aligned} K_1(t) &= \sum_{k=0}^{m'} \left(d_1(k,k,t) + d_2(k,k,t) \right), \\ K_2(t) &= \sum_{k=0}^{m'} \left(d_3(k,k,t) + d_4(k,k,t) \right), \end{aligned} \tag{55}$$

and it is straightforward to show that $K_1(t) = K_1(0)$ and $K_2(t) = K_2(0)e^{-\Delta m^2 \Gamma L}$. From Equations (2.10) in Chapter 2 and (53), the parity signal of a mm' state under both photon loss and phase fluctuation can be shown to be

$$\langle \hat{\Pi}_{mm'} \rangle = K_1(t) + (-1)^{m+m'} K_2(t) \cos(\Delta m \phi). \tag{56}$$

This gives rise to the phase-sensitivity for the parity detection for a mm' state under both photon-loss and phase fluctuations as

$$\delta\phi_{mm'} = \sqrt{\frac{1 - \left\{ K_1(t) + (-1)^{m+m'} K_2(t) \cos(\Delta m \phi) \right\}^2}{\left\{ \Delta m K_2(t) \sin(\Delta m \phi) \right\}^2}}, \tag{57}$$

where linear error propagation method in Equation (12) is employed. Notice that when loss is negligible this sensitivity recovers Equation (2.13) in Chapter 2.

A relative visibility with respect to both loss and phase fluctuations can be defined as

$$\begin{aligned} V_{mm'} &= \frac{\langle \hat{\Pi}_{mm'} \rangle_{\max} - \langle \hat{\Pi}_{mm'} \rangle_{\min}}{\langle \hat{\Pi}_{mm'}(\Gamma = 0, L = 0) \rangle_{\max} - \langle \hat{\Pi}_{mm'}(\Gamma = 0, L = 0) \rangle_{\min}}, \\ &= K_2(0) e^{-\Delta m^2 \Gamma L} \end{aligned} \tag{58}$$

where $L = R_b$ characterizes the loss in the upper path and R_a is set to be zero as aforementioned. In the limit of $L \to 0$, $K_2(0)$ approaches one and the visibility reduces to the previous result. Notice the dephasing only affects the off-diagonal terms of the density matrix while loss affects both diagonal and off-diagonal terms. However, because of the linearity of the Mach-Zehnder interferometer, the effect from photon loss is independent of that from phase fluctuation, as expected. All results in this section apply to N00N states with $N = m$ and $m' = 0$.

Appendix B: Structural decompositions of the bosonic Gaussian channels [3]

Here we review, for completeness, in detail an argument for the structural decompositions of the noisy bosonic communication channels using the symplectic formalism [146, 160]. In this formalism, the action of a Gaussian channel is characterized by two matrices X and Y which act as follows on covariance matrix Γ

$$\Gamma \longrightarrow \Gamma' = X\Gamma X^T + Y, \tag{59}$$

where X^T is the transpose of the matrix X. Such a map is called as the symplectic map which applies to any Gaussian channel. Below we describe the symplectic transformations for each of the channels $\mathcal{N}_{\bar{n}}$, $\mathcal{E}_{\eta,0}$, $\mathcal{A}_G$, and $\mathcal{E}_{\eta,N_B}$:

- The additive noise channel $\mathcal{N}_{\bar{n}}$ with variance $\bar{n}$ is given by

$$X = \mathbb{I} \text{ and } Y = 2\bar{n}\ \mathbb{I}, \tag{60}$$

  where $\mathbb{I}$ represents the identity matrix.

- The pure-loss channel $\mathcal{E}_{\eta,0}$ with transmissivity $\eta < 1$ is given by

$$X = \sqrt{\eta}\ \mathbb{I} \text{ and } Y = (1-\eta)\ \mathbb{I}. \tag{61}$$

- The thermal noise channel $\mathcal{E}_{\eta,N_B}$ with transmissivity $\eta < 1$ and noise photon number N_B is given by

$$X = \sqrt{\eta}\ \mathbb{I} \text{ and } Y = (1-\eta)(2N_B+1)\ \mathbb{I}. \tag{62}$$

- The amplifier channel $\mathcal{A}_G$ with gain $G > 1$ is given by

$$X = \sqrt{G}\ \mathbb{I} \text{ and } Y = (G-1)\ \mathbb{I}. \tag{63}$$

We now show that the additive noise channel $\mathcal{N}_{\bar{n}}$ can be regarded as a pure-loss bosonic channel $\mathcal{E}_{\eta,0}$ with $\eta = 1/(\bar{n}+1)$ followed by an amplifier channel $\mathcal{A}_G$ with $G = (\bar{n}+1)$. To do so, we substitute

$$\begin{aligned} X_1 &= \sqrt{1/(\bar{n}+1)}\mathbb{I}, \\ Y_1 &= (1-(1/(\bar{n}+1))\ \mathbb{I}, \\ X_2 &= \sqrt{(\bar{n}+1)}\ \mathbb{I}, \\ Y_2 &= \bar{n}\ \mathbb{I}. \end{aligned}$$

[3] This appendix previously appeared in B. Roy Bardhan and Mark M. Wilde, Physical Review A **89**, 022302 (2014) (Copyright(2014) American Physical Society) [158]. It has been updated and adapted to the disseration format by permission of the American Physical Society. See Appendix C for the copyright permission from the publisher.

in (61) and (63), where (X_1, Y_1) and (X_2, Y_2) correspond to the pure-loss bosonic channel $\mathcal{E}_{\eta,0}$ and the amplifier channel $\mathcal{A}_G$, respectively. The covariance matrix Γ_{12} for the composite map $(\mathcal{A}_{\bar{n}+1} \circ \mathcal{E}_{\frac{1}{\bar{n}+1},0})$ is then obtained as $\Gamma_{12} = X_2(X_1 \Gamma X_1^T + Y_1)X_2^T + Y_2 = \Gamma \, \mathbb{I} + 2\bar{n} \, \mathbb{I}$, which represents the additive noise channel $\mathcal{N}_{\bar{n}}$ [(60)]. Thus, we recover the decomposition in (5.14)

$$\mathcal{N}_{\bar{n}}(\rho) = (\mathcal{A}_{\bar{n}+1} \circ \mathcal{E}_{\frac{1}{\bar{n}+1},0})(\rho) \, .$$

Following a similar approach for the thermal noise channel $\mathcal{E}_{\eta,N_B}$, we can find the structural decompositions

$$\begin{aligned} \mathcal{E}_{\eta,N_B}(\rho) &= \left(\mathcal{N}_{(1-\eta)N_B} \circ \mathcal{E}_{\eta,0}\right)(\rho), \\ \mathcal{E}_{\eta,N_B}(\rho) &= \left(\mathcal{A}_G \circ \mathcal{E}_{\eta,0}\right)(\rho). \end{aligned}$$

Appendix C:
Copyright Permissions

- Copyright permission from the journal Physical Review A (PRA) of the American Physical Society (APS):

  Here I copy the relevant text (from the website https://journals.aps.org/copyrightFAQ.html):

  "As the author of an APS-published article, may I include my article or a portion of my article in my thesis or dissertation?

  Yes, the author has the right to use the article or a portion of the article in a thesis or dissertation without requesting permission from APS, provided the bibliographic citation and the APS copyright credit line are given on the appropriate pages."

  The email from the American Physical Society indicating its permission to reuse the materials from the papers authored by me is also shown below:

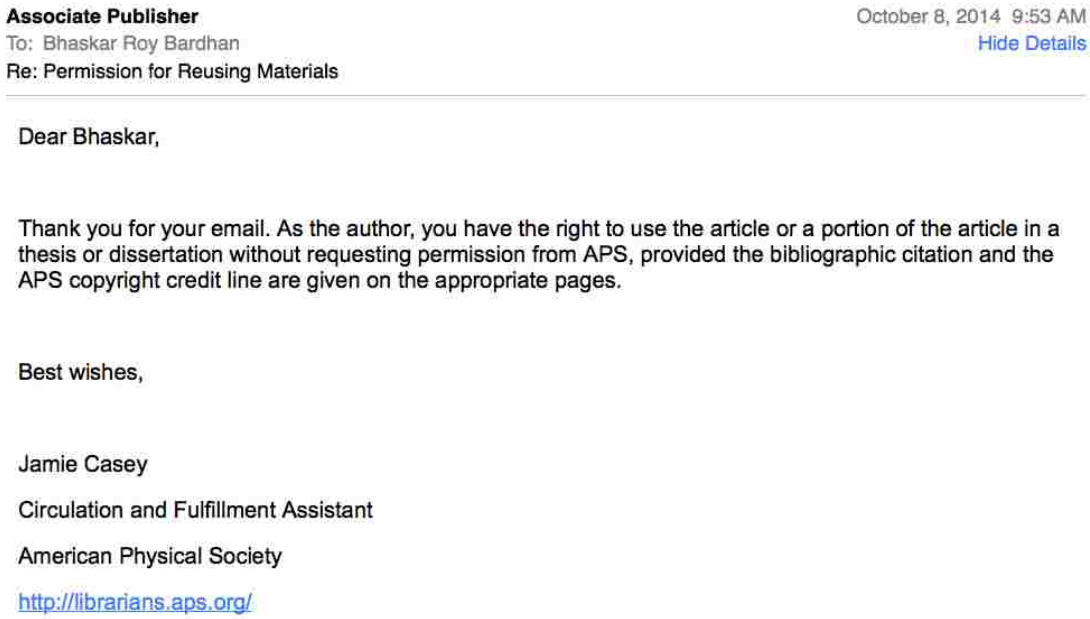

Associate Publisher October 8, 2014 9:53 AM
To: Bhaskar Roy Bardhan Hide Details
Re: Permission for Reusing Materials

Dear Bhaskar,

Thank you for your email. As the author, you have the right to use the article or a portion of the article in a thesis or dissertation without requesting permission from APS, provided the bibliographic citation and the APS copyright credit line are given on the appropriate pages.

Best wishes,

Jamie Casey

Circulation and Fulfillment Assistant

American Physical Society

http://librarians.aps.org/

- Copyright permission from the Institute of Electrical and Electronics Engineers (IEEE):

Title: Strong converse for the capacity of quantum Gaussian channels

Conference Proceedings: Information Theory (ISIT), 2014 IEEE International Symposium on

Author: Bardhan, B.R.; Garcia-Patron, R.; Wilde, M.M.; Winter, A.

Publisher: IEEE

Date: June 29 2014-July 4 2014

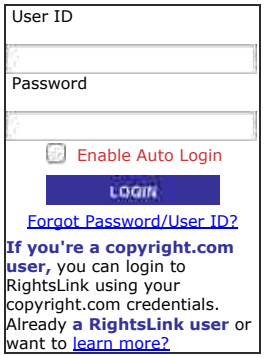

Thesis / Dissertation Reuse

The IEEE does not require individuals working on a thesis to obtain a formal reuse license, however, you may print out this statement to be used as a permission grant:

Requirements to be followed when using any portion (e.g., figure, graph, table, or textual material) of an IEEE copyrighted paper in a thesis:

1) In the case of textual material (e.g., using short quotes or referring to the work within these papers) users must give full credit to the original source (author, paper, publication) followed by the IEEE copyright line © 2011 IEEE.
2) In the case of illustrations or tabular material, we require that the copyright line © [Year of original publication] IEEE appear prominently with each reprinted figure and/or table.
3) If a substantial portion of the original paper is to be used, and if you are not the senior author, also obtain the senior author's approval.

Requirements to be followed when using an entire IEEE copyrighted paper in a thesis:

1) The following IEEE copyright/ credit notice should be placed prominently in the references: © [year of original publication] IEEE. Reprinted, with permission, from [author names, paper title, IEEE publication title, and month/year of publication]
2) Only the accepted version of an IEEE copyrighted paper can be used when posting the paper or your thesis on-line.
3) In placing the thesis on the author's university website, please display the following message in a prominent place on the website: In reference to IEEE copyrighted material which is used with permission in this thesis, the IEEE does not endorse any of [university/educational entity's name goes here]'s products or services. Internal or personal use of this material is permitted. If interested in reprinting/republishing IEEE copyrighted material for advertising or promotional purposes or for creating new collective works for resale or redistribution, please go to http://www.ieee.org/publications_standards/publications/rights/rights_link.html to learn how to obtain a License from RightsLink.

If applicable, University Microfilms and/or ProQuest Library, or the Archives of Canada may supply single copies of the dissertation.

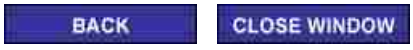

Vita

Bhaskar Roy Bardhan was born in Kolkata, a major city in the eastern part of India. He earned a bachelor's degree in physics (honors) from St. Xavier's College, University of Calcutta, India in July 2006. He then pursued his master's degree in physics in Indian Institute of Technology Guwahati and obtained his master's degree from there in May 2008. After spending a brief period as a graduate teaching assistant at the University of Connecticut, he enrolled in the doctoral degree program at the Physics and Astronomy Department at the Louisiana State University in June 2009. His research work is focused on quantum optics, quantum control and quantum information theory. During his doctoral studies he received the Charles E. Coates research grant for the academic year 2013-2014 from Louisiana State University, and was also recipient of several conference travel awards from the American Physical Society and Institute of Electrical and Electronics Engineers. He will join the research group of Professor Jeffrey Shapiro at the Massachusetts Institute of Technology as a postdoctoral researcher beginning in November 2014, and continue his work in the field of optical quantum communication.